LONG RANGE MATERIALS RESEARCH

Robert A. Huggins

Stanford University

Prepared for:

Defense Advanced Research Projects Agency

31 December 1973

AD776 240

FIRST SEMI-ANNUAL TECHNICAL REPORT

July 1 - December 31, 1973

Long Range Materials Research

Sponsored by
Defense Advanced Research Projects Agency
ARPA Order No. 2470

Program Code Number: 3D10

Contractor: Stanford University

Effective Date of Contract: June 1, 1973

Contract Expiration Date: May 31, 1974

Amount of Grant: $265,000

Grant Number: DAH C15 73 G15

Principal Investigator: Robert A. Huggins
Phone: (415) 321-2300, ext. 4118

Short Title: Long Range Materials Research

159

Center for Materials Research
Stanford University
Stanford, California 94305
(415) 321-2300, ext. 4118

CMR-74-2

1.

TABLE OF CONTENTS

I. INTRODUCTION

I. INTRODUCTION

This is the first semiannual technical report on the research program entitled "Long Range Materials Research," covering the period July 1 through December 31, 1973. This program is composed of four separate programs as follows:

1. Harmonic Generation and Detection of X-Ray Radiation
2. Superplasticity and Warm Working of Metals and Alloys
3. Synthesis of New Types of Catalyst Materials
4. Development of Elevated Temperature Electrocrystallization Techniques

Progress in each of the subareas during the initial portion of this program will be described separately in the succeeding sections of this report.

II. GENERATION OF COHERENT VACUUM ULTRAVIOLET AND SOFT X-RAY RADIATION

S. E. Harris

Professor of Electrical Engineering

and

J. F. Young

Research Associate, Hansen Laboratories

A. Introduction

A number of programs in our laboratory are now aimed at the development of techniques for the generation of coherent, vacuum ultraviolet, and soft x-ray radiation. A program aimed at the application of this radiation to sub-micron fabrication and to holographic microscopy is also underway. These programs are supported by a number of different contracts and grants from various DOD agencies, from NASA, and from the AEC. During this past year, funds from the ARPA program were used toward the partial purchase of a grazing incidence monochromator with a spectral range of 2 Å through 2000 Å. This instrument, when it arrives, will be used in general support of many of the above programs. In the present report and proposal we summarize the status of certain of these programs, and note the directions in which they are likely to proceed during the forthcoming year. For this forthcoming period, the ARPA funds will be used in part toward the purchase of a tunable laser to be described below, and in part for salary and equipment costs associated with the generation of radiation in the several hundred angstrom region.

A list of publications originating during the previous period is attached as Section H.

B. Conversion from 1.064μ to 3547 Å

Although not immediately germane to the subject of this report, we report progress on an AEC-supported program aimed at efficiently tripling 1.064μ radiation to 3547 Å radiation. The motivation for this program is to allow frequency tripling of lasers having very high peak powers and energies. The technical basis of the program is nonlinear optical techniques in phase-matched metal vapors. These vapors allow breakdown densities in excess of 10^{11} W/cm^2, as opposed to comparable densities in crystals of at most 10^{10} W/cm^2. Metal vapor inert gas cells might also be scaled to diameters of 30 cm, thus allowing areas several hundred times greater than that obtainable using nonlinear crystal techniques.

To date, the largest conversion efficiency which we have obtained in this program is 2.7%. The present experimental arrangement makes use of a concentric heat pipe oven, 40 cm in length, and operated at a pressure of 3 Torr of Na vapor. Scaling options for increased efficiency include increasing the Na pressure, substituting Rb for Na, length scaling, reducing the phase-matching ratio by substituting another metal vapor for the presently employed inert gas, and the introduction of quenching agents for reducing the lifetime of the excited state. Without going into further detail here, it seems likely that efficiencies approaching, or in excess of, 50% should be obtainable with continued experimental effort.

Techniques developed in this spectral region will also be directly applicable to generation of vacuum ultraviolet and soft x-ray laser radiation. These techniques include the development of sophisticated single and double heat pipe ovens, studies of focusing properties of metal vapor and inert gas cells, and a more general understanding of limits imposed by multi-photon ionization.

C. Generation of Vacuum Ultraviolet Radiation

A summary of experiments which have thus far been performed to extend the frequency tripling technique into the vacuum ultraviolet is shown in Fig. 1. In early experiments, we employed a phase-matched mixture of Cd and Ar in the ratio of 1 part Cd to 25 parts Ar to generate 1773 Å. In a second experiment, one photon of 1.06μ radiation was mixed with two photons of 3547 Å to yield an output at 1520 Å. Although a third experiment in this same system allowed the generation of a very weak signal at 1182 Å, a much better technique was soon discovered.

In this newer technique we use a second inert gas as the negatively dispersive medium. Using a phase-matched mixture of Xe and Ar in a ratio of about 430 parts Ar to 1 part Xe, we obtained approximately 3% conversion efficiency from 3547 Å to 1182 Å.

In attempting to scale this technique to higher efficiency, we have recently encountered a rather severe gas mixing problem. In general, it appears to take as much as 12 to 15 hours for sufficiently homogeneous mixing of the Xe and Ar to occur. This makes continuous scans and optimization of focusing and operating conditions very difficult. We are now developing

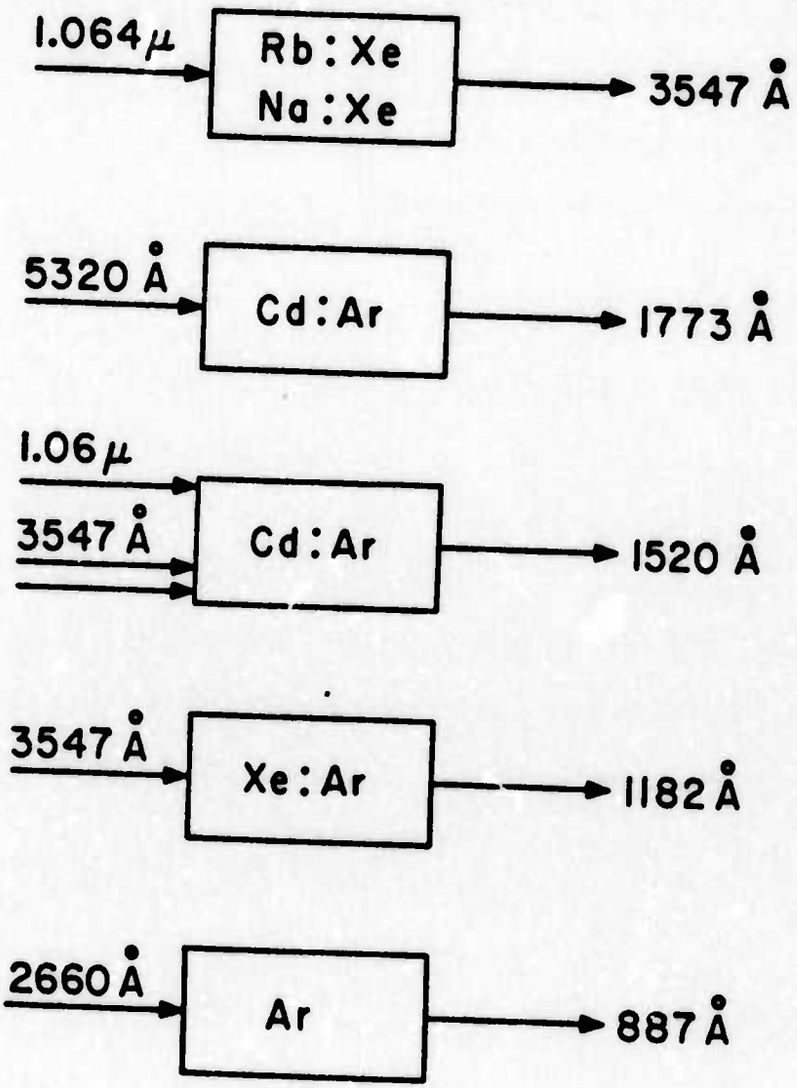

FIG. 1 --Summary of experiments for generation of vacuum ultraviolet radiation.

techniques for continuous circulating systems to allow dynamic mixing of these gases and more meaningful experiments. Unfortunately, this problem represents a set-back to some of our earlier plans for using high power radiation at 1182 Å to in turn generate soft x-ray radiation. Until the efficiency of the 1182 Å conversion process can be improved, or until we have at our disposal a higher power fundamental frequency driving laser, we will have to modify our plans and change to an approach not dependent on having very high power densities at 1182 Å. We note, however, that the aforementioned mixing problem should be solvable within several months, and might again allow us to proceed along the originally proposed route.

D. Soft X-ray Generation

A number of approaches are available to extend nonlinear optical techniques into the soft x-ray region of the electromagnetic spectrum. Options include: (1) the cascading of several efficient third-order nonlinear processes, for instance, $1.064\mu \rightarrow 3547$ Å $\rightarrow 1182$ Å $\rightarrow 394$ Å ; (2) the use of higher order nonlinear processes to allow direct conversion from ultraviolet frequencies to soft x-ray frequencies; and (3) the use of tunable laser techniques and resonantly enhanced nonlinear optical susceptibilities to obtain very high conversion efficiencies in relatively simple experimental arrangements. It should be noted that any nonlinear optical technique yields a beam having the same characteristics as the fundamental driving frequency. It is thus polarized, of picosecond time scale, and diffraction limited.

In recent months we have uncovered a tie between multi-photon ionization and nonlinear optical susceptibilities which leads to the prediction

of quite high conversion efficiencies, allowing that certain experimental conditions can be obtained. Without going into unnecessary detail, the gist of recent analyses is that the same atomic phenomena which leads to the multi-photon ionization of atoms also leads to the creation of higher order nonlinear optical polarizabilities. In a recent theoretical paper, we have shown that subject to the assumption that, first, the incident laser power density is bounded by multi-photon absorption to a non-allowed transition, and, second, the coherence length of the process is determined by an atomic level close to the generated frequency, that the conversion efficiency from incident laser power to harmonic power is given by $T_2/T_1\ (\mu_{ij}^2/\mu_{0j}^2)$. In this formula, T_2 and T_1 are the dephasing and decay times of the non-allowed transition, and μ_{ij}^2 over μ_{0j}^2 is a ratio of certain matrix elements which in typical atomic systems exceeds 10. Using typical values for T_2 and T_1 , we predict conversion efficiencies which are very high – in fact, in many cases, in excess of 100%. The key to obtaining these high conversion efficiencies is a tunable laser system which allows the sum of an even number of photons to be in coincidence with a non-allowed transition. Analysis shows that within certain limits the detuning for the non-allowed transition, and thus implicitly the linewidth of the pumping laser, does not enter into the predicted conversion efficiency. Larger detunings require larger power densities, but yield the same conversion efficiency. Also, again within certain limits, theory predicts that the same conversion efficiency should be obtainable irrespective of the order of the nonlinear optical susceptibility which is involved. Thus, again allowing for the existence of tunable high power radiation, it should be possible to do

direct efficient seventh harmonic or ninth harmonic generation. As part of our work on the forthcoming program, it will be necessary to develop high power tunable picosecond pulsed laser systems. Our general approach to this problem will be to start with a commercially available lower power source, at perhaps the 10 kW to 50 kW level and to pass this laser radiation through a picosecond pumped dye laser amplifier. By using this technique we expect that a peak tunable output power of at least 10 MW should be obtainable.

E. Holography in the Vacuum Ultraviolet

One of the interesting applications of short wavelength radiation is holographic microscopy of sub-micron specimens. Radiation generated by a nonlinear optical technique has approximately the same coherence properties as that of the fundamental frequency laser source, and should be immediately useful for recording high quality holograms. Our general approach to the microscopy problem is to record a far-field or Fraunhofer hologram of a small object onto a grainless photosensitive media, and then to use an electron microscope and computer techniques to read-out the hologram and reconstruct the object. Figure 2 shows the general approach for taking a Fraunhofer hologram. For sub-micron particles, the far-field distance may itself be very small, and spacings on the order of a micron between the object and the photosensitive surface are sufficient to place the object in the far-field. In the far-field the object does not cast a shadow and thus the focused illumination acts as both the object illumination wave and the reference wave. The input laser beam may be tightly focused, and an additional reference beam is not required. This technique also has

FRAUNHOFER – HOLOGRAM

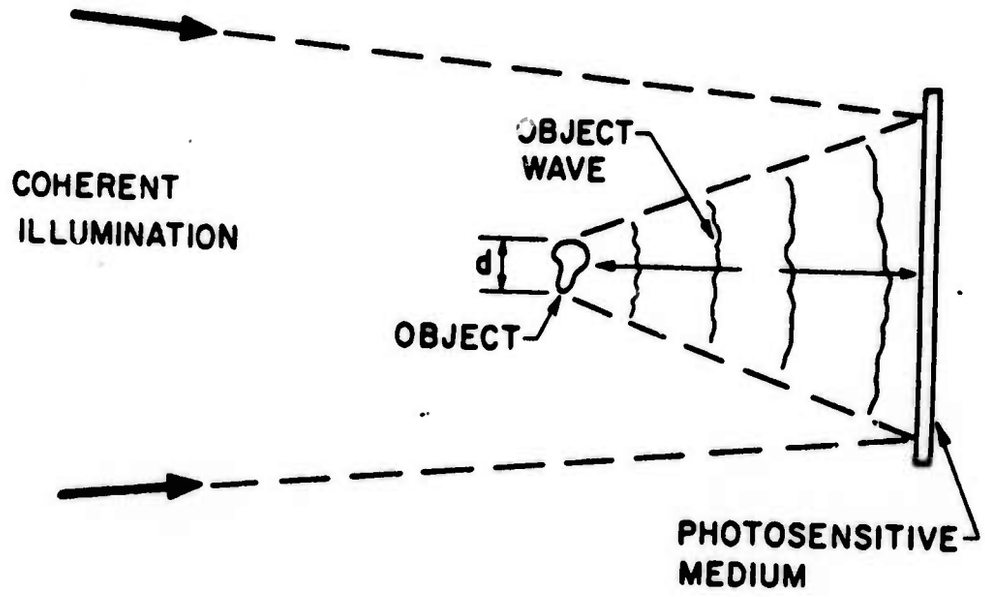

FAR FIELD DISTANCE = d^2/λ

$d = 1000\,\text{Å}$

$\lambda = 300\,\text{Å}$

FAR FIELD = $0.3\,\mu$

FIG. 2 --Schematic of holographic technique for application at soft x-ray wavelengths.

the advantage of not requiring large f-number high precision optics, or Fresnel lenses. As a first step in the holographic program, we have used the harmonically generated beam of 1182 Å radiation to construct a holographic grating on a polymethyl methacrylate (PMMA) substrate. To date, holographic fringes with a spacing of 836 Å have been constructed. Fringe construction of this type allows the spatial frequency response of different recordings to be examined and may also have application to sub-micron fabrication.

F. Inner-Shell-Depletion X-ray Lasers

One application for a coherent radiation in the vacuum ultraviolet is the construction of x-ray lasers operating on transitions between a normal outer state and a selectively depopulated inner shell. Although the population of the inner shell will be accomplished by selective multi-photon ionization, it may be shown that there exists a region of wavelengths in the vacuum ultraviolet that at sufficient intensity have a higher probability for photoionizing an inner electron than for an outer electron. Rough estimates indicate that a process of this type will only allow a generated frequency of about a factor of 3, and thus the output may have no practical advantage over that obtainable by the nonlinear optical techniques described previously. The scientific interest in this experiment would be in the construction of an early x-ray laser, and in the study of transition probabilities and lifetimes which would help to determine whether other techniques such as pumping with an x-ray flashlamp are worth further investigation.

G. Futu is

In summary, we will investigate a number of techniques which allow the generation of short wavelength laser radiation. During the start of the year principle effort will be concentrated on improving the efficiency of the 3547 Å to 1182 Å frequency converter. Depending on the success of this project, we will then proceed to generate higher harmonics using eicher 7 photons of 1182 Å to yield 168 Å in ionized Li^+, or, alternately, if sufficient 1182 Å has not been obtained, we will fall back to an easier experiment utilizing 2660 Å and ionized Rb. We will also continue analytical work which is now underway to delineate the limits of perturbation theory and in particular to show the effect of higher order frequency shifts on calculations which have thus far been performed. We will begin work on the resonant processes described previously with particular emphasis on obtaining high efficiency at lower incident power densities. This work may also have important application to visible laser techniques; for instance, it may lead to efficient up-conversion of broadband infrared signals into the visible. The holographic program described above will be continued with emphasis on holography of small objects. According to present plans, we are several weeks away from the first photograph of a 1000 Å object.

H. References

1. S. T. K. Nieh and S. E. Harris, "Aperture-Bandwidth Characteristics of the Acousto-Optic Filter," J. Opt. Soc. Amer. 62, 672 (May 1972).
2. A. H. Kung, J. F. Young, G. C. Bjorklund, and S. E. Harris, "Generation of Vacuum Ultraviolet Radiation in Phase Matched Cd Vapor," Phys. Rev. Letters 29, 985 (October 1972).
3. A. H. Kung, J. F. Young, and S. E. Harris, "Generation of 1182 Å Radiation in Phase Matched Mixtures of Inert Gases," Appl. Phys. Letters 22, 301 (March 1973).
4. R. B. Miles and S. E. Harris, "Optical Third Harmonic Generation in Alkali Metal Vapors," IEEE J. Quant. Elect. QE-9, 470 (April 1973).
5. S. E. Harris, "Generation of Vacuum Ultraviolet and Soft X-Ray Radiation Using High-Order Nonlinear Optical Polarizabilities," Phys. Rev. Letters 31, 341 (August 1973).
6. S. E. Harris, A. H. Kung, E. A. Stappaerts, and J. F. Young, "Stimulated Emission in Multiple-Photon-Pumped Xenon and Argon Excimers," Appl. Phys. Letters 23, 232 (September 1973).
7. S. E. Harris, J. F. Young, A. H. Kung, D. M. Bloom, and G. C. Bjorklund, "Generation of Ultraviolet and Vacuum Ultraviolet Radiation," Proceedings of the Laser Spectroscopy Conference, Vail, Colorado, June 1973 (to be published).
8. S. E. Harris and D. M. Bloom, "Resonantly Two-Photon Pumped Frequency Converter," (submitted for publication).

III. DETECTION OF X-RADIATION

C. W. Bates, Jr.

Associate Professor of Materials Science
and Engineering

A. Introduction

Sodium activated cesium iodide CsI(Na) is one of the most rugged, stable and efficient room temperature alkali halide scintillator materials to come along in recent years (1965). Its large x-ray stopping power relative to the other alkali halides, its high conversion efficiency (12%) at its emission maximum of 4200Å makes it an ideal detector of x-rays in conjunction with a photocathode surface, radiographic film or a photomultiplier tube. It has made x-ray sensing systems employing zinc sulphide or calcium tungstate almost extinct[1,2]. Its narrow spectral output when bombarded by particles in the mev. range makes it also an excellent nuclear particle detector[3,19]. In spite of its immense practical possibilities and current uses, little work has been done on determining the specific luminescent mechanism in this material. As experimental techniques become more refined, it is becoming increasingly obvious that many of the activated alkal-halides which were originally thought to be well understood, such as KI(TI) and KCI(TI) need to be re-examined[20]. Another reason for studying CsI(Na) is that in at least one way, it is a simpler system to study than the thallium activated alkali halides. In CsI(Na), the emission at 4200Å cannot be due to transitions between crystal field split levels of the sodium ion in the CsI host crystals because no such levels exist to give this emission. The luminescent mechanism can thus be due to a trapping of a center or complex, already existing in the crystal by the sodium ion, or the creation of a center or complex due to the introduction of the sodium. In the thallium activated materials, evidence exists that the emission is due to transitions between crystal field split states of the thallium ion as well as the center responsible

for the intrinsic emission in these crystals[20]. Thus CsI(Na) offers the unique possibility of studying centers responsible for the intrinsic emission in the alkali halides at temperatures higher than normally observed, without the complicating effects of other emissions.

B. Research Progress to Date

A measurement of the temperature dependence of the luminescent efficiency of CsI(Na) has suggested that the room temperature 4200Å emission is due to a radiative recombination of a trapped hole (V_k center) with an electron trapped nearby. This results from the following considerations. The luminescent efficiency of CsI(Na) under x-ray irradiation increases in a linear fashion, with increasing temperature from liquid nitrogen up to 80°C, after which it begins to decrease. This is somewhat unusual for activated phosphors which normally have the opposite temperature dependency of luminescent efficiency. At low temperatures, under ionizing radiation (x-rays, electrons, etc.), electrons and holes are formed in the intrinsic alkali halides. The free holes are spontaneously trapped to form a covalent bond between two adjacent halide ions (X_2 or V_k centers). The electrons can either recombine with V_k centers giving rise to the characteristic intrinsic emission or can be trapped at defects already present in the crystal or created by the radiation. Above a certain temperature, recombination at nonradiative sites becomes more probable and the efficiency begins to decrease. These trapping processes allow of the possibility to have stable V_k centers. Their number is a function of the concentration and of the efficiency of the electron traps. Lamatch et al.[21] have determined that electrons are trapped quite efficently by the sodium. We have previously observed structure on the absorption edge of CsI(Na) at room temperature which did not exist on the absorption edge for a pure crystal. The absorption edge itself is also shifted to longer wavelengths. In addition, we found that some severely

strained crystals of CsI gave identical emission spectra to crystals of CsI(Na). The absorption edge data suggests some experiments to be performed, whereas, the strained crystal results support the ($V_k + e^-$) radiative recombination mechanism. This is due to the presence of defects created by the strains that can trap the electrons. However, the nature of these traps is still nuclear. These preliminary experiments support our proposed mechanism of recombination of a V_k center with a trapped.

Our first sets of experiments which should be finished by the end of March, consist of looking at the structure on the absorption edge of CsI(Na), from liquid helium through room temperature for sodium concentrations of 0.01 - 0.3 mole percent. This should identify all of the absorption bands due to the sodium. Also, we plan to look at the emission and excitation spectra of CsI(Na) and CsI to determine which absorption bands give rise to emissions. We are planning to use a theory first advanced by F. Bassini and N. Inchauspé[22], to determine the position of these absorption bands in the tail of the fundamental absorption band. This calculation is in progress.

Experiments to follow these fundamental ones consist of observations of the degree of polarization of the V_k center emission after illumination with light to align the V_k centers along their molecular axes and ESR and ENDOR experiments to determine hyperfine interactions.

C. References

1. C. W. Bates, Jr. Adv. in Electronics and Electron Physics 28a, 545 (1969).

2. C. W. Bates, Jr. Applied Optics 12, 938 (1973).

3. R. Hofstader, Phys. Rev. 74, 100 (1948); 75, 976 (1949).

4. H. Kallmann, Phys. Rev. 75, 623 (1949).

5. E. C. Farmer, H. B. Moore, and C. Goodman, Phys. Rev. 76, 454 (1949).

6. C. E. Mandeville, and H. O. Albrecht, Phys. Rev. 80, 299 (1950).

7. R. Hofstader, J. A. McIntyre, and H. I. West, Phys. Rev. 82, 749 (1951).

8. M. Furst and H. Kallman, Phys. Rev. 82, 964 (1951).

9. J. Bonanomi and J. Rossel, Helv. Phys. Acta. 25, 725 (1952).

10. W. Van Sciver and R. Hoffstader, Phys. Rev. 87, 522 (1952).

11. B. Hahn and J. Rossel, Helv. Phys. Acta. 26, 271, 803 (1953).

12. J. Schenck, Nature 1711, 513 (1953).

13. A. W. Schardt and W. Bernstein, AEC Report BNL 1156 (1953).

14. F. S. Eby and W. K. Jentschtke, Phys. Rev. 96, 911 (1954).

15. W. Van Sciver and R. Hofstader, Phys. Rev. 97, 1181 (1955).

16. W. Van Sciver IRE Trans. on Nucl. Sci. NS-3, 39 (1956).

17. W. Van Sciver and L. Bogart, IRE Trans. on Nucl. Sci. NS-5, 90, (1958).

18. W. Van Sciver, Phys. Rev. 120, 1193 (1960).

19. F. S. Mozer, E. Bogott, and C. W. Bates, Jr., IEEE Trans. on Nucl. Sci. NS-15, 144 (1968).

20. J. Donahue and K. Teegarden, J. Phys. Chem. Solids 29, (1968).

21. H. Lamatsch, J. Rossel, and Saurer, Phys. Stat. Sol. 41, 605 (1970); ibid 46, 687 (1971; ibid 48, 311 (1971).

22. F. Bassani and N. Inchauspé, Phys. Rev. 105, 819 (1957).

IV. SUPERPLASTICITY AND WARM WORKING OF PLAIN HIGH CARBON STEELS

O. D. Sherby

Professor of Materials Science
and Engineering

J. C. Shyne

Professor of Materials Science
and Engineering

and

C. M. Young

Research Associate, Materials Science
and Engineering

A. Introduction

During these past six months we have been engaged in the development of high carbon steels (from 0.8 to 1.9%C) containing the second phase, Fe_3C, in the form of spheroids dispersed in a ductile α-Fe matrix. Since most steels contain carbon in the range 0.2 to 0.3 percent these high carbon materials are a clear departure from the nominal compositions used for structural steels and are approaching carbon compositions commonly thought of as cast irons. Yet the results already obtained in this study suggest that a whole new class of inexpensive structural steels with excellent strength and formability can be produced by unique combinations of thermal-mechanical processing, with the key step being warm working. [We define warm temperature to be in the range 0.35 - 0.65 T_m, where T_m is the absolute melting temperature of the material]. The warm range of temperature is important for the following reasons: (1) The atomic diffusivity is high enough so that microstructural changes are rapid compared to low temperature; (2) The deformation stresses are relatively high so that fine spheroidized cementite (Fe_3C) microstructures result [previous work has shown that fine spheroidized structures are produced at high stresses[1,2]]; (3) The ductility is sufficiently great at warm temperatures so that the fairly large strains necessary to produce homogenous microstructures are possible before fracture; and (4) There is no recrystallization due to a phase transformation on cooling from warm working temperature to ambient temperature.

The research to date has focused on two main areas of investigation. In the first area, we have attempted to optimize the ambient temperature properties of high carbon steels after various elevated temperature thermal-mechanical treatments. The goal here is to produce a

material with both a high yield strength and good ductility. The second area of research has been an attempt to optimize the fabrication characteristics of these high carbon spheroidized structures. The hope here is to develop true superplasticity in such simple, inexpensive materials after appropriate processing at warm temperature.

B. Ambient Temperature Properties

Our earlier warm working studies have lead to the development of ultra fine spheroidized structures in eutectoid composition steel[1,2] of commercial purity (grain size ≃ 0.5 microns and particle sizes considerably smaller than 0.1 microns). Such materials were shown to exhibit ambient temperature yield strengths in the order of 150 to 180 ksi. The tensile ductility of the fine spheroidized material, however, was fairly low (about 2 to 4% elongation). In order to determine if the impurity content played an important role in obtaining such low ductility, we obtained, and are now studying, a high purity eutectoid composition steel (Fe - .8%C). In the following paragraphs we describe some of the results obtained in the past six months on this material.

Fine spheroidized structures have been obtained in the high purity eutectoid composition steel after warm rolling the pearlitic structure at 550°C to a true strain of $\varepsilon = 2.0$. The warm rolled structure consisted of fine spheroidized particles of Fe_3C(≃ 0.45μm in size) with a high dislocation density. At room temperature, this material exhibited 127 ksi yield strength and 12% true strain to fracture as shown by curve I in Figure 1.

To improve the ductility low temperature annealing treatments (500°C for 100 hrs) were performed on the warm rolled material. This annealing increased the ductility to 27.5% true strain while the yield stress dropped to 93 ksi (curve II Figure 1). This reduction in flow stress apparently resulted from the annihillation of dislocation tangles within subgrains. Particle coarsening or subgrain growth did not occur during this annealing treatment.

To improve further the ductility of the annealed material, cold

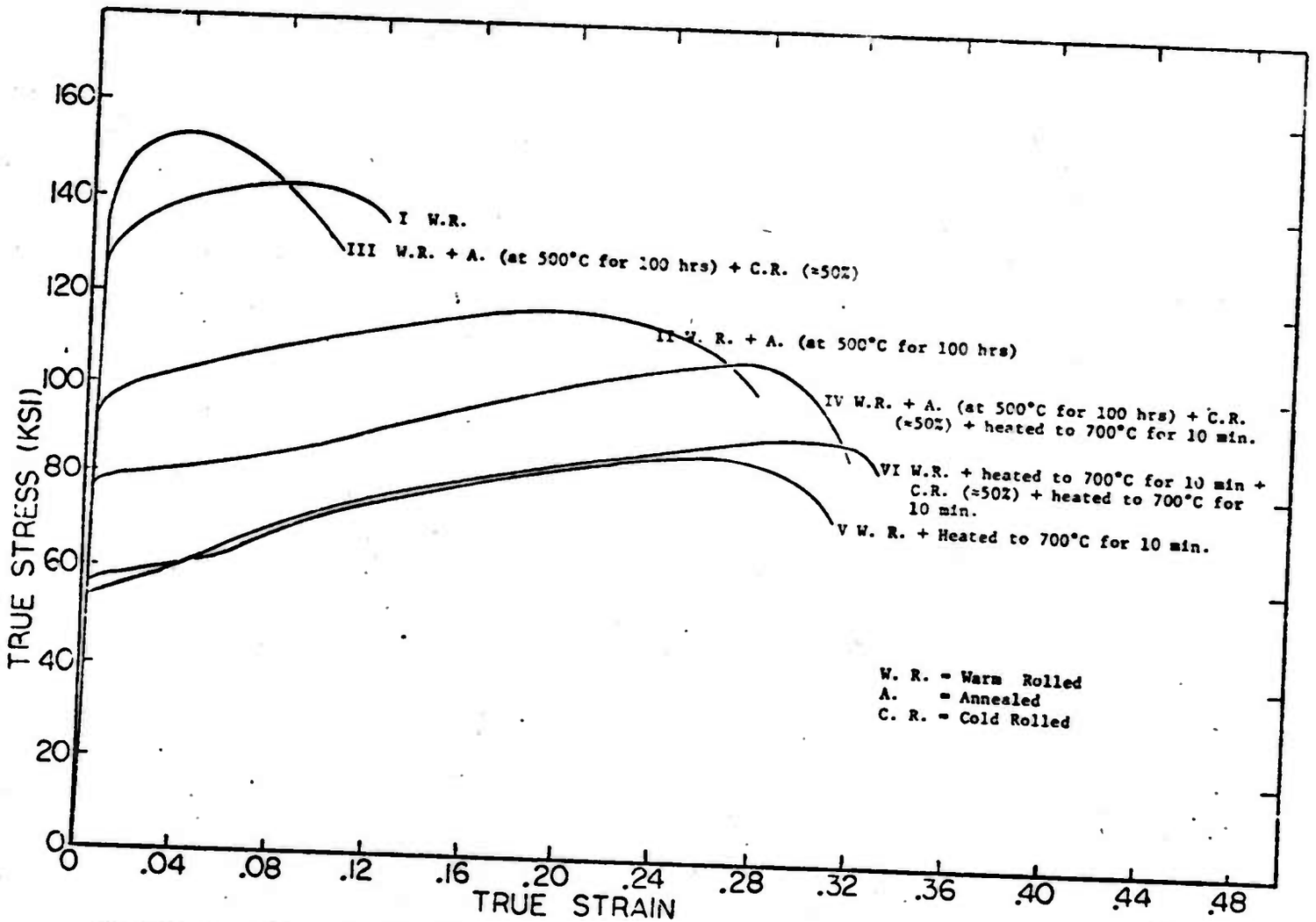

Figure 1. True stress-true strain curves for the high purity eutectoid composition steel at room temperature following the various processing histories indicated. The high yield strengths and excellent ductility of this material suggest many possible structural applications. All tests were performed in tension.

rolling followed by a heat treatment for recrystallization was performed. Cold rolling was done at room temperature up to 50% reduction in area and the recrystallization anneal heat treatment was performed at 700°C for 10 minutes. The cold rolled material exhibited 138 ksi yield strength and 10.5% true strain to fracture at room temperature (curve III Fig. 1). These results show that the material is still ductile after cold rolling to 50% reduction in area and has a high yield strength. After the heat treatment of this cold rolled material at 700°C for 10 minutes, the material exhibited 77 ksi yield strength and 31.5% true frcature strain at room temperature (curve IV Figure 1).

The (warm rolled), (warm rolled + annealed) and (warm rolled + annealed + cold rolled + heat treated at 700°C for 10 minutes) materials all exhibited fairly high yield strengths, a very low strain hardening rate, and very high ductility. After the 500°C anneal, the particle size did not change appreciably as observed by transmission electron microscopy but after the final heat treatment at 700°C some particle coarsening was observed.

Another thermal-mechanical process was investigated for the high purity eutectoid composition steel involving direct heating to 700°C for 10 minutes after warm working. This was done to reduce the dislocation density within subgrains to allow greater strain hardening during cold rolling. It was hoped that heating followed by cold rolling 50% and reheating to 700°C again for 10 minutes would induce recrystallization. The ambient temperature stress-strain curves for each step are shown by curves V and VI in Fig. 1. The intent of this treatment was to produce a recrystallized fine grain size material containing high angle boundaries while retaining the fine spheroidized carbides. Although this last thermal-mechanical treatment resulted in the weakest ambient temperature material it was hoped that it would produce the high angle grain boundaries necessary for developing superplastic characteristics at elevated temperature (this subject will be discussed in the next section). Thus far, we are not certain that the grain boundaries created during high temperature annealing are indeed

high angle.

Commercial foundry castings of Fe-1.3%C, Fe-1.6%C and Fe-1.9%C have been obtained for the warm working studies. In addition we are attempting to obtain high purity heats of the 1.3%C and 1.9%C steels because of the marked influence of impurities on the mechanical properties, principally ductility, found in the Fe-0.8%C steels. We have sucessfully warm rolled billets from each of the commercial purity high carbon steels by various thermal-mechanical processes. All of the alloys, even the 1.9%C, are remarkably ductile during warm rolling once the lamellar Fe_3C begins to spheroidize which is very exciting because it indicates that these materials will have good formability. Microstructures of the Fe-1.6%C and Fe-1.9%C steels are shown in Figure 2 in the as-cast condition and after warm working. The spheroidization of the cast structure is nearly complete with a homogeneous distribution of spheroids for the 1.6%C. However, in the case of the 1.9%C steel the spheroidization is incomplete and fairly inhomogeneous. This seems to be the result of the much larger regions of massive cementite in the 1.9%C casting compared to the lower carbon castings and may require greater strain during warm rolling to completely spheroidize the cementite. We are greatly encouraged by the high temperature formability of the 1.9%C alloy, however, since this composition borders on that composition region commonly thought of as cast iron. Our results suggest that investigations into the spheroidization of white cast irons by warm working may be very worthwhile pursuing. The interparticle spacing for a given volume fraction of Fe_3C can be varied by changing the warm working temperature, strain rate and strain as well as the thermal-mechanical history prior to warm working. We are exploring several of the most promising thermal-mechanical treatments to evaluate the effect of each of the variables on both the microstructure and mechanical properties for these alloys.

The most promising combination of mechanical properties has been obtained in the 1.3%C alloy; Figure 3 shows the true stress-true strain curves for this alloy following warm working at 565°C (1050°F) and after

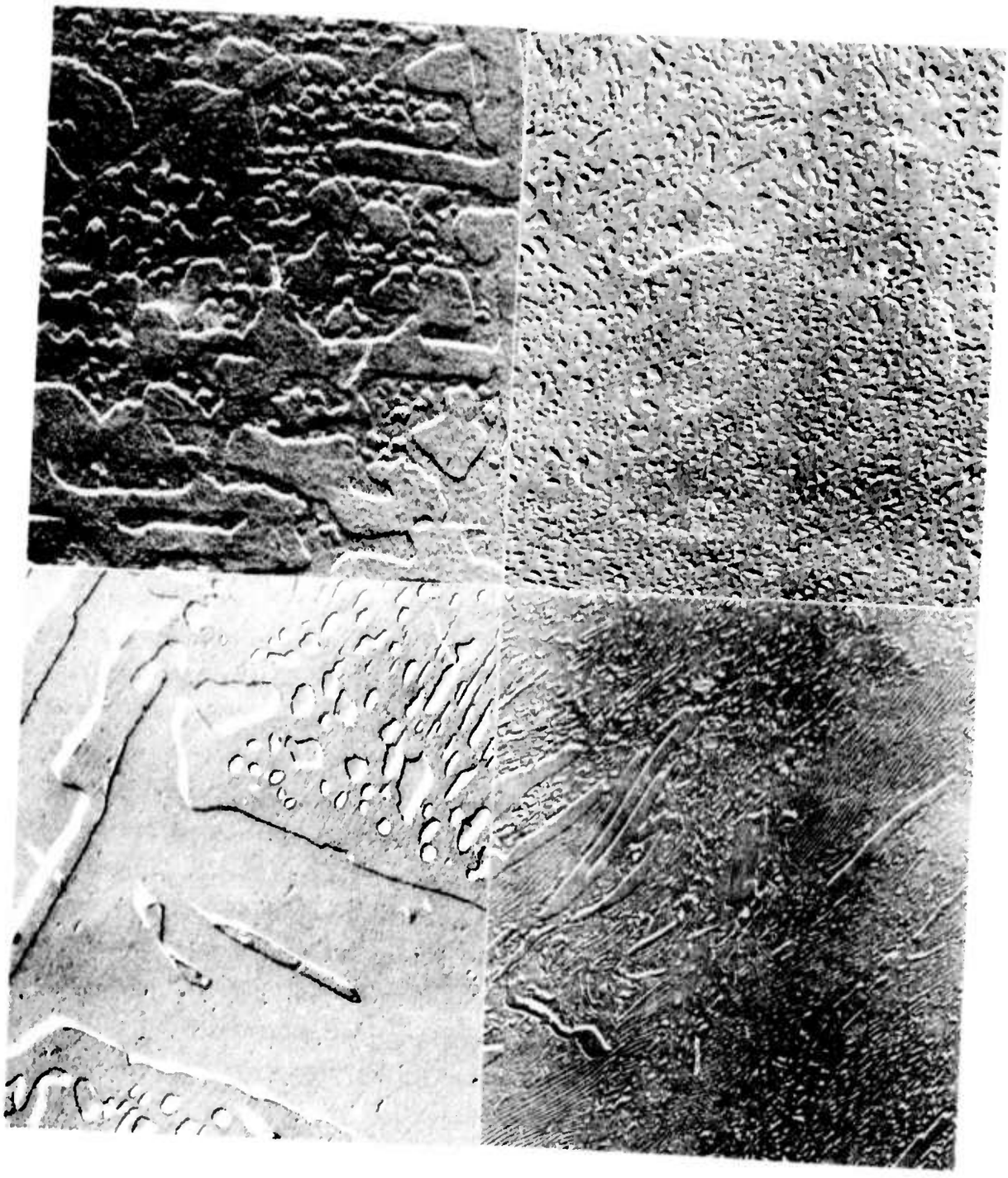

Figure 2. Carbon replica transmission electron micrographs of the high carbon steels. Top left, 1.6%C as-cast; top right 1.6%C after warm working; bottom left, 1.9%C as-cast; bottom right 1.9%C after warm working. (3750M)

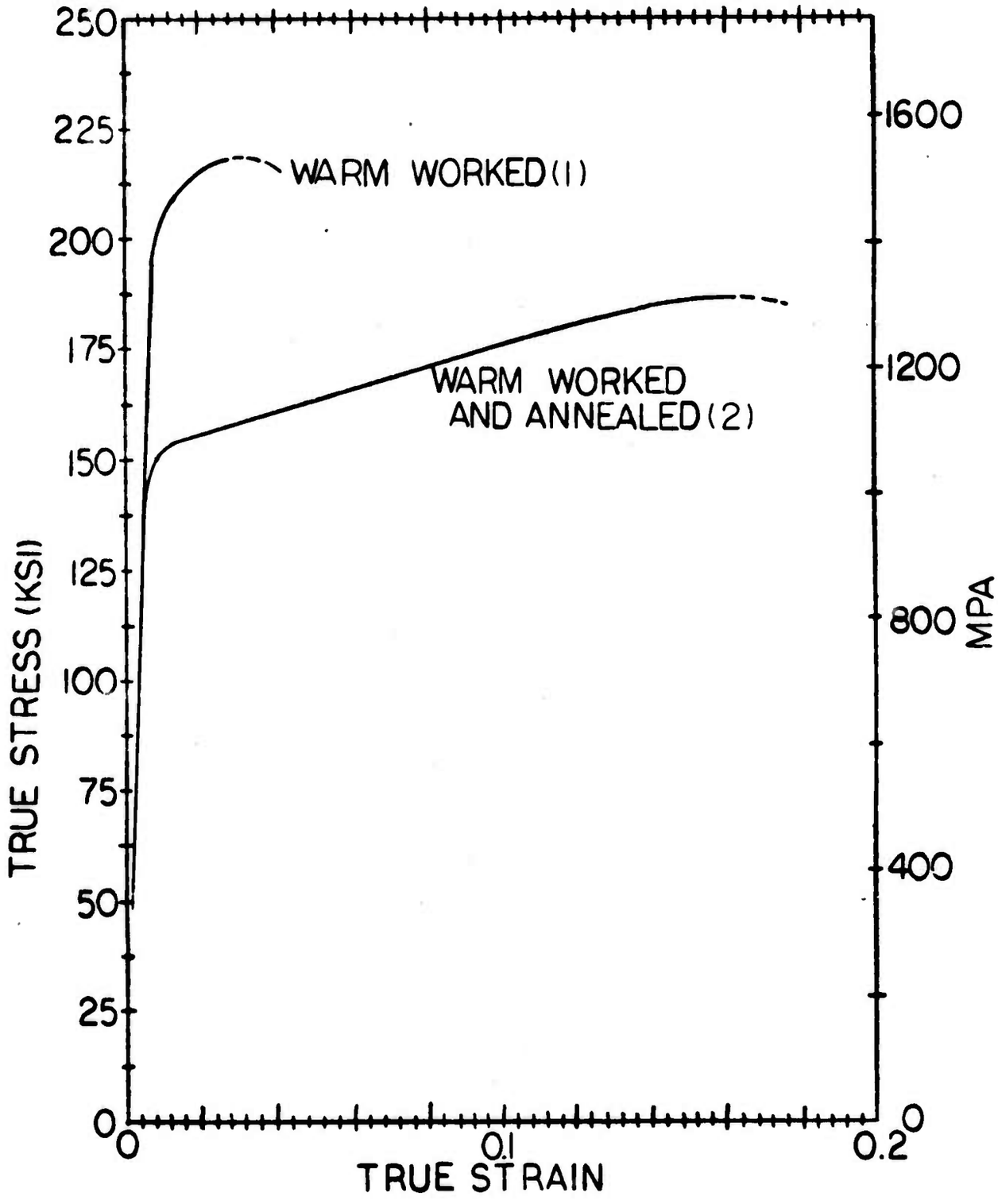

Figure 3. True stress-true strain curves for the Fe-1.3%C alloy at room temperature[1] after warm working at 565°C (1050°F) and (2) after annealing following warm working.

a subsequent annealing treatment (650°C for 20 min). The as-warm worked material has a yield strength about 195,000 psi, a 215,000 psi ultimate tensile strength, and 4% tensile elongation which is a very attractive combination of properties. The ductility can be improved by annealing with a resultant decrease in the yield strength as shown by the second curve in Figure 3. We believe that even more attractive mechanical properties can be obtained from not only this 1.3%C alloy by optimizing the warm working parameters but from the 1.6 and 1.9% carbon alloys where the amount of second phase is increased. We have successfully rolled plates of the 1.6%C steel and produced a uniform fine dispersion of spheroidized Fe_3C by a warm working technique. As warm rolled, the material is not ductile at room temperature (as determined by bend tests). However, following a similar annealing treatment to that used on the 0.8%C steel, the material is quite ductile (>6% bend ductility) at room temperature. We are presently machining tensile specimens for more precise ambient temperature evaluation of the microstructure developed during these rolling experiments.

The first rolling experiments on the 1.9%C steel (Figure 2, bottom) did not result in complete spheroidization of the Fe_3C but did indicate good formability at warm working temperature. This 1.9%C structure was very brittle at room temperature, possibly due to a very poor casting structure.

The above results reveal the wide range of properties we have been able to obtain in a plain carbon steel by various thermal-mechanical processing treatments. We are currently attempting to relate the properties obtained to the corresponding microstructure especially as assessed by transmission electron microscopy.

C. Elevated Temperature Formability Investigation (Superplasticity)

The second area of interest in this investigation is the behavior of these warm worked structures developed in the high carbon steels (as a result of warm working) when reheated the deformed at slow strain rates. We have studied the potential superplastic characteristics of our fine spheroidized eutectoid composition (0.8%C) steel at elevated temperature.

The results obtained to date look promising and elongations in the order of 100 to 160% have been obtained in the temperature range 600 to 700°C (Figure 4). These elongations are in fact the highest of any reported to date on isothermal testing of Fe-C alloys[3,4]. The stress exponent, n, (in $\dot{\varepsilon}|_T = k\sigma^n$) was found to be about 3 to 3.5 between 650 and 700°C whereas superplastic materials typically exhibit n = 2[5,6].

A comparison of the strength of the fine spheroidized steel with that of pure iron is given in Figure 5. The comparison is made by plotting the diffusion compensated strain rate, $\frac{\dot{\varepsilon}}{D}$, against the modulus normalized stress, $\frac{\sigma}{E}$. The pure iron data is from Watanabe and Karashima[8] and the modulus data from Köster[9]. As can be seen, at low values of the diffusion compensated strain rate, the eutectoid composition steel is only about a factor of two stronger than pure iron. On the same graph (Fig. 5) we have also plotted some limited data on the strength of the high purity eutectoid composition steel warm worked to yield a fine spheroidized structure. It is of interest to note that this material is almost as weak as pure iron at low stresses; we would wish to attribute this behavior to the fine grain size present in the high purity eutectoid composition steel (g.s. ≃ 5 microns). The higher strength of the commercial purity 1080 steel than that observed in the high purity eutectoid steel must be attributed to the presence of impurities such as Mn, Si and Cu. Of interest to note, however, was that the tensile ductility of the pure spheroidized steel was not higher than that observed in the commercial grade material (~120 percent elongation to fracture).

In Figure 5, the values of the strain rate and stress at 700°C are given on the right hand and top portions of the graph respectively. An important observation to note is that at high strain rates at 700°C the resistance to plastic flow is only in the order of 30,000 psi. This would suggest that, even at high forming rates, the power consumption in shaping such fine spheroidized materials would not be very high.

A factor which may have prevented attainment of a superplastic state in our studies of the fine spheroidized steel (0.80 wt. percent carbon)

Figure 4. Tensile specimens of 1080 steel. Top, undeformed sample. Bottom, deformed specimen at 650°C, $\dot{\varepsilon} = 1.11 \times 10^{-4}$/s to about 160% elongation ($\varepsilon = 0.96$). A second neck can be observed just to the left of the fracture. The formation of multiple necks is often found in materials with a high strain rate dependence of the stress.

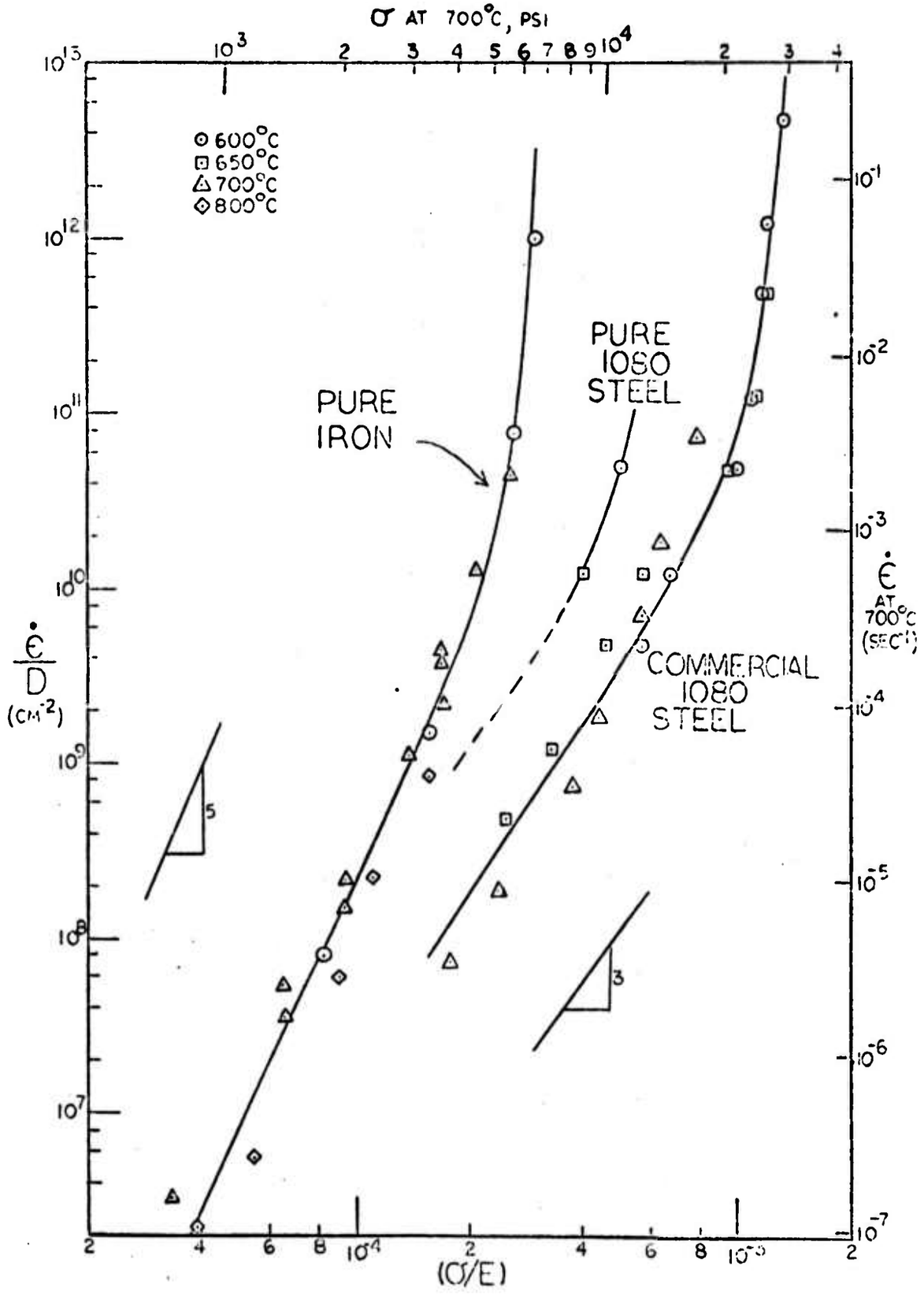

Figure 5. A comparison of the high temperature strength of a commercial grade and a high purity fine spheroidized 1080 steel with that of pure iron. The strain rate is compensated by the diffusivity and the applied stress is compensated by the modulus to allow comparison to be made at different temperatures.

is that a fair amount of subgrain growth occurred during elevated temperature testing. Deformed samples revealed grain sizes in the order of 3-5 microns in contrast to the original 0.5 micron subgrain size. We believe we can produce and stabilize a fine grain size by the presence of a higher concentration of cementite than exists in a eutectoid composition steel. Most superplastic materials consist of two phases with the second phase generally in excess of 20 to 30 percent by volume[10,11]. With this observation in mind, we have prepared high carbon steels containing, 1.3, 1.6 and 1.9 weight percent carbon. The material will be warm worked in the gamma as well as in the ferrite range to develop a fine spheroidized structure. In this manner, the cementite content will be varied from 12.5 to 29 percent by volume. Such materials should have more promising high temperature superplastic properties than those obtained earlier from our eutectoid composition steel if the low angle subgrain boundaries present after warm working can be replaced by high angle grain boundaries. We therefore propose to take our warm worked and annealed fine spheroidized high carbon steels and cold work them at room temperature. After cold working, the material will be recrystallized in the ferrite range, with the expectation that high angle bounlaries will form. The recrystallized material will be studied for its superplastic tendency at high temperatures as well as for its low temperature tensile characteristics as was done on the eutectoid composition steel.

D. References

1. M. J. Harrigan, L. Chamagne, C. Sauve and O. D. Sherby, Transactions Quarterly, ASM, 62, (1969) 575.
2. M. J. Harrigan and O. D. Sherby, Materials Science and Engineering, 7, (1971) 177.
3. A. R. Marder, Trans. AIME, 245, (1969) 1337.
4. G. R. Yoder and V. Weiss, Met. Trans., 3, (1972) 675.
5. H. W. Hayden, R. C. Gibson, H. F. Merrick and J. H. Brophy, Transactions, ASM, 60, (1967) 3.
6. A. Ball and M. M. Hutchison, Metal Science Journal, 3, (1969) 1.
7. O. D. Sherby and P. M. Burke, Progress in Materials Science, 13 (1968) 325.
8. T. Watanabe and S. Karashima, Metallurgical Transactions, 2, (1971) 1359.
9. W. Köster, Z. Metallkunde, 39, (1948) 1.
10. R. H. Johnson, Metallurgical Reviews No. 146, September 1970 (Metals and Materials, 4, (1970) 115.
11. O. D. Sherby, Science Journal, 5, (1969) 75.

V. SUPERPLASTICITY OF Pb-Sn AND Pb-Sn-Au ALLOYS

C. R. Barrett

Associate Professor of Materials Science
and Engineering

and

A. E. Geckinli

Research Associate of Materials Science
and Engineering

This portion of the investigation has been concerned with two aspects of superplastic flow in Pb-Sn eutectic alloys. First, the influence of a fine precipitate distribution on superplastic flow and fracture is being investigated. The second and related aspect of the study is the possibility of strengthening the normally soft superplastic alloys by a precipitation heat treatment. This would be useful for improving the strength properties of superplastic materials following forming treatments.

To date, the majority of experiments have been carried out on the Pb-Sn-Au system. The alloy composition is the Pb-Sn eutectic composition with about 0.1% Au. Samples are melted, cast, and then cold rolled to produce an equiaxed grain structure, with average grain size of 3μ. Aging the alloys in the temperature range 120 - 160°C prior to cold rolling causes $AuSn_4$ precipitation with an average precipitate spacing of about 0.1μ. The flow properties of these alloys are being evaluated using stress relaxation techniques, tensile tests, and carrying out dynamic studies in the scanning electron microscope using a special tensile stage. The results obtained thus far are listed below.

Stress relaxation tests have been carried out at room temperature over a range of relaxation rates (strain rates) of 10^7. The data for pure Pb-Sn and Pb-Sn-Au (aged for a variety of times at 120° or 160°C) show similar characteristics. Namely, at low relaxation rates (low stresses) Newtonian viscous deformation is observed (directional diffusion creep) and the flow stress is increased the dominant deformation mode is grain boundary sliding and superplastic flow is observed. At high stresses recovery-work hardening creep associated with the generation and motion of dislocations is observed. At low stresses the Pb-Sn and Pb-Sn-Au data superimpose whereas in the superplastic flow region and recovery work hardening creep region the Pb-Sn-Au samples have a flow stress about twice the Pb-Sn samples at the same strain rate. Although the flow stresses differ, the maximum strain rate sensitivity is the same for the two alloys, being about 0.33-0.4. This strengthening of the Pb-Sn-Au precipitate hardened alloys in the superplastic flow region does not result in any noticeable change in the

mechanism of plastic flow. The scanning electron microscope date suggest that the predominant deformation moue is grain boundary sliding for both alloys. The only grain deformation observed is localized to the region of the grain boundaries and is associated with the preservation of coherence between grains.

The origin of the increase in the flow strength of the Pb-Sn-Au alloys is as yet undefined. Two possibilities are (1) a slight change in diffusivity with addition of Au to the Pb-Sn alloy and (2) an influence of the $AuSn_4$ precipitates on the accomodation deformation accompaning grain boundary sliding. The weak stress dependence of the strain rate during superplastic flow means that a small change in diffusion coefficient will be translated into a similar magnitude change in flow stress at constant strain rate. That is, if the diffusion coefficient were to change by a function of three, we could expect to see a two-fold or so change in flow stress. The second possibility listed above relates to the influence of the $AuSn_4$ precipitates on the plastic deformation which must accompany grain boundary sliding if grains are to maintain coherency. The acommodation deformation may take place either by diffusional flow or grain boundary sliding. There is considerable data in the literature to suggest that a fine distribution of precipitates or dispersed particles may alter the local flow characteristics for either of these flow conditions. Present work is directed to examining the various possibilities listed above.

One further aspect of the study involves the influence of $AuSn_4$ precipitates on the fracture properties of Pb-Sn-Au alloys. It is observed that the total strain to failure is lower in the precipitation hardened alloys (about two or three times less than that observed for Pb-Sn alloys tested under identical conditions). Scanning electron microscope studies to date indicate considerable porosity generation in the Pb-Sn-Au alloys during superplastic flow. This feature probably accounts for the decreased ductility. Work is underway to establish the cause of this porosity and determine what influence it may have on the formability of the Pb-Sn-Au alloys.

VI. SYNTHESIS OF NEW TYPES OF CATALYST MATERIALS

J. P. Collman
Professor of Chemistry

and

M. J. Boudart
Professor of Chemical Engineering
and Chemistry

A. Introduction

The following three individual research reports encompass research done in J. P. Collman's laboratory under collaborative supervision by Michel Boudart and is concerned with the preparation and study of hybrid heterogeneous-homogeneous hydrogenation catalysts. The initial stage of this project has addressed several problems: the synthesis of silated ligands and their transition metal complexes, methods for attaching these silated homogeneous catalysts to porous silica, studies of the reactivity of the resulting catalysts by kinetic analyses and physical studies of these substances by electron microscopy.

The first and longest report is by Makoto Takeda, who was visiting Stanford from the Mitsubishi Chemical Company. Takeda prepared a series of silated ligands and their transition metal complexes. Using an atmospheric pressure apparatus for determining the kinetics of catalytic hydrogenation, Takeda established a reproducible and well behaved rate law for these reactions and made comparisons between these catalysts and a traditional commercial rhodium on alumina. Future work will include studies of rhodium on silica as this should make a better comparison.

Marrocco attempted to reproduce Takeda's results and; although this reports suggests difficulties in reproducing these active catalysts, most recent studies (since December 1 and therefore not included in this six month report) demonstrate that the same active catalysts can be produced and that the problem with inactivity stems from peroxide impurities in the olefins which were employed. Marrocco's electron microscopy studies

suggest the presence of metal crystallites in these new catalyst systems and raise a serious question concerning the actual structure of the active catalysts. We intend to address ourselves to this question by examining substrate reactivities, the effect of low levels of poisoning, and the use of chiral ligands. Initial synthetic studies of chiral ligands are included in Takeda's report.

Howard Heitner (a postdoctoral who has gone to work at the DuPont Photo Products Laboratory) has described some sulfur bearing hybrid catalysts. His report emphasizes substrate reactivity patterns as criteria for differentiating classic heterogeneous catalysts from the new hybrid homogeneous-heterogeneous catalysts and provides preliminary evidence suggesting the presence of homogeneous analogues in his systems.

In its present state the principal investigators do not consider that this work is in a final publishable form since major questions remain to be answered. Future work will be directed toward the areas of selective catalyst poisoning, the use of chiral ligands, substrate reactivity studies, and the synthesis of chelating silated ligands (these should render the hybrid catalysts more stable towards the formation of metallic aggregates). During this time, we shall also begin to study conducting surfaces as a preclude to our eventual work on electrochemical catalysis. Before that work can be carried out, we must have firmly in hand well established methodologies for preparing hybrid homcgeneous-heterogeneous catalyst materials.

B. Preparation and Characterization of Hybrid Homogeneous-Heterogeneous Catalyst Materials:. I. Synthesis and Catalytic Activity

M. Takeda

Introduction

In the past few years supported metal complexes have attracted attention as potential catalysts, as means of studying the comparisons of homogeneous and heterogeneous catalysts, and as models for enzyme systems.[1-4]

Attempts to use polystyrene (Biobeads SX-2) and silica gel (Cabosil HS-5) as supports have been studied in the Collman group[2, 5-8]. Biobeads SX-2, polystyrene-2% divinylbenzene copolymer have been found to be mobile enough to allow ligands attached to the polymer to act as chelates (eq. 1-1)[2, 5]. However, Grubbs and his co-workers[3] reported there is much less chelation, i.e., less mobility of the polymer structure in the 20% crosslinked than in the 2% crosslinked copolymer. Using the 20% crosslinked polystyrene they have found the effectiveness of the polymer-attached $(C_2H_5)_2TiCl_2$ as a catalyst for hydrogenation of olefins is enhanced by a factor of about six over the correspondingly reduced titanocene dichloride or benzyltitanocene dichloride (eq. 1-2).

The use of silica gel as a support has been reported by Deuel, et. al.[9] Working with silica gel having 22.5 mμ diameter and 150 m^2/g surface area they obtained 0.32 meq/g of OBu by the reaction of chlorinated silica gel with n-butanol in the presence of a base (eq. 2-1). The problems with

Scheme I.

Functionalization of Polystyrene

1-1 Collman, et. al., 1972

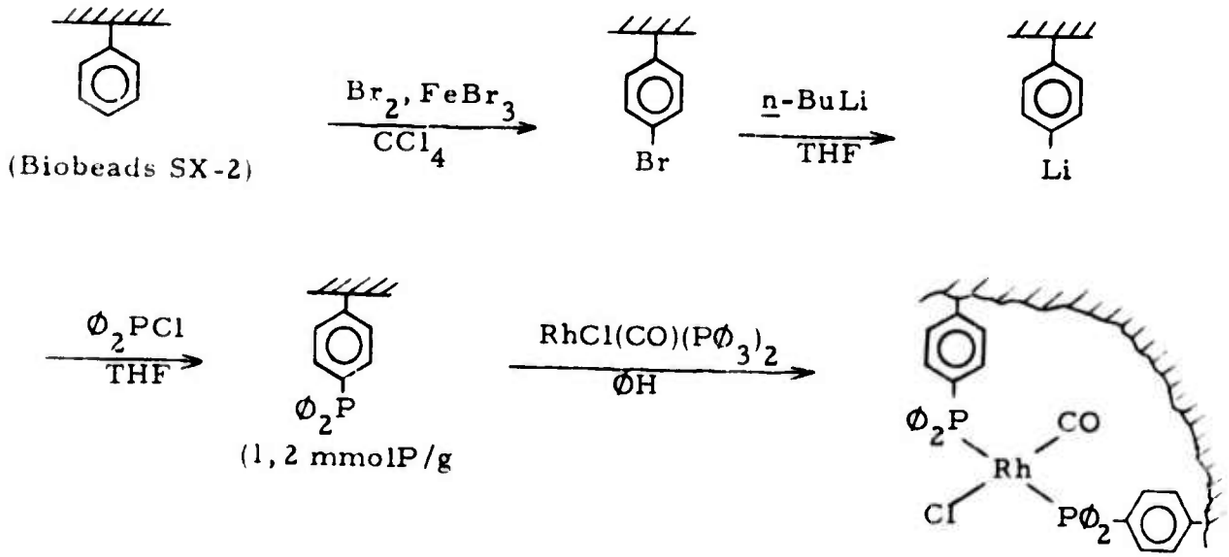

1-2 Grubbs, et. al., 1973

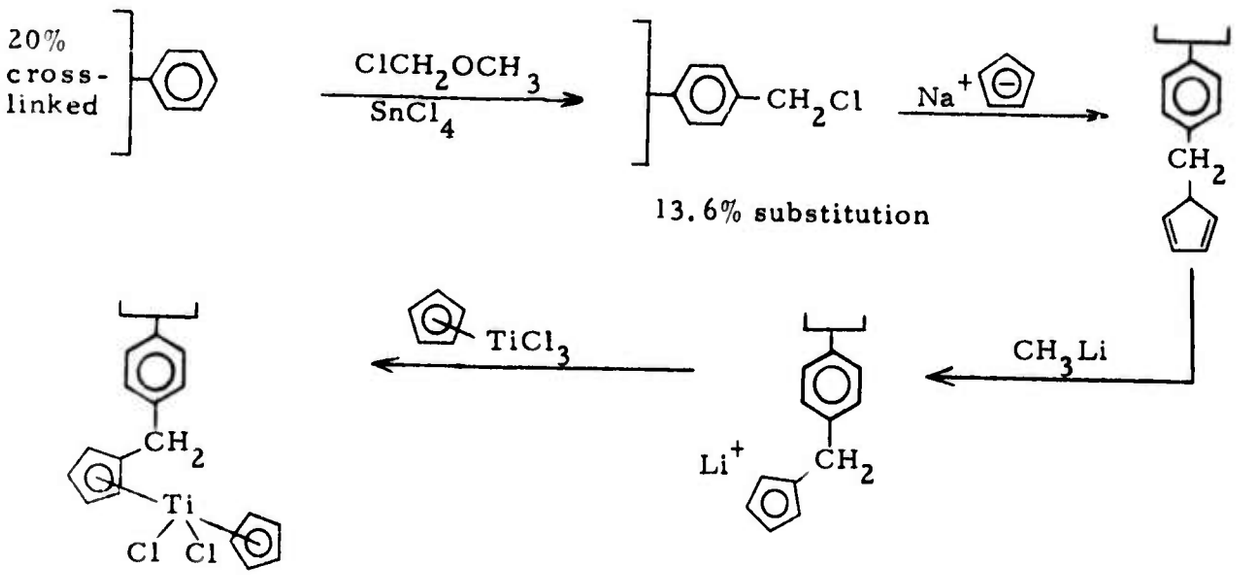

Scheme II.

Functionalization of Silica

2-1. Deuel, et. al., 1959

$$\equiv SiOH + SOCl_2 \xrightarrow[\Delta]{\emptyset H} \equiv SiCl + SOCl_2 + HCl$$

$$\equiv SiCl + \underline{n}\text{-}BuOH \xrightarrow[\Delta]{Base} \equiv SiO\text{-}\underline{n}Bu + HCl.base$$

2-2. Parr and Grohman, 1971

$$\equiv SiOH + Cl_3Si\text{-}C_6H_4\text{-}CH_2Br \longrightarrow \equiv SiO\underset{|}{Si}\text{-}C_6H_4\text{-}CH_2Br$$

(porous glass) (0.08 meq Br/g)

$$\equiv Si\text{-}O\text{-}Si\text{-}C_6H_4\text{-}CH_2Br + LiPPh_2 \longrightarrow \equiv Si\text{-}O\text{-}\underset{|}{Si}\text{-}C_6H_4\text{-}CH_2PPh_2$$

2-3. Allum, et. al., 1972

$$\equiv SiOH + (EtO)_3SiCH_2CH_2P\emptyset_2 \xrightarrow[\Delta]{Toluene} \equiv SiO\underset{|}{Si}CH_2CH_2P\emptyset_2$$

(1.0-1.4 wt%P)

the approach are (1) the hydrolytic instability of the Si-O-C linkages formed and (2) the removal of the base-HCl salt from the silica gel[6].

The approach to get hydrolytically stable Si-C bonds has been developed by Parr and Grohman[10]. Their approach is to react $R\text{-}SiCl_3$ with the silanol groups on the glass surface (Bio-Glass 2500) forming $\equiv Si\text{-}O\text{-}S\text{-}R$ (eq. 2-2).

This report is concerned with the synthesis of the attached complex catalysts on silica gel (Cabosil HS-5 and Grace 62) and their catalytic reactions, primarily hydrogenation of olefins and benzene.

Results and Discussion

1. Syntheses of Supported Rhodium Complexes

Scheme III shows the preparation of the silated phosphine ligands. The reactions proceeded by irradiation of an equimolar mixture of diphenylphosphine and vinylsilanes under mild conditions and produced no observable side products (by nmr). The products were isolated by fractional vacuum distillation (yield 81 ~ 83%).

Scheme III.

Preparation of Silated Phosphine Ligands

$$C_2H_5O\overset{\overset{CH_3}{|}}{\underset{\underset{CH_3}{|}}{Si}}-CH=CH_2 \xrightarrow[r.t.,\ 40\ hr.]{HP\phi_2,\ h\nu} C_2H_5O\overset{\overset{CH_3}{|}}{\underset{\underset{CH_3}{|}}{Si}}CH_2CH_2P\phi_2 \equiv L \qquad (3)$$

1a (81%)
colorless liq.
bp 136-138°/0.13mm

$$(C_2H_5)_3OSi-CH=CH_2 \xrightarrow[r.t.,\ 48\ hr]{HP\phi_2,\ h\nu} (C_2H_5)_3SiCH_2CH_2P\phi_2 \equiv L^* \qquad (4)$$

1b (83%)
colorless liq.
bp 130-132°/0.05 mm

Scheme IV shows the preparation of several rhodium complexes with silated phosphine ligands. The dimer $[Rh(CO)_2Cl]_2$ reacted readily with the silated phosphines to form the phosphine carbonyl chlorides [LRh(CO)Cl] in 91-93% yields (eq. 5). The cyclooctadiene (COD) rhodium dimer, $[Rh(COD)Cl]_2$ also reacted with the phosphines to give monomeric complexes in 85-88% yields (eq. 6).

Dodecacarbonyltetrarhodium $[Rh_4(CO)_4]$ reacted with the phosphines in hexane under a stream of nitrogen to give $Rh_4(CO)_4L_2$ and unidentified compounds (eq. 7). Purification by chromatography on silica gel gave low yields (37%-61%) of the analytical pure compounds 7a and 7b.

Scheme IV.

Preparation of Rhodium Complexes with Silated Phosphine Ligands

$$1/2\ [Rh(CO)_2Cl]_2 + 2L \xrightarrow[\text{r.t., 30min.}]{\text{ØH}} L_2Rh(CO)Cl + CO \qquad (5)$$

L=L 3a (93%)
L=L* 3b (91%)

$$1/2\ [Rh(COD)Cl]_2 + L \xrightarrow[\text{r.t., 10min}]{CH_2Cl_2} LRh(COD)Cl \qquad (6)$$

L=L 5a (85%)
L=L* 5b (88%)

$$Rh_4(CO)_{12} + 2L \xrightarrow[\text{r.t., 24 hr}]{\text{hexane, } N_2 \text{ flow}} L_2Rh(CO)_{10} \qquad (7)$$

L=L 7a (61%)
L=L* 7b (37%)

$$L = C_2H_5O\overset{\overset{CH_3}{|}}{\underset{\underset{CH_3}{|}}{Si}}CH_2CH_2P\text{Ø}_2, \quad L^* = (C_2H_5O)_3SiCH_2CH_2P\text{Ø}_2$$

The supported catalysts were prepared by reacting the metal compounds with silica gel (Cabosil HS-5 or Grace 62) in refluxing toluene (Path A, Scheme V), or by reacting the phosphinated silica gel with the organometallic complexes (Path B, Scheme V). Tables 1 and 2 present the conditions and results of the preparation of the several supported complexes. Table 2 also shows the preparation of the supported complexes with a sulfur ligand.

Scheme V.

Preparation of Supported Catalysts

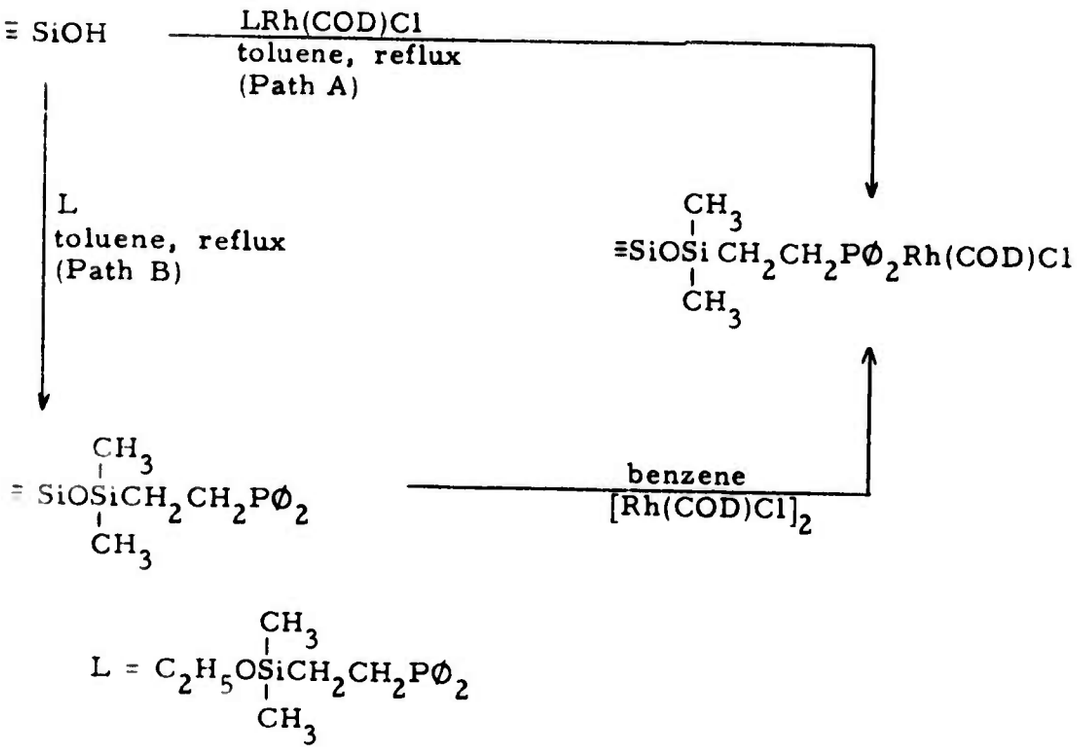

Table 1. Preparation of Supported Catalysts from Silica Gel and Metal Complexes

Exp. No.	Silica gel (g)	Metal complexes (mg)	Toluene (ml)	Temp. (hr)	Rh (%)	Other constituents (%
MT-I-37	Cabosil HS-5 (1.0)	$L_2Rh(CO)Cl$ (150)	40	reflux (18)	1.94	C, 7.04; H, 0.80 P, 0.95
MT-I-65	" (1.8)	LRh(COD)Cl (100)	60	" (3)	0.55	
MT-II-3	" (1.5)	" (70)	50	" "	0.59	
MT-I-52	" "	" (50)	"	" (6)	0.93	C, 4.14; H, 0.51
MT-II-14	Grace 62 (4.5)	" (600)	40	" (18)	1.14 (0.95)	P, 0.37; Cl, 0.39
MT-II-7	Cabosil HS-5 (1.3)	" (300)	50	" (24)	1.15	
MT-I-68	" (1.0)	" (200)	40	" "	1.30	
MT-I-39	" (1.0)	" (150)	40	" (18)	1.63	
MT-I-69	" (1.0)	L* Rh(COD)Cl (150)	40	" "	1.37	
MT-I-70	" (0.9)	$L_2Rh_4(CO)_{10}$ (450)	30	" "	8.13	
MT-I-47	" (0.28)	" (100)	15	" "	8.41	c, 6.81; H, 0.90

$L = C_2H_5O\overset{\overset{CH_3}{|}}{\underset{\underset{CH_3}{|}}{Si}}CH_2CH_2P\phi_2$ $\qquad$ $L^* = (C_2H_5O)_3SiCH_2P\phi_2$

Table 2. Preparation of Supported Catalysts from Functionalized Silica Gel and Metal Complexes

MT-II-23

$$\equiv SiOH + (C_2H_5O)_3SiCH_2CH_2P\phi_2 \xrightarrow[48\ hr.]{\text{toluene, r.t., } N_2 \text{ flow}} \equiv SiO\overset{OC_2H_5}{\underset{OC_2H_5}{Si}}CH_2CH_2P\phi_2$$

(Grace-62)

P, 0.95%

MT-II-25

Procedure identical to MT-II-23 except reflux for 18 hr. P, 0.97%.

MT-II-28

$$\equiv SiO\overset{OC_2H_5}{\underset{OC_2H_5}{Si}}CH_2CH_2P\phi_2 + [Rh(COD)Cl]_2 \xrightarrow[r.t., 1\ hr.]{\text{benzene}} \equiv SiO\overset{OC_2H_5}{\underset{OC_2H_5}{Si}}CH_2CH_2P\phi_2Rh(COD)Cl$$

(P, 0.97%)

Rh, 2.88%; P, 0.98%; Cl, 0.98%.

MT-II-4 & -9

$$\equiv SiOH + (CH_3O)_3CH_2CH_2CH_2SH \xrightarrow[reflux,\ 18\ hr]{\text{toluene, } N_2} \equiv SiO\overset{OCH_3}{\underset{OCH_3}{Si}}CH_2CH_2CH_2SH$$

(Cabosil HS-5)

MT-II-4, S: 0.79%, C: 1.87%, H: 0.43% (=Cabosil-SH_1)

MT-II-9, S: 0.63%, C: 1.20%, H: 0.29%, (=Cabosil-SH_2)

MT-II-5

$$\text{Cabosil-}SH_1 + L''Rh(COD)Cl \xrightarrow[2)Et_3N,\ 1\ hr]{1)Bz,\ r.t.,\ 1\ hr} \left(\equiv SiO\overset{OCH_3}{\underset{OCH_3}{Si}}CH_2CH_2CH_2S\right)\underset{L''}{Rh}(COD)$$

($L''=PPh_3$)

Rh: 1.39%, S: 0.71:, Cl: 0.39% (=Cabosil-SC_1)

MT-II-10

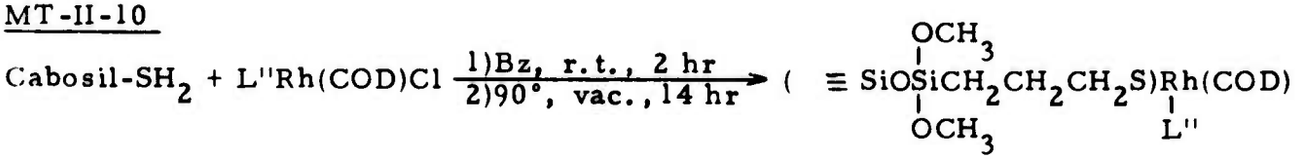

Rh:0.77%, S:0.44%, Cl:0.23%, P:0.34% (=Cabosil-SC_2)

MT-II-6

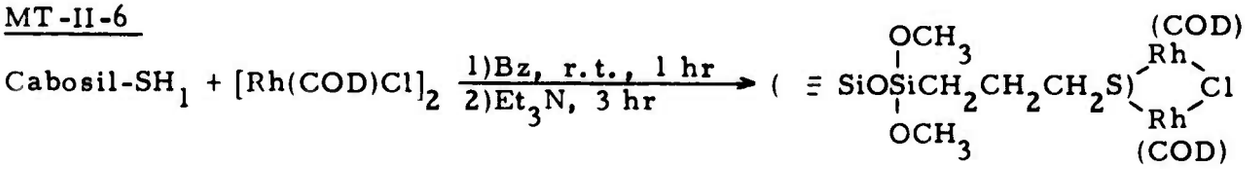

Rh:2.16%, S:0.79%, Cl:0.74%, N:0.32% (=Cabosil-SD)

MT-II-13

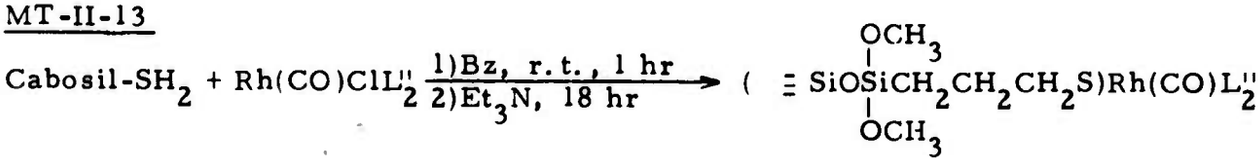

Rh: 0.82% (=Cabosil-SV)

2. Hydrogenation of Olefins and Benzene by Homogeneous and Supported Rhodium Complexes

Tables 3, 4, and 5 show the results of hydrogenation of olefins and benzene by various catalysts. Details of the apparatus and the procedure used are given in the Experimental Section.

1) Reproducibility of Hydrogenations with Supported Catalysts.

The kinetic data described later indicate that the reproducibility of the hydrogenation is quite good if the catalyst of the same batch was used and previously activated under hydrogen. However, the induction periods of the first reaction may differ dramatically depending on the time elapsed since synthesis.

Figure 1 represents two runs, MT-II-20 (25 days after synthesis) and MT-II-27 (46 days after synthesis) using the same batch of catalyst (MT-II-14). After the first run, 5 mmol more 1-decene was added and each hydrogenation was continued (MT-II-20-2 and MT-II-27-2). This figure demonstrates the following:

a) There is a big difference (about one order of magnitude) in the periods of the first runs.

b) Rates of the second runs are about ten times larger than the first runs.

c) The reproducibility of the rates (especially of the second runs) is quite good.

These three points indicate that the supported complex catalysts are partially deactivated on standing with possible oxygen concentration, but

Table 3. Hydrogenation of Olefins and Benzene by Attached and Homogeneous Rhodium Complexes
(Temp. 25°, H_2 pressure 46 psi)

Exp. No.	Catalyst (Rh g.atom x 10^5, Rh%)	Substrate (mmol)	Solvent (ml)	Rate (mmol H_2/hr)	Time (hr)	Product (%)[e]
MT-I-66	$RhCl(PPh_3)_3$ (2.5, -)	1-Decene(2.5)	Benzene(10)	0.95	20	Decane (93.2) CHX(0.022 mmol)
MT-I-66-2[a]	"	"	"	3.42	7.5	Decane (99.0) CHX (0.018 mmol)
MT-I-41	$L_2Rh(CO)Cl(=A)$ (10, -)[d]	1-Decene (2.6) Benzene (5.6)	THF (5)	0.024	24	Decane (18.3)
MT-I-43	Cabosil-A (10, 1.94)	"	"	0.0085	96	" (22.3)
MT-I-46	LRh(COD)Cl(=B) (5, -)	"	"	0.0063	144	" (23.2)
MT-I-45	Cabosil-B (5, 1.63)	"	"	5.40	1.5	" (100) CHX (0.09)
MT-I-58	" (2.5, 0.93)	1-Decene (2.5)	Benzene(10)	3.88	2	Decane (100)
MT-I-61	"	1-Methylcyclo hexane (2.5)	"	0.082	21	Me-CHX (28.0) CHX (0.34 mmol)
MT-I-44	" (2.5, 1.63)	2,3-Dimethyl-futene (2.5)	"	0.0065	48	CHX (0.10 mmol)
MT-I-67	" (2.5, 0.55)	1-Decene (2.5)	"	0.41	24	Decane (99.2) CHX (0.21 mmol)
MT-II-16	" (1.25, 0.59)	"	"	0.0076	13 days	Decane (31.3)

Table 3. (continued-2)

Exp. No.	(Rh g.atom x 10^5, Rh%)	Substrate (mmol)	Solvent (ml)	Rate (mmolH_2/hr)	Time (hr)	Product(%)
MT-I-63	Cabosil-B(2.5, 0.93)	1-Decene (2.5)	THF (10)	4.24	2	Decane(100)
MT-I-63-2[a]	"	"	"	9.13	"	"
MT-I-63-3[a]	"	"	"	8.91	"	"
MT-II-15	" (2.5, 1.15)	"	Benzene(10)	6.17	20	Decane(100) CHX(1.70 mmol)
MT-II-15-2[a]	"	"	"	17.9	7.5	Decane (100) CHX (0.59 mmol)
MT-II-15-3[b]	"	--	"	0.20	11 days	CHX (3.45 mmol)
MT-II-17	Grace-B(2.5, 0.95)	1-Decene (2.5)	"	1.44	18	Decane (100) CHX (1.44 mmol)
MT-II-17-2[a]	"	"	"	7.72	6	Decane (100) CHX (0.98 mmol)
MT-II-17-3[c]	"	"	"	7.69	17	Decane (100) CHX (3.80 mmol)
MT-II-17-4[a]	"	--	"	6.89	--	--
MT-II-22	Cabosil-B[f] (2.5, 1.37)	1-Decene (2.5)	"	10.72	6	Decane (100) CHX (0.16 mmol)
MT-II-22-2[b]	"	"	"	0.51	40	CHX (6.72 mmol)
MT-II-33	Cabosil-B[g](2.5, 2,88)	"	"	4.47	5	Decane (100) CHX (0.472 mmol)
MT-II-33-2[b]	"	--	"	0.671	20	--
MT-II-33-3[a]	"		"	17.94	25	--

Table 3. (continued-3)

Exp. No.	Catalyst (Rh g.atom x 10^5, Rh%)	Substrate (mmol)	Solvent (ml)	Rate ($mmolH_2$/hr)	Time (hr)	Product (%)
MT-II-33-4[a]	Cabosil-B[g](2.5, 2.88)	1-Decene (2.5)	Benzene (10)	20.52	20	--
MT-I-60	$L_2Rh_4(CO)_{10}$(=C)(2.5)	1-Decene (2.5)	THF (10)	1.95	3	Decane (98.0)
MT-I-62	"	Benzene (2.5)	"	0.017	27	CHX (5.8)
MT-II-32	Cabosil-C (2.5, 8.13)	1-Decane (2.5)	Benzene (10)	9.03	0.75	Decane (100) CHX (0.83 mmol)
MT-II-32-2[b]	"	--	"	0.51	0.59	CHX (0.10 mmol)
MT-II-32-3[a]	"	1-Decene (2.5)	"	14.16	0.5	Decane (100) CHX (0.03 mmol)
MT-I-59	" (0.625, 8.41)	Benzene (25)	THF (10)	1.00	21	CHX (41.0)
MT-I-48	" (10, 8.41)	1-Decene (2.5)	Benzene (10)	4.32(?)	2.5	Decane (100) CHX (2.19 mmol)
MT-I-48-2[b]	"	--	"	3.03	3.43	CHX (2.57 mmol)

a) Additional substrate added to preceding solution and repressured to 46 psi of hydrogen.

b) Preceding run was repressed to 46 psi of hydrogen. c) The catalyst was filtered in air and reused under the identical condition as preceding. d) L=$C_2H_5O\overset{CH_3}{\underset{CH}{Si}}CH_2CH_2P\phi_2$. e) CHX=cyclohexane, Me-CHX=methylcyclohexane. f) B=$(C_2H_5O)_3SiCH_2CH_2P\phi_2$)Rh(COD)Cl. g) Cabosil-B" was prepared from phosphinated silica gel and $[Rh(COD)Cl]_2$ (MT-II-25).

Table 4. Hydrogenation of Olefins and Benzene by Supported Rhodium Complexes with Sulfur Ligands

(Temp. 25°, H_2 pressure 46 psi)

Exp. No.	Catalyst (Rh g .atom x 10^5)	Substrate (mmol)	Solvent (ml)	Rate (mmol H_2/hr)	Time	Product(%)
MT-II-21	Cabosil-SV(2.5, 0.82)	1-Decene (2.5)	Benzene	0.768	20	Decane (100) CHX (0.034 mmol)
MT-II-21-2[b]	"	--	"	0.0036	48	CHX (0.14 mmol)
MT-II-21-3[c]	"	1-Decene (2.5)	"	7.38	2	Decane (100)
MT-II-8	Cabosil-SC_1(2.5, 1.39)	1-Decene (2.5)	Benzene (10)	0.30	22	Decane (100) CHX (0.027 mmol)
MT-II-8-2[a]	"	"	"	3.25	2	Decane (100) CHX (0.011 mmol)
MT-II-8-3[a]	"	"	"	4.00	1.5	Decane (100) CHX (0.009 mmol)
MT-II-12	Cabosil-SC_2[f](2.5, 0.77)	"	"	0.25	43	Decane (100) CHX (0.046 mmol)
MT-II-12-2[a]	"	"	"	0.52	21	Decane (100) CHX (0.057 mmol)
MT-II-11	Cabosil-SD[g](2.5, 2.16)	"	"	0.19	48	Decane (100) CHX (0.158 mmol)
MT-II-11-2[a]	"	"	"	2.22	41	Decane (100) CHX (0.143 mmol)
MT-II-11-3[a]	"	"	"	1.47	21	Decane (100) CHX (0.113 mmol)
MT-II-29	Grace-SN[h](2.5, 3.0)	"	"	0.987	22	Decane (100) CHX (0.304 mmol)

Table 4 (continued-2)

Exp. No.	Catalyst (Rh g.atom x 10^5)	Substrate (mmol)	Solvent (ml)	Rate (mmol H_2 hr)	Time	Product(%)
MT-II-29-2[a]	Grace-SN[h] (2.5, 3.0)	1-Decene (2.5)	Benzene (10)	1.05	21	Decane (100) CHX (0.04 mmol?)

a), b), c) See Table 3. d), e), f), g) See Table 2. h) 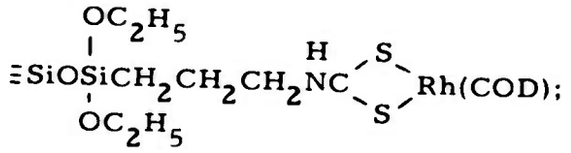

H. Heitner, NB 52-2.

Table 5. Hydrogenation of Olefins and Benzene by Attached and Homogeneous Rhodium Complexes

(Temp. 25°, H_2 pressure 665 mm)

Exp. No.	Catalyst[d] (Rh g.atom x 10^5, Rh%)	Substrate (mmol)	Solvent (ml)	Rate (ml H_2/min)	Time hr	Product(%)
MT-II-18	Rh/Alumina (2.5, 5)	1-Decene (5.0)	Benzene (20)	47.0	0.05	Decane (98.4) CHX (0.540 mmol)
MT-II-18-2[b]	"	--	"	5.0	--	--
MT-II-19	Rh/Alumina (0.5, 5)	1-Decene (5.0)	"	9.3	0.4	Decane (95.0)
MT-II-20	Grace-B (2.5, 0.95)	"	"	0.30	19	Decane (100) CHX (0.766 mmol)
MT-II-20-2[a]	"	"	"	3.90	2	Decane (100) CHX (0.358 mmol)
MT-II-20-3[c]	"	"	"	3.80	1.5	Decane (100) CHX (0.328 mmol)
MT-II-53	Cabosil-B (2.5, 0.55)	"	"	0.034	96	Decane (91.3) CHX (0.02 mmol)
MT-II-53-2[a]	"	"	"	0.27	44	--
MT-II-47	Cabosil-B' (2.5, 2.88)	"	"	2.78	1.3	Decane (100) CHX (0.23 mmol)
MT-II-47-2[b]	"	--	"	0.062	10	--
MT-II-47-3[a]	"	1-Decene (5.0)	"	5.30	1.0	--
MT-II-51	Cabosil-B (2, 5, -)	"	"	0.051	28.5	Decane (84.2)
MT-II-55	Cabosil-C (2.5, 8.13)	"	"	3.47	0.75	Decane (100) CHX (0.692mmol)

Table 5 (continued-2)

Exp. No.	Catalyst[d] (Rh g. atom x 10^5, Rh%)	Substrate (mmol)	Solvent (ml)	Rate (ml H_2/min)	Time (hr)	Product(%)
MT-II-55-2[b]	Cabosil-C (2.5, 8.13)	--	Benzene (20)	0.790	0.5	--
MT-II-55-3[a]	"	1-Decene (5 mmol)	"	7.45	0.5	--
Mt-II-55-4[b]	"	--	"	0.775	1.0	--
MT-II-27	"	1-Decene (5mmol)	"	0.31	4 days	Decane (100) CHX (1.16 mmol)
MT-II-27-2[a]	"	--	"	3.25	2	Decane (100) CHX (0.342 mmol)

a) Additional substrate added to the preceding solution and hydrogenation was continued.

b) Preceding run was continued to measure the rate of hydrogenation of benzene.

c) The catalyst was filtered in air and reused under the identical condition as preceding run.

d) Table 2.

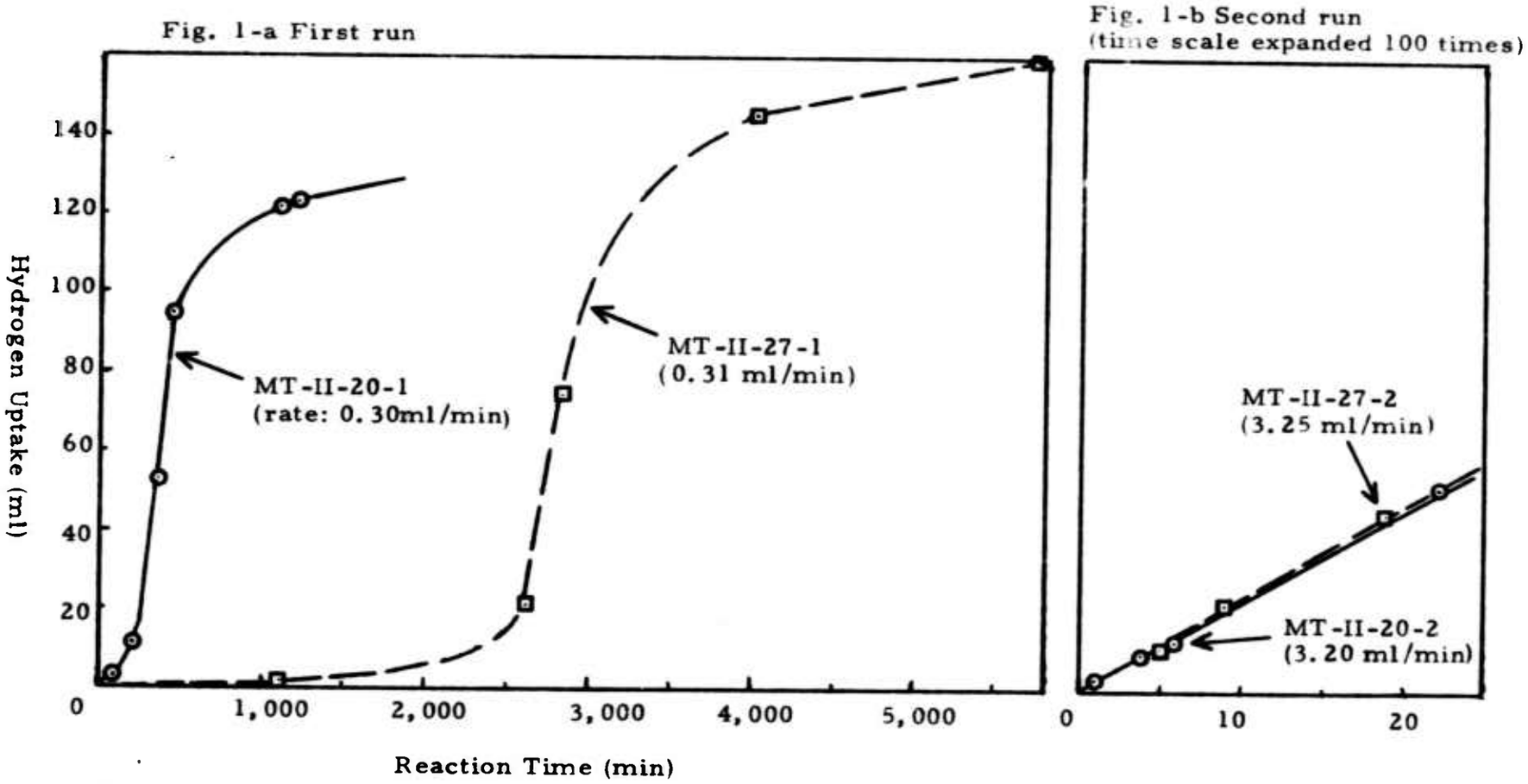

Fig. 1. Reproducibility of Hydrogenation with a Supported Catalyst.

Catalyst: Grace-B (MT-II-14; Rh, 0.95%), 2.5×10^{-5} Rh g. atom,

1-Decene: 5 mmol, Benzene: 20 ml, H_2: 665 mm, 25°.

are reactivated by atmospheric hydrogen. Agitation of the solution was affected by a shaker or a 4 cm Teflon coated magnetic stirring bar. The shaker gives very efficient agitation of hydrogen, and hydrogen absorption rates of up to ca. 50 ml/min have been observed with Rh/Al_2O_3 without any apparent limitation due to hydrogen diffusion control (cf. MT-II-18 and MT-II-19).

The repeat runs in Figure 1, MT-II-20 (agitation by the shaker) and MT-II-27 (agitation by the stirrer) show that the stirrer is sufficient for the reactions up to approximately 4 ml/min. The kinetic study (section 2-(5)) also substantiates that the reactions dealt with in this paper are not diffusion controlled even when magnetically stirred.

The catalyst can easily be separated by simple filtration and reused with little change in activity (see MT-II-17, MT-II-20 and MT-II-21).

Table 6 demonstrates that little rhodium is lost from the support during catalysis under mild conditions (H_2:1 atom, 3 days). Under more severe conditions (H_2:46 psi, 4-6 days, or especially in the hydroformylation) proportionally more rhodium is lost from the catalyst.

2) Comparison of Supported and Homogeneous Rhodium Complex Catalysts

Table 7 compares the reduction rates of 1-decene by supported and homogeneous rhodium catalysts. The order of activity is approximately as follows: Cabosil-C > Cabosil-B $\gg$ C $\gg$ B $\approx$ Cabosil-A $\approx$ A

(A=$L_2Rh(CO)Cl$, B=$LRh(COD)Cl$, C=$L_2Rh_4(CO)_{10}$, L=$C_2H_5O\overset{CH_3}{\underset{CH_3}{Si}}CH_2CH_2P\phi_2$)

Note the striking difference in activity of B and C when supported and the lack of such difference with A.

Table 6. Rhodium Loss from the Support During Catalysis

Catalyst (Rh, %)	Reaction No.	Condition	Time (day)	Rh(%) After Catalysis	Rh Loss (%)
Cabosil-B (1.66)	MT-I-45	H_2, 46 psi	6	1.42	12.9
Cabosil-B (0.93)	MT-I-58	"	4	0.73	21.5
Grace-B (1.14) (P, 0.37 Cl, 0.39)	MT-II-20	H_2, 1 atm	3	1.11 (P, 0.34; Cl, 0.34)	2.6
Cabosil-C (8.41)	MT-I-48	H_2, 46 psi	1	8.22	2.3
"	MT-I-59	"	4	6.33	24.7
"	MT-II-1	CO, 25 psi H_2, 25 psi	12	3.38	59.8

Table 7. Comparison of Supported and Homogeneous Rhodium Complex Catalysts

Catalyst[a] (Rh g. atom x 10^5, Rh(%))	1-Decane (mmol)	Solvent (ml)	Rate (mmol H_2/hr)
(H_2, 46 psi)			
$L_2Rh(CO)Cl$(=A)(10, -)	2.6	THF(5)	0.024
Cabosil-A		Benzene (0.5)	0.009
LRh(COD)Cl(=B)(10, 1.94)	"	"	0.006
Cabosil-B (5, 1.63)	"	"	5.40
Cabosil-B (2.5, 0.93)	2.5	Benzene (10)	3.88
$L_2Rh_4(CO)_{10}$(=C)(2.5, -)	"	THF (10)	1.95
Cabosil-C (2.5, 8.13)	"	Benzene (10)	9.03
(H_2, 1 atm)			
B (2.5, -)	5.0	Benzene (20)	0.127
Cabosil-B' (2.5, 2.88)	"	"	7.28
Cabosil-C (2.5, 8.13)	"	"	9.09

a) See Table 1.

3) Effect of Rhodium Content on Catalytic Activity.

Figures 2-1 and 2-2 shows that the activity for hydrogenation increases with increasing rhodium content. This trend is the reverse of platinum on alumina catalyst as studied by Hussey, et al.[29]

4) Reduction Rates of Other Olefins.

A cursory study of the rates of reduction of various substrates by Cabosil-B catalyst shows the difference of the reduction rates between two, three and four substituted olefins is quite large. 2,3-Dimethylbutene is not hydrogenated even under 46 psi hydrogen.

Substrate: 1-Decene > 1-methylcyclohexane > benzene > 2,3-dimethylbutene

Rate: (3.88) (0.082) (0.006) (0.001)

The literature results are not sufficiently clear to enable a comparison with heterogeneous analogs.

5) Kinetic Study.

For the kinetic study, Grace-B, $(\equiv SiO\overset{\overset{CH_3}{|}}{\underset{\underset{CH_3}{|}}{Si}}CH_2CH_2P\phi_2)Rh(COD)Cl$ (MT-II-14; Rh 0.95%) was used after previous activation by 1 atmosphere hydrogen. The standard conditions are as follows:

Catalyst: Grace B (1.19 mM), 1-Decene: 0.238M, Benzene: 20 ml, Temp.: 25°, H_2: 665 mm.

(i) Dependence on temperature.

Rates were measured at three temperatures ranging from 5-25° for 1-decene hydrogenation in benzene. On plotting the log of the rate data versus 1/T we obtained a straight line (Figure 3). This indicated that our reaction is not diffusion controlled. From Figure 3, a value

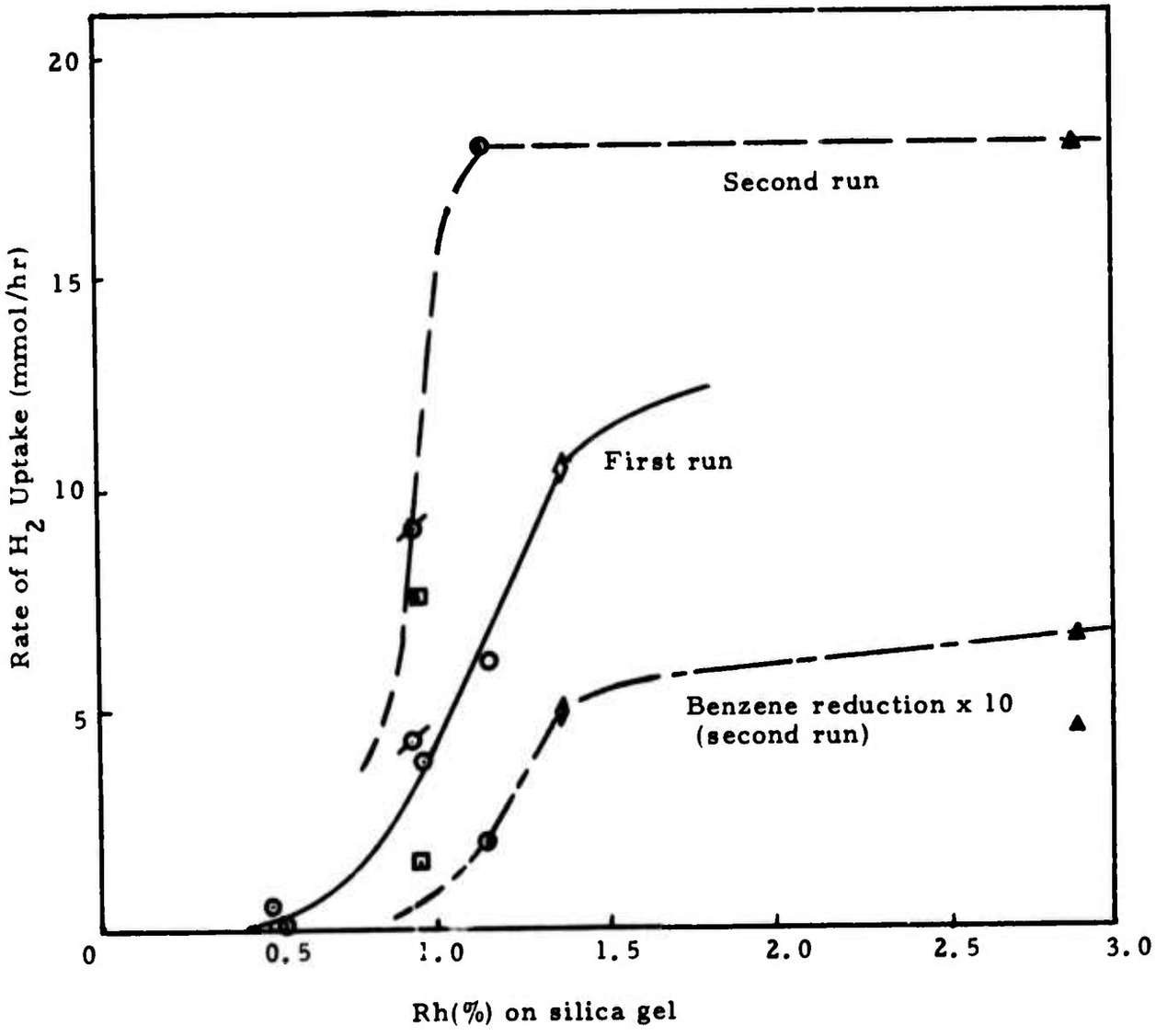

Fig. 2-1. Activity as a Function of Rhodium Content

Conditions Catalyst: 2.5×10^{-5} Rh g. atom
1-Decene: 2.5 mmol
Benzene: 10 ml
H_2: 46 psi

⊙ Cabosil-B, ⊘ Cabosil-B (Solvent THF)
⊡ Grace-B, ◊ Cabosil-B'
△ Cabosil-B'' (see Table 3)

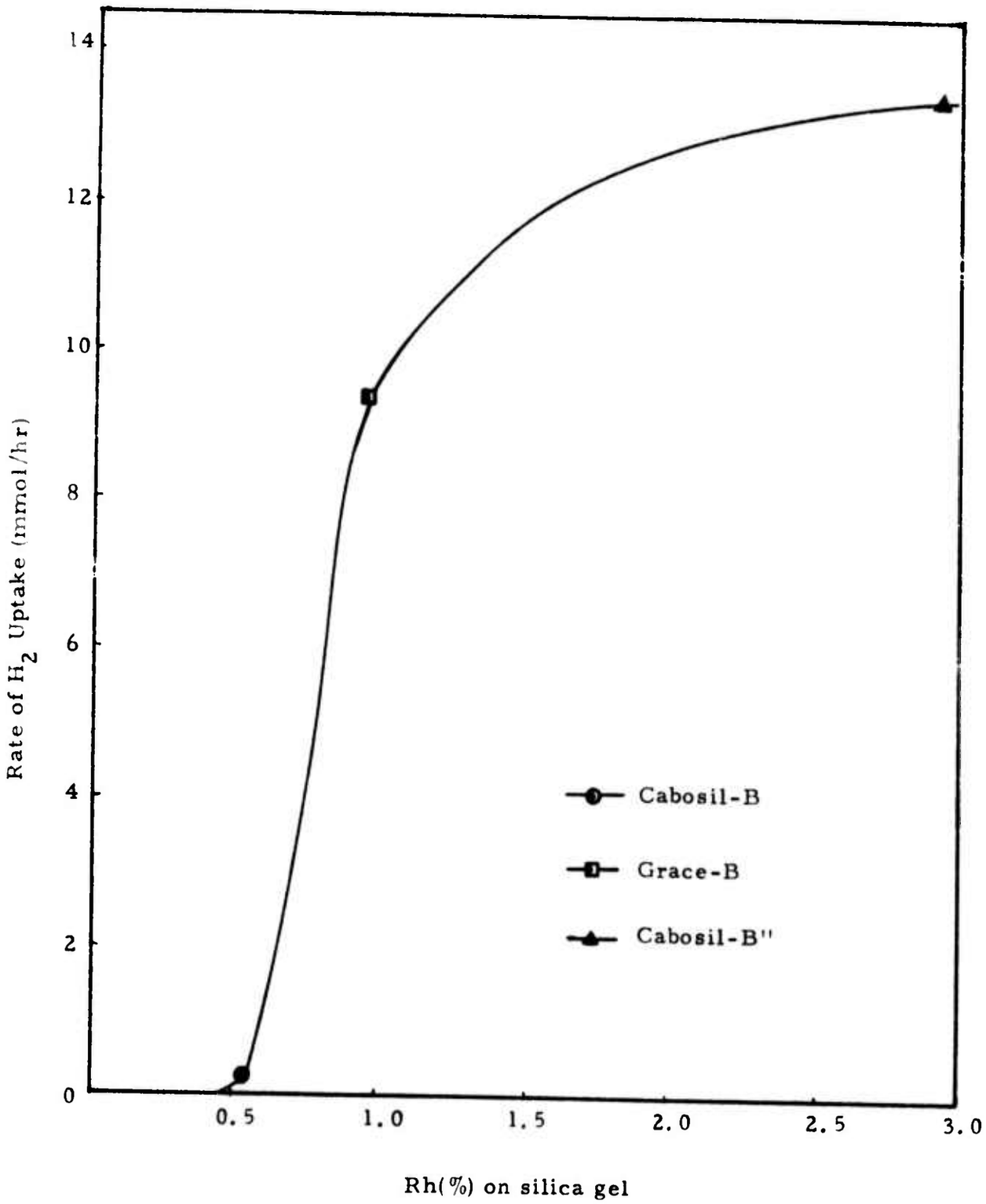

Fig. 2-2. Activity as a Function of Rhodium Content

Conditions
Catalyst: 2.5×10^{-5} Rh g.atom (second run)
1-Decene: 5 mmol
Benzene: 20 ml
H_2 : 665 mm

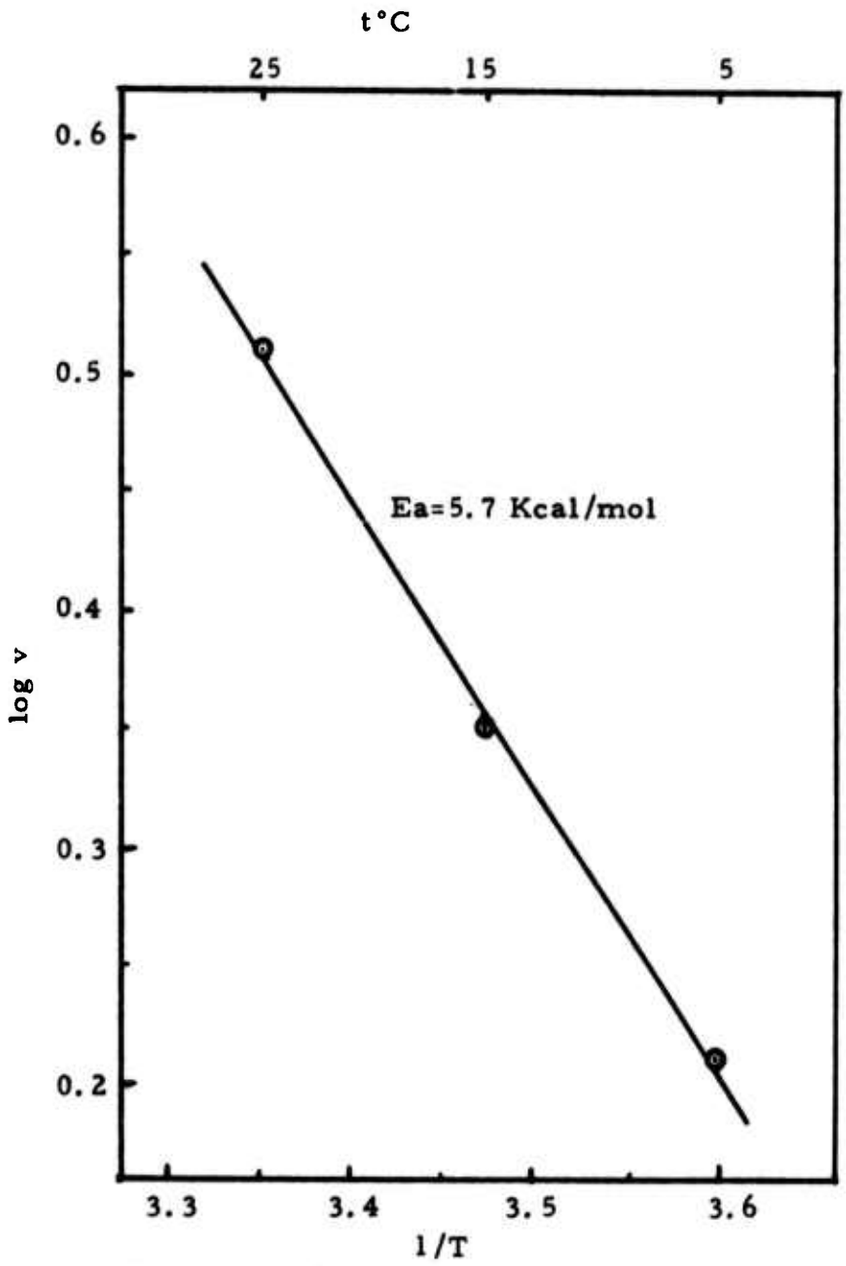

Fig. 3. Arrhenius plot for hydrogenation rates at 665 mm H_2, 1.19 mM Rh, 0.238 M -1decene in benzene.

for the apparent activation energy, Ea, of 5.7 Kcal/mole is obtained. This value is good agreement with the activation energy, 5.7-6.5 Kcal/mole for the hydrogenation of cycloalkenes in the liquid phase on a platinum-alumina catalyst[29]. For comparison, the activation energy for the homogeneous hydrogenation of cyclohexene with $RhCl(PPh_3)_3$ is 22.9 Kcal/mole[19], and for the gas phase hydrogenation of ethylene with Pt/SiO_2 is 9 Kcal/mole[31].

(ii) Dependence on catalyst concentration.

From results under standard conditions using various catalyst concentrations (0.3-1.2 mM), it is clear that the plot of rate against catalyst concentration is linear with zero intercept (Fig. 4).

(iii) Dependence on hydrogen pressure.

A linear relationship was also found between hydrogen pressure and rate of hydrogenation for 250-665 mm pressure of hydrogen (Fig. 5).

(iv) Dependence on 1-decene concentration

Fig. 6 illustrates the plot of rate of hydrogenation against 1-decene concentration. The rate does not increase linearly with increasing olefin concentration. The plot of the reciprocal of this rate against the reciprocal of the olefin concentration (Fig. 7) is linear with a positive intercept on the y-axis.

(v) Discussion of kinetic results.

The experimental data for the hydrogenation of 1-decene in benzene solution with supported rhodium complex, fit a rate law of the form,

$$d[H_2]/dt = \frac{\alpha[Rh][H_2][Decene]}{1 + \beta[Decene]} \qquad (8)$$

where α and β are constants.

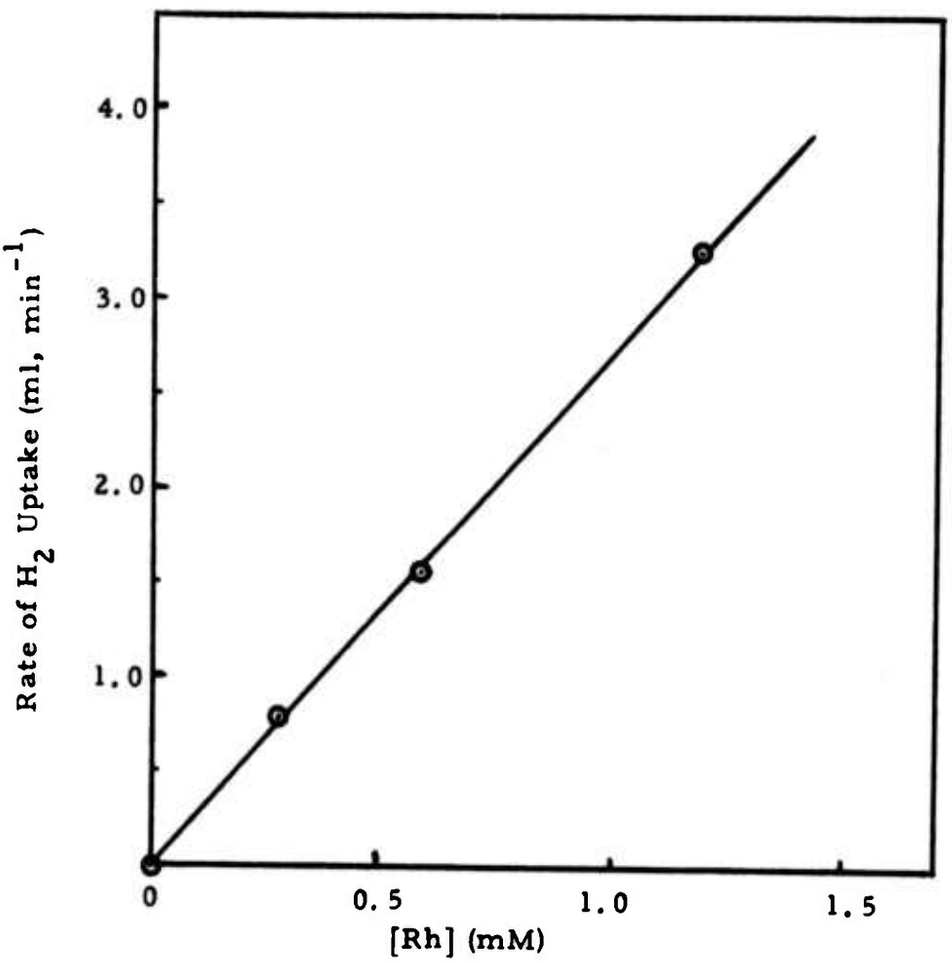

Fig. 4. Dependence of the rate of hydrogenation of [Rh] at 25°, 665 mm H_2, 0.238 M 1-decene in benzene (20 ml).

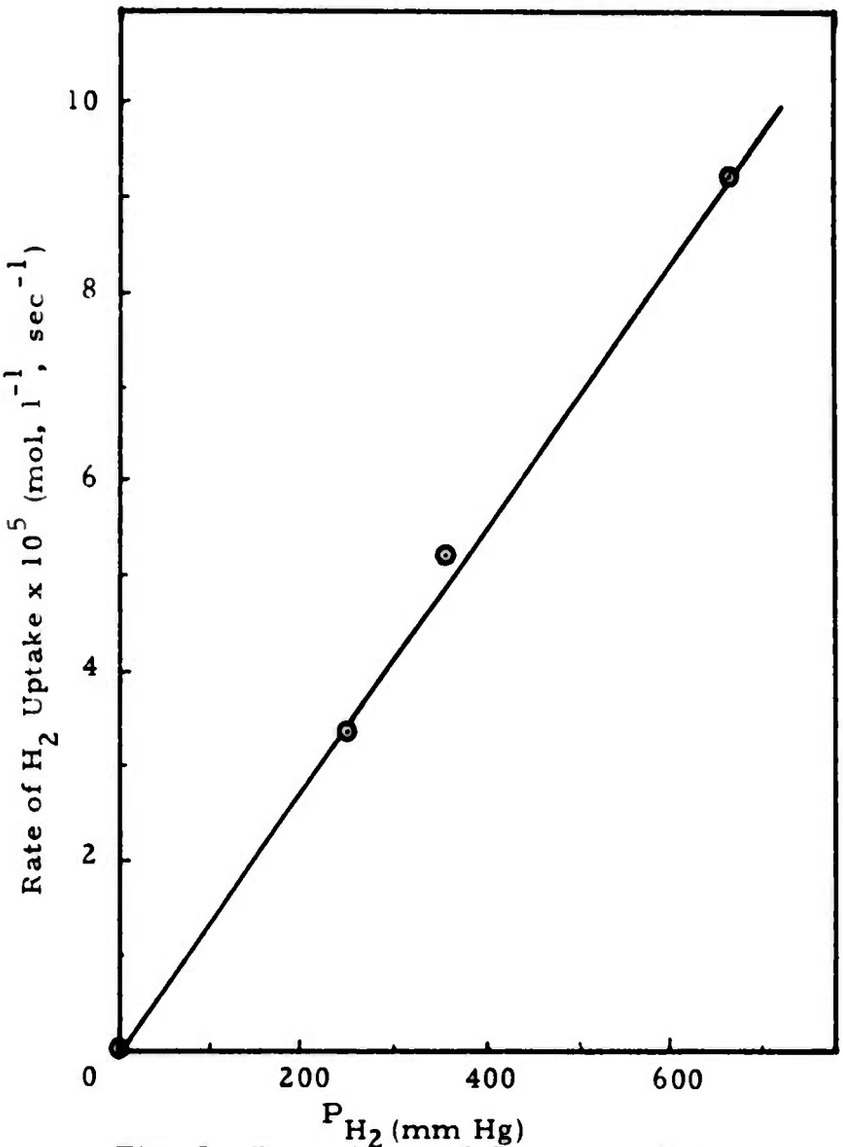

Fig. 5. Dependence of the rate on hydrogen pressure at 25°, 1.19 mM Rh, 0.238 M 1-decene in benzene (20 ml).

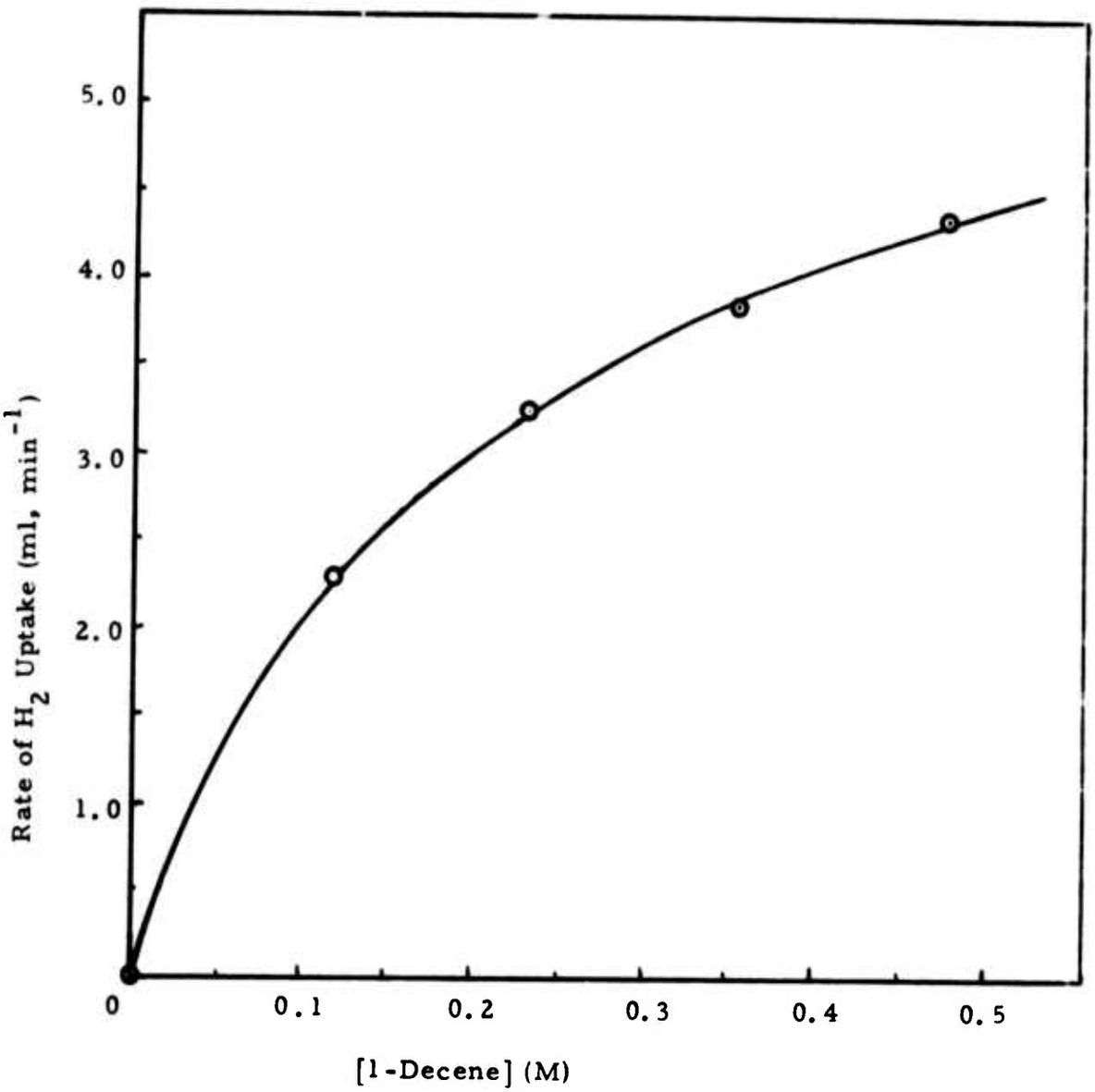

Fig. 6. Dependence of the reduction rate on [1-decene] at 25°, 1.19 mM Rh, 665 mmH_2 in benzene (total volume, 21 ml).

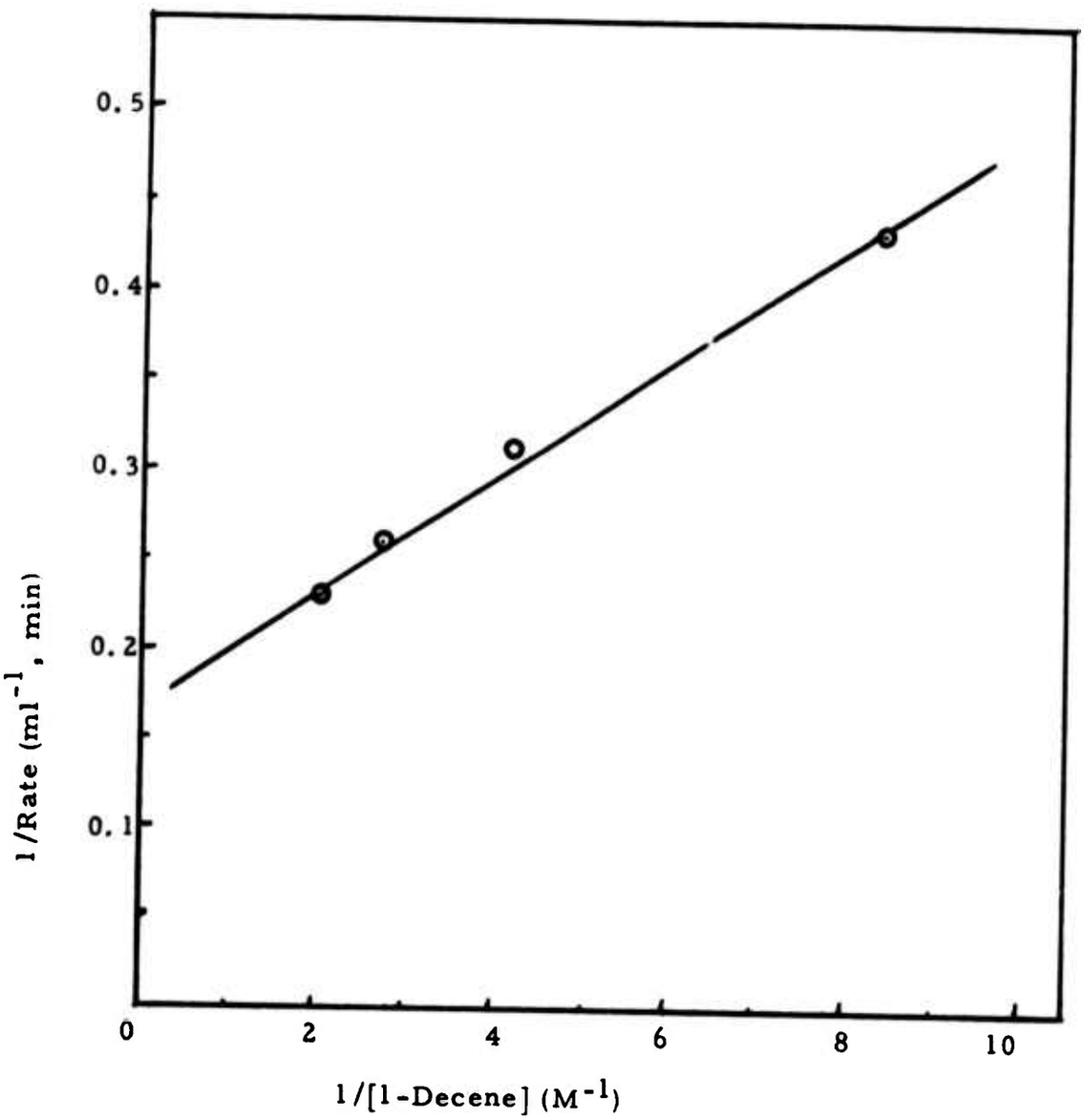

Fig. 7. Plot of reciprocal of rate of hydrogenation of 1-decene against the reciprocal of 1-decene concentration in benzene (total volume, 21 ml) at 25°, 1.19 m M Rh, 665 mm H_2.

The most generally satisfactory mechanism for the hydrogenation of olefins using $RhCl(PPh_3)_3$ is that proposed by Wilkinson, et al.,[19] which is summarized in Scheme V.

Scheme V

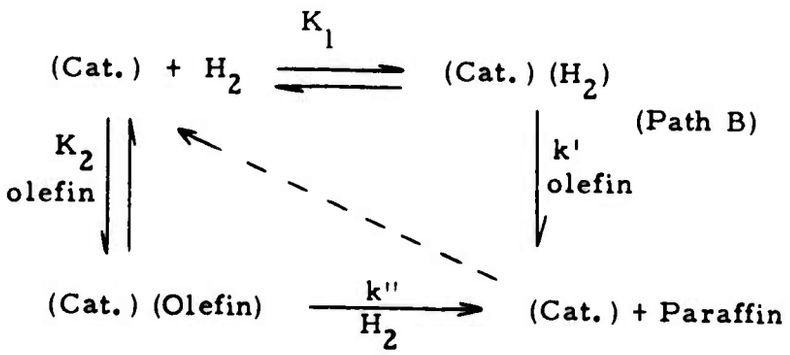

The rate of this reaction conforms to the rate expression,

$$R = \frac{(k'K_1 + k''K_2)[H_2]\,[\text{Olefin}]\,[\text{Catalyst}]}{1 + K_1\,[H_2] + K_2\,[\text{Olefin}]} \qquad (9)$$

Our rate expression (8) is of the same form as (9) if $K_1 = 0$, and the path (A) mechanism in Scheme V is operative.

Hence, our rate expression can be written as follows:

$$R = \frac{k''K_2\,[H_2]\,[\text{Olefin}]\,[\text{Catalyst}]}{1 + K_2\,[\text{Decene}]}$$

3. Hydroformylation of 1-Hexene with Supported Rhodium Complexes

The phosphine complexes of rhodium, e.g., $RhCl(CO)(P\emptyset_3)_3$, are reported to be highly reactive in addition to being considerable more stable and selective compared to $Co_2(CO)_8$[32]. However, the primary disadvantage is in the separation of the soluble catalysts from the reaction products. Therefore, the heterogeneous catalyst is industrially very attractive.

Our preliminary experiments shown below suggest that our supported catalysts are not so reactive and that much rhodium comes off from the support as illustrated in Table 6.

MT-II-1

1-Hexene (2.5 mmol) —[Cabosil-C(Rh 8.41%, 1.25×10^{-5} g . atom); CO/H_2(1/1) 50 psi, r.t., 10 hr; Benzene (10 ml)]→ Aldehydes (2.72%) n/iso = 2.2

MT-II-2

1-Hexene (2.5 mmol) —[Cabosil-B (Rh 1.63%, 2.5×10^{-5} g . atom); "]→ Aldehydes (0.05%)

4. Studies Directed Toward the Asymmetric Reduction with Supported Chiral Rhodium Complexes

Recently, a number of transition metal complex catalysts for stereoselective homogeneous hydrogenation have been developed[28]. Knowles, et al.,[33] got optical yields up to 90%, in the catalytic reduction of α-acylaminoacrylic acids to α-amino acids using rhodium complexes with chiral phosphines.

A recent report by Dang, et al.,[25] indicates that in order to obtain asymmetric reduction using rhodium phosphine complexes the chiral center does not have to be on phosphorus. Using the rhodium complex with the chiral phosphine 13 in Scheme VI (13 is now available from Strem Chemicals Inc., $22.00/g in 1 g lots), optical yields in the range of 70-80% were obtained in the reduction of β-substituted α-acetamido-acrylic acids. They attributed the high stereoselectivity of this reaction to the conformational rigidity of the diphosphine chelating the rhodium.

This study was initiated to get practical catalysts for asymmetric reduction and evidence that our supported rhodium catalysts are working in the form of the complex rather than metallic rhodium.

Scheme VI shows the synthesis of the chiral rhodium complex supported on silica gel 13. The catalyst 13 have found moderate activity for the hydrogenation of 1-decene in benzene solution at 46 psi H_2.

MT-II-60

1-Decene (2.5 mmol) —[Cat 13 (Rh 1.78%, 2.5×10^{-5} g . atom), Benzene (10 ml), H_2 46 psi, 25°, 20 hr.]→ Decane (100%), CHX (0.02 mmol)

Rate = 0.54 mmol H_2/hr.

The second run (MT-II-60-2) obtained by adding 2.5 mmol of 1-decene after the first run (MT-II-60) was completed, yielded a second rate = 3.34 m mol H_2/hr.

Scheme VI

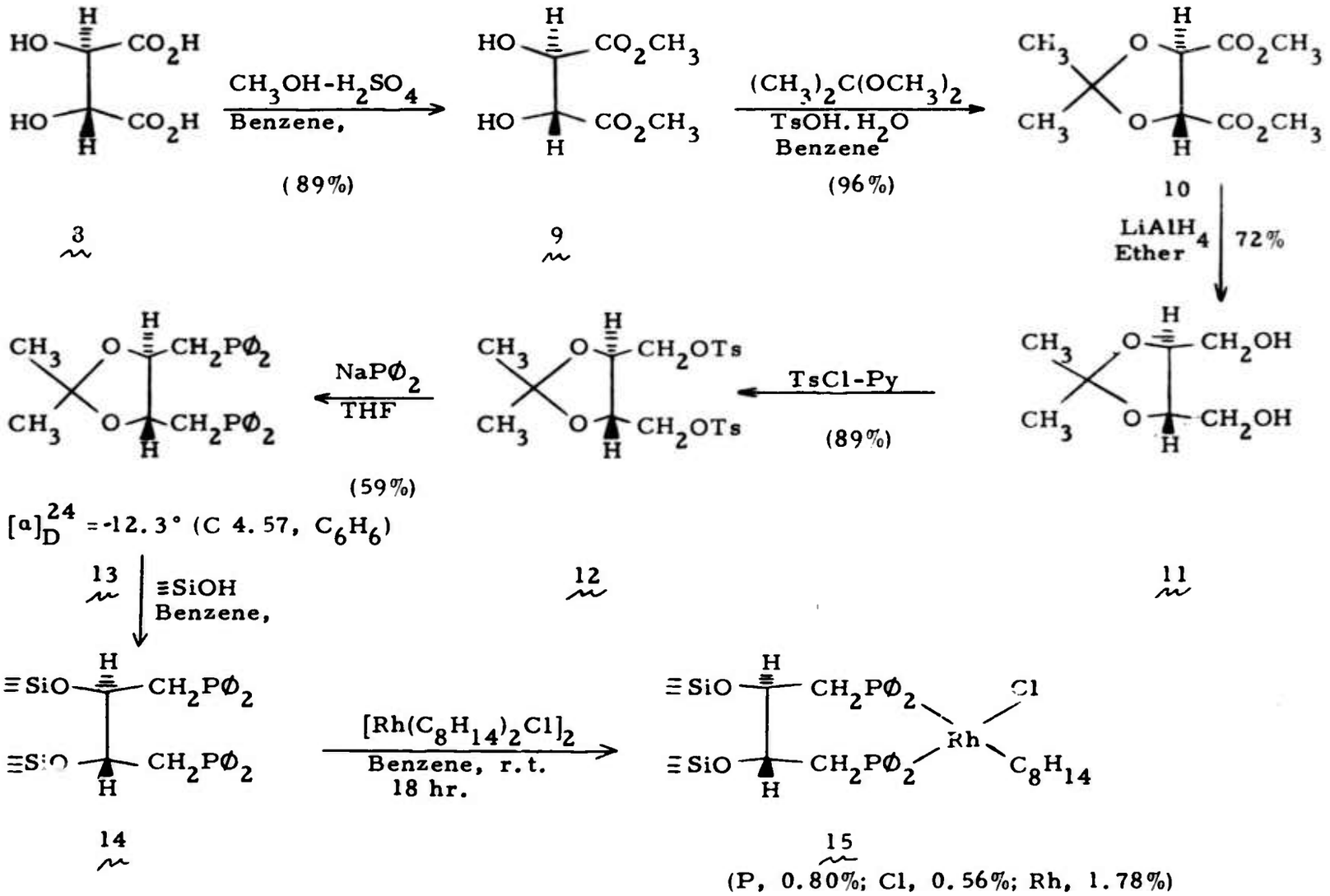
CH3OH-H2SO4
Benzene,
(89%)
(CH3)2C(OCH3)2
TsOH.H2O
Benzene
(96%)
LiAlH4
Ether
72%
TsCl-Py
(89%)
NaPØ2
THF
(59%)
[α]D24 = -12.3° (C 4.57, C6H6)
≡SiOH
Benzene,
[Rh(C8H14)2Cl]2
Benzene, r.t.
18 hr.
(P, 0.80%; Cl, 0.56%; Rh, 1.78%)

EXPERIMENTAL

N.m.r. spectra were measured on a Varian T-60, A-60 or XL-100 instrument. Infrared spectra were recorded on a Perkin-Elmer Model 457 spectrometer. Elemental analyses and molecular weight (osmometric) determinations were performed by the Stanford Microanalysis Laboratory. The melting points (uncorrected) were taken on a microscope melting point apparatus.

Glc measurements were made with Hewlett-Packard's F & M Scientific 5750 employing a 3-meter 10% carbowax on chroma wax column. Peak areas were obtained with a Vidar-6300 digital integrator. All preparations were carried out under nitrogen or argon atmosphere unless otherwise specified. Non-volatile air-sensitive substances were handled in a HE 43-2 Vacuum Atmosphere inert atmosphere chamber. Optical rotations were determined electronically on a Perkin-Elmer Model 141.

Materials. Thiophene free benzene and tetrahydrofuran (THF) were distilled under nitrogen from sodium-potasium alloy and calcium hydride, respectively. The substrates for hydrogenation were freed from peroxides by passage under nitrogen through a 20-cm column of freshly activated (400°, 3 hr) alumina and were stored under nitrogen and protected from light. Cabosil HS-5 (Cabot Co., Boston) was heated in a muffle furnace to 500° for 18 hr, and kept in a desiccator under nitrogen.

The hydrogen used for the hydrogenations was purified by a "deoxo" unit and a molecular sieve drier. All pressure reactions were carried

out in a Fischer-Porter bottle. The hydrogenation was carried out at falling hydrogen pressure. A Matheson 100 psi range gauge was used to determine the pressure at different times. The detailed procedure is described later in this section.

Apparatus for Hydrogenation at Constant Pressure

Figure 1 shows the apparatus for hydrogenation at constant pressure. This system and procedure was patterned after that used by Professor Boudart's group. The monostat system has been described in their paper[18].

The reaction vessel was a 200 ml flask with four vertical indentations to facilitate agitation and an outer jacket for water-cooling. It was attached with flexible teflon tubing to the vacuum system described above.

Procedure for Hydrogenation at Constant Pressure

1) Evacuate the catalyst (2.5×10^{-5} Rh g . atom) and reactor for 2 hr below 1 μ pressure.

2) Add 1 atm of hydrogen and shake gently for 10 min to remove oxide layer on the catalyst.

3) Evacuate the reactor and catalyst again for 1/2 hr.

4) Open stoppers to manometer and burette.

5) Add hydrogen until almost 1 atm.

6) Add solvent (benzene 20 ml) to the reactor via sampling tube through septum.

7) Let the temperature in reactor reach equilibrium.

8) Add substrate (1-decene, 5 mmol).

9) Add hydrogen until exactly 1 atm pressure.

10) Start shaker or timer simultaneously and take readings.

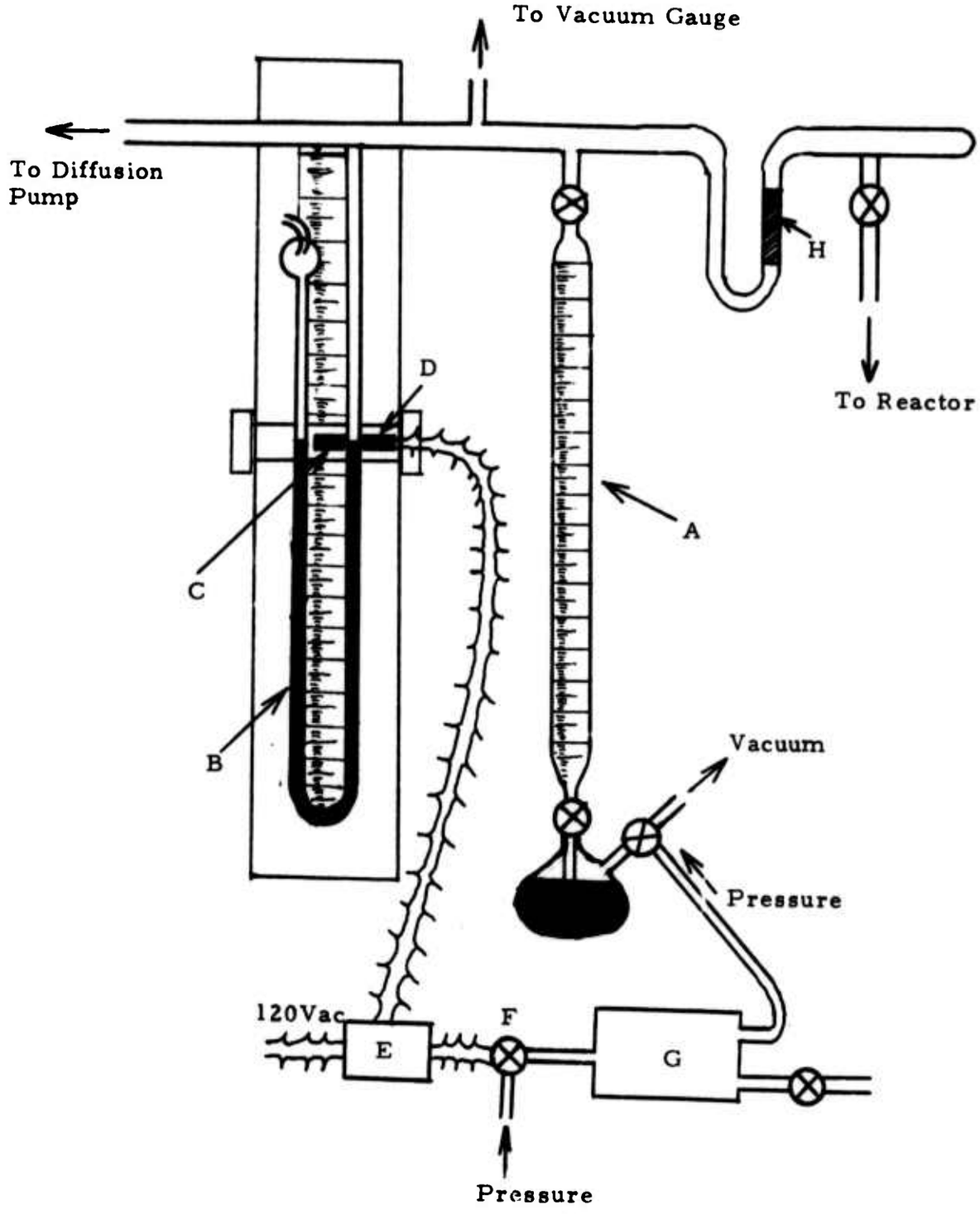

Fig. 1. Reaction Apparatus

A. Gas burette, B. Manometer, C. Light source, D. Photoelectric cell, E. Relay, F. Selencid valve, G. Surge tunk, H. Gold trap

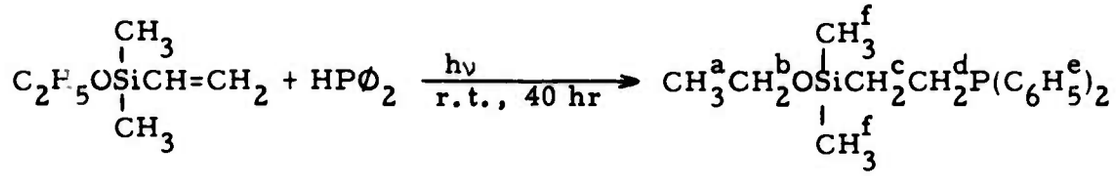

1a (80.5%)

(2-Dimethylethoxysilylethyl)diphenylphosphine 1a (MT-I-16)

This compound was prepared by the method of Niebergall[11]. A solution of freshly distilled vinyldimethylethoxysilane (3.91 g, 30 mmol) and diphenylphosphine (5.59 g, 30 mmol) was irradiated for 40 hr using a water-cooled quartz apparatus with a low-pressure mercury arc lamp. The product was distilled at 0.13 mm, bp 136-138°, giving 7.64 g (80.5%) of 1a: nmr ($CHCl_3$) δ 0.10 (S, 6H, H^f), 0.51-1.04 (m, 2H, H^c), 1.26 (t, 3H, J_{ab} = 7.0H_z, H^a), 1.97-2.36 (m, 2H, H^d), 3.73 (q , 2H, J_{ab} 7.0H_z, H^b), 7.32-7.77 (m, 10H, H^e); ir (neat) 3070, 3052, 2969, 2925, 2895, 1586, 1481, 1434, 1390, 1250 (S), 1150, 1105 (S), 1077 (S), 1027, 1000, 955.

Anal. Calcd. for $C_{18}H_{25}OSiP$: C, 68.31; H, 7.96. Found: C, 68.39; H, 8.03.

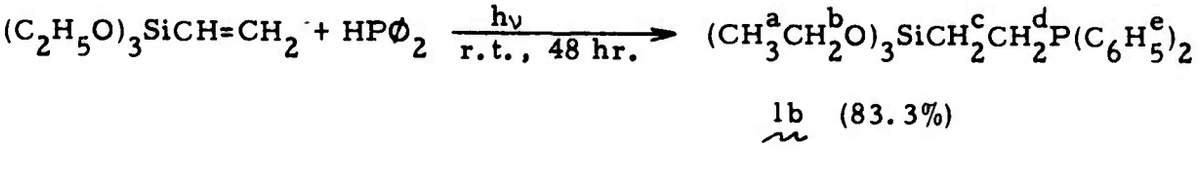

1b (83.3%)

(2-Triethoxysilylethyl)diphenylphosphine 1b (MT-I-1 and 2)

The same procedure as in the preparation of 1a was followed, using vinyltriethoxy silane (3.80 g, 20 mmol) and diphenylphosphine (3.72 g, 20 mmol). The solution was irradiated for 48 hr and then distilled at

0.05 mm, 130-132°, giving 6.26 g (83.3%) of 1b: nmr (CCl_4) δ 0.32-0.84, 2H, H^c), 1.14 (t, 9H, J_{ab}=6.9 Hz, H^a), 1.80-2.27 (m,, 2H, H^d), 3.71 (q, 6H, J_{ab}=6.9Hz, H^b) 7.02-7.48 (m, 10H, H^e); ir (neat) 3070, 2978 (S) 2925, 2890, 1587, 1481, 1434, 1391, 1260, 1166 (S), 1100 (S), 1080 (S), 1027, 1000, 957 (S), tlc ($CHCl_3$) Rf 0.52.

Anal. Calcd. for $C_{20}H_{29}O_3SiP$: C, 63.80; H, 7.76. Found: 63.60; H, 7.88.

$$1/2\ [Rh(CO)_2Cl]_2 + 2L \xrightarrow[\text{r.t., 30 min.}]{\text{ØH}} L_2Rh(CO)Cl + CO$$

2 1a 3a (92.6%)

$$(L = CH_3^aCH_2^bO\overset{\overset{CH_3^f}{|}}{\underset{\underset{CH_3^f}{|}}{Si}}CH_2^cCH_2^dP(C_6H_5^e)_2)$$

Chlorocarbonylbis[diphenyl(2-dimethylethoxysilylethyl)phosphine]rhodium 3a (MT-I-33)

Dichlorotetracarbonyldirhodium 2 was prepared by the method of McCleverty and Wilkinson[12] from $RhCl_3 \cdot 3H_2O$ and carbon monoxide (yield 95%), mp 124-125° (MT-I-55).

Using the method of McCleverty[13], a solution of silated phosphine 1a (1.266 g, 4 m mol) in benzene (10 ml) was added dropwise to a solution of rhodium dimer 2 (0.389 g, 1 m mol) in benzene (10 ml). Carbon monoxide was evolved and the solution changed in color from orange to yellow. After 30 min the solution was evaporated to about one-tenth its original volume, and 30 ml of ethanol was added. The solution was allowed

.o stand in a refrigerator (-22°) for 18 hr. The yellow crystals were filtered from the solution, washed with cold ethanol (5 ml x 3), and dried in vacuo. The yield of the rhodium complex 3a was 1.48 g (92.6%): tlc ($CHCl_3$) R_f 0.09; nmr ($CDCl_3$) δ 0.05 (S, 6H, H^f), 0.44-1.10 (m, 2H, H^c), 1.12 (t, 3H, J_{ab}=6.9 Hz, H^a), 2.25-2.78 (m, 2H, H^d), 3.57 (q, 2H, J_{ab}=6.9Hz, H^b), 7.20-7.83 (m, 10H, H^e); ir (KBr) 1952 (νCO).

Anal. Calcd. for $C_{30}H_{50}O_3Si_2P_2RhCl$: C, 55.60; H, 6.31; P, 7.75; Rh, 12.88; Cl, 4.44. Found: C, 55.67; H, 6.27; P, 8.05; Rh, 13.1; Cl, 4.70.

$$1/2[Rh(CO)_2Cl]_2 + 2\ L^* \xrightarrow[\text{r.t., 10 min.}]{\emptyset H} L^*_2\,Rh(CO)Cl + CO$$

2 3b (91.4%)

($L^* = (CH_3^aCH_2^bO)_3SiCH_2^cCH_2^dP(C_6H_5^e)_2$)

Chlorocarbonylbis[diphenyl(2-triethoxysilylethyl)phosphine]rhodium 3b (MT-I-5)

This compound 3b was prepared from rhodium dimer 2 and triethoxysilane 1b by the same method as used for 3a in a yield of 91.4% as yellow crystals: mp 108.5-109.5; tlc ($CHCl_3$) Rf 1.10; ir (KBr) 3072, 3060, 2979 (S), 2025, 2892, 1963 (vs), 1482, 1437 (S), 1392, 1264, 1164 (S), 1098 (S), 1070 (S), 1027, 1005, 965; nmr ($CDCl_3$) δ 0.70-1.10 (m, 4H, H^c), 1.12 (t, 18H, J_{ab}=6.9Hz, H^a), 2.38-2.82 (m, 4H, H^d), 3.77 (q, 12H, J_{ab}=6.9Hz, H^b), 7.22-7.96 (m, 20H, H^e).

Anal. Calcd. for $C_{41}H_{58}O_7Si_2P_2RhCl$: C, 53.56; H, 6.36; Cl, 3.86. Found: C, 53.17, H, 6.27, Cl, 3.67.

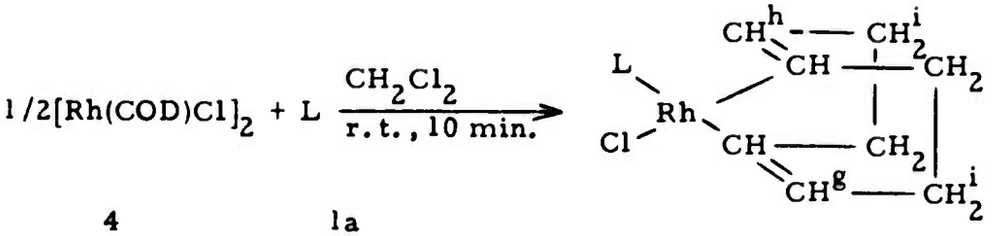

4 1a 5a (84.7%)

(L = $CH_3^aCH_2^bOSi(CH_3^f)_2CH_2^cCH_2^dP(C_6H_5^e)_2$)

Cycloocta-1,5-diene-(2-dimethylethoxysilylethyl)diphenylphosphinechlororhodium 5a. (MT-I-50)

Bis(cycloocta-1,5-diene)-μ,μ'-dichlororhodium 4 was prepared by the procedure of Chatt and Venanzi[14] from rhodium trichloride trihydrate and 1,5-cyclooctadiene in 66% yield (MT-I-49).

A solution of the silated phosphine 1a (1.266 g, 4 m mol) in methylene chloride (10 ml) was added dropwise to a solution of the rhodium dimer 4 (0.986 g, 2 m mol) in methylene chloride (10 ml). After 10 min at room temperature, the solution was evaporated and the product was washed with cold pentane. Recrystallization from methylene chloride-hexane afforded 1.905 g (84.7%) of rhodium complex 5a as yellow crystals: mp 96-97°; tlc (2% CH_3OH-$CHCl_3$) Rf 0.61; nmr ($CHCl_3$) δ 0.10 (S, 6H, H^f), 0.42-1.10 (m, 2H, H^c), 1.16 (t, 3H, J_{ab}=7.0Hz, H^a), 1.50-2.75 (m, 10H, H^d and H^i), 3.04 (bs, 2H, H^h), 3.65 (q, 2H, J_{ab}=7.0Hz, H^b),

5.46 (bs, 2H, H^g), 7.22-7.84 (m, 10H, H^e); ir 1434, 1250, 1100, 1076.

Anal. Calcd. for $C_{26}H_{37}OSiPClRh$: C, 55.47; H, 6.63; mol wt, 563. Found: C, 55.20; H, 6.63; mol wt, 543 (by osomometry in chloroform).

$$1/2[Rh(COD)Cl]_2 + L^* \xrightarrow[r.t., 10\ min.]{CH_2Cl_2} L^*Rh(COD)Cl$$

4 1b 5b (87.5%)

($L^* = (CH_3^aCH_2^bO)_3SiCH_2^cCH_2^dP(C_6H_5^e)_2$)

Cycloocta-1,5-diene-(2-triethoxysilylethyl)diphenylphosphinechlororhodium 5b (MT-I-8 and 64)

This compound 5b was prepared in 87.5% yield, starting with rhodium dimer 4 (493 mg, 1 m mol) and the silated phosphine 1b (753 mg, 2 m mol). Following the procedure used for 5a, yellow crystals were obtained from methylene chloride-hexane, recrystallization, mp 86-87°: tlc (2% CH_3OH-$CHCl_3$) Rf 0.57; nmr ($CDCl_3$) δ 1.0-1.3 (m, 2H, H^c), 1.19 (t, 9H, J_{ab}=6.8Hz, H^a), 1.6-2.8 (m, 10H, H^c and H^h), 3.03 (bs, 2H, H^h), 3.81 (q, 6H, J_{ab}=6.8Hz, H^b), 5.43 (bs, 2H, H^g), 7.13-7.92 (m, 10H, H^e); ir (KBr) 3052, 2972, 2922, 2880, 2831, 1483, 1433, 1390, 1262, 1163, 1100 (S), 1072 (S), 958, 760, 730, 693.

Anal. Calcd. for $C_{28}H_{41}O_3ClSiPRh$: C, 53.98; H, 6.63; mol wt, 623. Found: C, 53.79; H, 6.61; mol wt, 633 (by osmometry in chloroform).

$$Rh_4(CO)_{12} + 2L \xrightarrow[\text{r.t., 24 hr}]{\text{hexane, } N_2 \text{ flow}} Rh_4(CO)_{10}L_2$$

6 1a 7a (61%)

$$(L=CH_3^aCH_2^bOSi(CH_3^f)_2CH_2^cCH_2^dP(C_6H_5^e)_2)$$

Bis[diphenyl(2-dimethylethoxysilylethyl)phosphine]decacarbonyltetrarhodium 7a (MT-I-56)

This compound 7a was prepared by the modified method of Booth, et al.[16] The silated phosphine 1a (127 mg, 0.4 m mol) in hexane (15 ml) was added slowly to a stirred solution of freshly recrystallized dodecacarbonyltetrarhodium[15,17] (150 mg, 0.2 m mol) in hexane (15 ml) at -22° and stirred under a stream of nitrogen. After 1 hr the reaction mixture was warmed to room temperature and stirred for 18 hr. Evaporation of solvent afforded 264 mg of reddish brown hard oil. This material was then chromatographed on silica gel, eluting with chloroform, and 162 mg (61%) of pure 7a was obtained as dark red solid: mp 50-53°; tlc ($CHCl_3$) Rf 0.31; nmr ($CDCl_3$) δ 0.05 (S, 6H, H^f), 0.25-0.80 (m, 2H, H^c), 1.10 (t, 3H, J_{ab}=6.8Hz, h^g), 2.06-2.62 (m, 2H, H^d), 3.53 (q, 2H, J_{ab}= 6.8Hz, H^b), 7.17-7.70 (m, 10H, H^e); ir (KBr) 2062 (S), 2038 (vs), 2000 (S), 1837 (S), 1821 (S).

Anal. Calcd. for $C_{46}H_{50}O_{12}Si_2P_2Rh_4$: C, 41.71; H, 3.80; mol wt, 1325. Found: C, 41.26; H, 3.79; mol wt, 1312 (by osmometry in chloroform).

$$Rh_4(CO)_{12} + 2L^* \xrightarrow[\text{r.t., 48 hr.}]{\text{hexane, } N_2 \text{ flow}} Rh_4(CO)L_2$$

6 1b 7b (37.1%)

($L^* = (CH_3^aCH_2^bO)_3SiCH_2^cCH_2^dP(C_6H_5^e)_2$)

Bis[diphenyl(2-triethoxysilylethyl)phosphine]decacarbonyltetrarhodium 7b

(MT-I-20)

This compound 7b was prepared and purified in a similar manner as dimethylethoxysilane analog 7a from the rhodium tetramer 6 and the triethoxysilylphosphine 1b in 37.1% yield: nmr ($CDCl_3$) δ 0.15-0.98 (m, 2H, H^c), 1.13 (t, 9H, J_{ab}=6.9 Hz, H^a), 2.10-2.70 (m, 2H, H^d), 3.72 (q, 6H, J_{ab}=6.9Hz, H^b), 7.10-7.75 (m, 10H, H^e); ir(KBr) 2061 (S), 2039 (vs), 2000 (S), 1839 (S) 1820 (S).

Anal. Calcd. for $C_{50}H_{58}O_{16}Si_2P_2Rh_4$: C, 41.56; H, 4.05; mol wt, 1445. Found: C, 41.30; H, 4.16; mol wt 1103 (by osmometry in chloroform).

$$\equiv SiOH + LRh(COD)Cl \xrightarrow[\text{reflux, 18hr}]{\text{toluene}} (\equiv Si\text{-}O\overset{CH_3}{\underset{CH_3}{Si}}CH_2CH_2P\phi_2)Rh(COD)Cl$$

5a 6a

Treatment of Cabosil HS-5 with LRh(COD)Cl 5a (MT-I-39)

Cabosil HS-5 (1g) and the rhodium complexes 5a (150 mg, 0.267 mmol) were placed in a nitrogen filled flask, and dry degassed toluene (40 ml) was added. The mixture was refluxed under nitrogen for 18 hr, filtered and washed with benzene (approximately 10 ml x 4) until the washings were colorless. The product 6a was vacuum dried and analyzed.

Anal. C, 5.84; H, 0.68; Rh, 1.63.

Hydrogenation of 1-Decene in a Fischer-Porter Bottle. (Mt-II-15)

A Fischer-Porter bottle was charged with 200 mg (Rh: 1.15%, 2.5×10^{-5} Rh g. atom) of rhodium complex on silica gel, ($\equiv SiO\overset{CH_3}{\underset{CH_3}{Si}}CH_2-CH_2P\phi_2$)Rh(COD)Cl and flushed with nitrogen. Benzene (10 ml) and 1-decene (0.47 ml, 2.5 mmol) were added under a stream of nitrogen, and the bottle was thoroughly flushed with hydrogen by pressuring to 46 psi four times. The mixture was stirred at 25° under 46 psi of hydrogen and the reaction was followed by hydrogen pressure drop and checked by glc analysis (MT-V-15-1).

Reaction rate: 6.17 m mol H_2/hr.

Glc analysis (reaction time, 20 hr): Decane (100%), cyclohexane (1.70 mmol).

After the reaction of MT-II-15-1, 1-decene (0.474 ml, 2.5 mmol) was added to the reaction mixture and the same procedure was followed (MT-II-15-2).

Reaction rate: 17.9 mmol H_2/hr.

Glc analysis (reaction time, 7.5 hr): Decane (100%), cyclohexane (0.59 mmol, total 2.29 mmol)

After the reaction of MT-II-15-2, the bottle was repressured to 46 psi without addition of 1-decene to measure the rate of reduction of benzene (MT-II-15-3).

Reaction rate: 0.204 mmol/hr.

Glc analysis (reaction time, 11 days): cyclohexane (3.45 mmol, total 5.74 mmol).

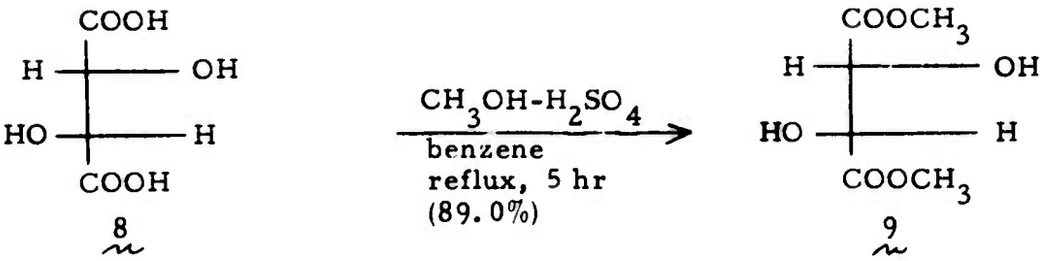

8 9

Dimethyl-L-tartrate 9 (MT-II-40)

Fifteen grams (0.1 mol) of L-tartaric acid 8, 108 ml (0.9 mol) of dry methyl alcohol, 60 ml of benzene, and 82 µl (0.15g) of concentrated sulfuric acid were placed in a 250 ml distilling flask. A distilling apparatus was attached and the system was heated with an oil bath. An azeotropic mixture of methanol, benzene, and water began to distill at 57.5°. Distillation was continued until the temperature rose to 59°, when further heating was suspended. After 54 ml (0.45 mol) of methanol and 30 ml of benzene were added, the flask was again heated until the temperature rose to 65°, when distillation was discontinued. Distillation of the residue after removal of solvents gave 13.51 g (75.9%) of a colorless oil 9, bp 116-118° (0.3 mm) [lit.[21] bp 158-158.5° (12 mm)].

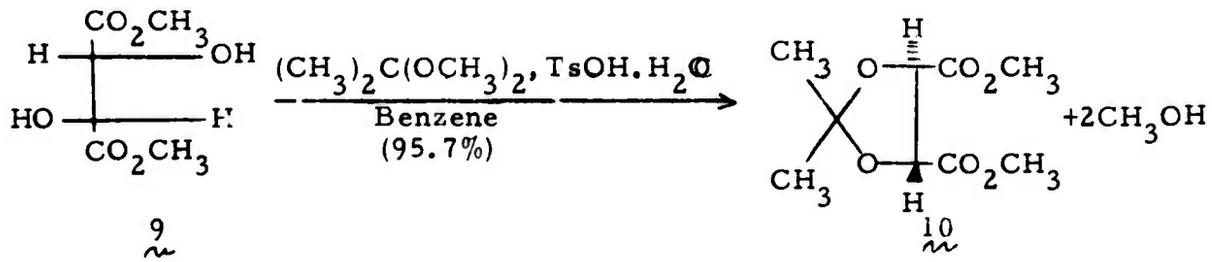

9 10

Dimethyl 2,3-O-isopropylidene-L-tartrate 10 (MT-II-42)

This acetonide 10 was prepared from dimethyl-L-tartrate 9 following a procedure similar to Carmack and Kelley[22].

A solution of 8.91 g (50 mmol) of dimethyl-L-tartrate 9, 6.25 g (60 mmol) of 2,2-dimethoxypropane, and 25 mg of p-toluenesulfonic acid monohydrate in benzene (20 ml) was refluxed; the benzene-methanol azestrope (bp 58°) was slowly removed at the head of a column packed with glass helices. After 3 hr, the temperature of the refluxing vapor had risen to 75°. The catalyst was neutralized with 50 mg of anhydrous potassium carbonate and the solvent and unreacted 2,2-dimethoxypropane were removed under reduced pressure. The product 10 was distilled as 10.45 g (95.7%) of a colorless liquid, bp 63-64° (0.02 mm).

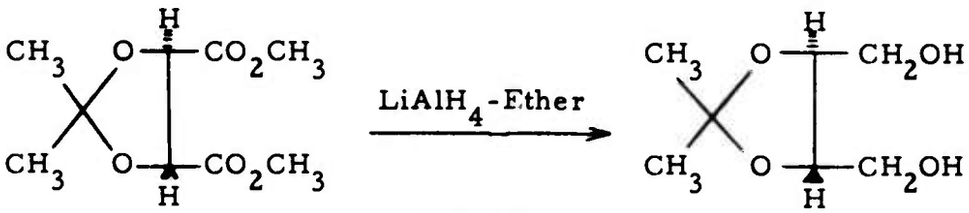

2,3-O-Isopropylidene-L-threitol 11 (MT-II-44)

This diol 11 was prepared from dimethyl 2,3-O-isopropylidene-L-tartrate 10 using the method of Feit[23].

A solution of $LiAlH_4$ (4.2 g, 0.111 mol) in diethyl ether (40 ml) was refluxed for 30 min with vigorous stirring. A solution of dimethyl 2,3-isopropylidene-L-tartrate 10 (10 g, 45.8 mmol) in diethyl ether (50 ml) was added dropwise without heating over a period of 1 hr, the heat of reaction causing a gentle refluxing. After additional heating for 2 hr ethyl acetate (5 ml) was carefully added, and the reaction mixture was cooled to 0°. After successive cautious additions of water (4.2 ml),

4N NaOH (4.2 ml), and water (13 ml), the inorganic precipitate which had formed was removed by filtration and extracted in a Soxhlet extractor with ether. The combined ethereal extracts were dried ($MgSO_4$) and evaporated under reduced pressure. Distillation of the residual yielded 2.3-O-isopropylidene-L-threitol 11 (5.36 g, 72.0%), bp 93.0-95.5° (0.02 mm) [lit.[23] bp 91-93° (0.01-0.02 mm)].

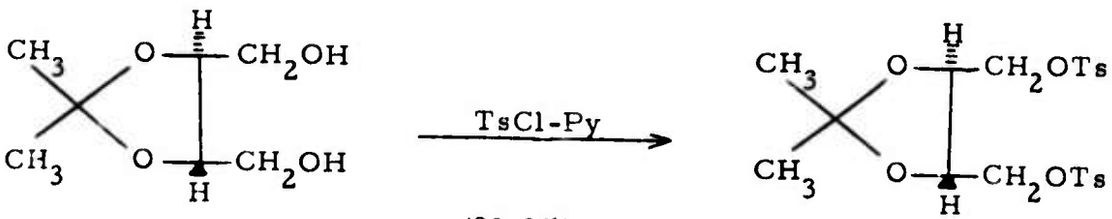

(89.2%)

1,4-Ditosyl-2,3-isopropylidene-L-threitol 12 (MT-II-46)

This ditosylate 12 was prepared by the method of Rubin et al[24]. To 3.0 g (18.5 mmol) of 2,3-isopropylidene-L-threitol 11 in 20 ml of dry pyridine, 7.6 g (40 mmol) of finely powdered, freshly recrystallized p-toluenesulfonyl chloride were added in one portion at -10°. The mixture was stirred until homogeneous and the flask was placed in a refrigerator (4°). After 20 hr, the reaction mixture was permitted to continue at 0° for 2 hr. The product was filtered and washed with 95% ethanol. It was recrystallized from 22 ml of ethanol giving 7.7 g (89.2%) of mp 91-92° [lit.[24] 91-92°]. $[\alpha]_D^{24}$ -12.3° (C5, chloroform) [lit.[24] $[\alpha]_D^{24}$ -12.4° (C5, chloroform)].

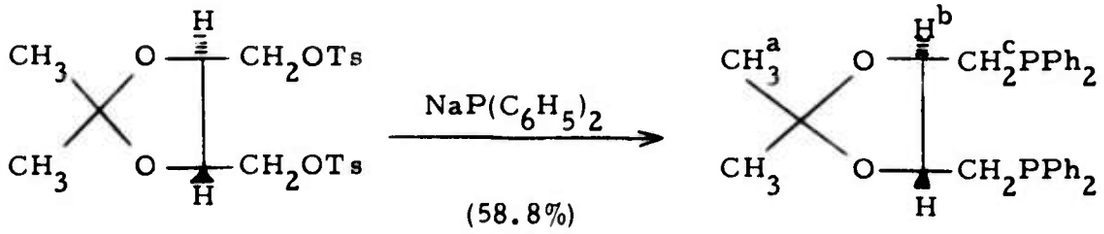

L-2,3-O-Isopropylidene-2,3-dihydroxy-1,4-bis(diphenylphosphino)-butane 13 (MT-II-49)

This diphosphine 13 was prepared by a modification of the method of Kagan and Dang[25].

A solution containing 5.28 g (24 mmol) of $P(C_6H_5)_2Cl$ and 2.3 g (0.1 mol) of sodium in 30 ml of dioxane was refluxed under nitrogen with rapid mechanical stirring for 4 hr. The yellow reaction mixture was allowed to cool to room temperature, whereupon 20 ml of dry THF was added. Ditosylate 12 (4.23 g, 9 mmol) in 10 ml of THF was added dropwise, and the mixture was stirred for another 2 hr and filtered. The precipitate was washed with benzene, and the combined filtrate and washings were evaporated to dryness under reduced pressure. The residue was taken up in 12 ml of ethanol and allowed to stand in a refrigerator (-22°). After 2 days the precipitate was filtered, washed with 1 ml cold ethanol, and dried under vacuum. The crude diphosphine was recrystallized twice from ethanol affording 2.83 g (58.8%) of pure 13; mp 88-89°; tlc ($CHCl_3$) Rf 0.45; $[\alpha]_D^{24}$ -12.3° (C 4.57, C_6H_6); nmr (CCl_4) δ 1.25 (S, 6H, H^a), 2.27 (bd, 4H, J_{bc}= 5.4 H_2, J_{pCH}=~0, H^c, 3.84 (bq, 2H, H^b), 7.08 (bs, aromatic).

Anal. Calcd. for $C_{31}H_{32}O_2P_2$: C, 74.70; H, 6.47; P, 12.43. Found: C, 74.75; H, 6.69; P, 12.54.

References

(1) R. H. Grubbs and L. C. Kroll, J. Amer. Chem. Soc., 93, 3062 (1971).

(2) J. P. Collman, L. S. Hegedus, M. P. Cooke, J. R. Norton, G. Dolcetti and D. Marquardt, ibid., 94, 1789 (1972).

(3) R. H. Grubbs, C. Gibbons, L. C. Kroll, W. D. Bonds, Jr., and C. H. Brubaker, Jr., ibid., 95, 2374 (1973).

(4) K. G. Allum, R. D. Hancock, S. McKenzie and Pitkethly, preprint of paper to be published in the Proceedings of the Fifth International Congress on Catalysis, Amsterdam, 1972.

(5) L. S. Hegedus, Research Report, April 1971.

(6) D. Valentine, Jr., Research Report, August 1971.

(7). D. N. Marquardt, Research Report, July 1972.

(8) J. R. Shapley, Research Report, August 1972.

(9) K. Deuel, J. Wartmann, K. Hutschnecker, U. Schobinger and C. Guedel, Helv. Chim. Acta, 42, 1160 (1959).

(10) W. Parr and K. Grohmann, Tet. Lett., 2633 (1971).

(11) Von Heinz Niebergall, Makromol. Chem., 52, 218 (1962).

(12) J. A. McCleverty and G. Wilkinson, Inorganic Syntheses, 211 (1966).

(13) J. A. McCleverty and G. Wilkinson, ibid., 8, 214 (1966).

(14) J. Chatt and L. M. Venanzi, J. Chem. Soc., 4735 (1957).

(15) S. H. H. Chaston, F. G. A. Stone, J. Chem. Soc. (A), 500 (1969).

(16) B. L. Booth, B. J. Else, R. Fields and R. N. Haseldine, J. Organometal. Chem., 27, 119 (1971).

(17) D. N. Marquardt, NP III, 39.

(18) M. Boudart, A. W. Aldah and M. A. Vannice, J. Catal. 18, 46 (1970).

(19) J. A. Osborn, F. H. Jardine, J. F. Young and G. Wilkinson, J. Chem. Soc. (A), 1711 (1966).

(20) C. O'Connor and G. Wilkinson, ibid., 2665 (1968).

(21) Y. Tsuzuki, K. Tanabe, K. Okamoto, M. Fukubayashi, Bull. Chem. Soc. Japan, 39, 1387 (1966).

(22) M. Carmack and C. J. Kelley, J. Org. Chem., 33, 2171 (1968).

(23) P. W. Feit, J. Med. Chem., 7, 14 (1964).

(24) L. J. Rubin, H. A. Lardy and H. O. L. Fisher, J. Amer. Chem. Soc., 74, 425 (1952).

(25) H. B. Kagan and Tuan-Phat Dang, ibid, 94, 6429 (1972).

(26) A. S. Hussey and Y. Takeuchi, J. Org. Chem., 35, 643 (1970).

(27) F. H. Jardine, J. A. Osborn and G. Wilkinson, J. Chem. Soc. (A), 1574 (1967).

(28) R. E. Harmon, S. K. Gupta and P. J. Brown, Chem. Rev., 73, 21 (1973).

(29) A. S. Hussey, G. W. Keulks, G. P. Nowack and R. H. Baker, J. Org. Chem., 33, 610 (1968).

(30) A. S. Hussey, Y. Takeuchi, J. Amer. Chem. Soc., 91, 672 (1969).

(31) J. C. Schlatter and M. Boudart, J. Catal., 24, 482 (1972).

(32) D. Evans, J. A. Osborn and G. Wilkinson, J. Chem. Soc. (A), 3133 (1968).

(33) W. S. Knowles, M. J. Sabacky and B. D. Vineyard, Chem. Commun., 10 (1972).

(34) M. L. Hair and W. Hertl, J. Phys. Chem., 73, 4269 (1969).

C. Preparation and Characterization of Hybrid Homogeneous-Heterogeneous Catalyst Materials: II. Synthesis and Structural Characterization

M. Marrocco

Introduction

Silica surfaces, due to uses in chromatography, and widespread and variagated employment in industry, find themselves among those most thoroughly investigated. Silica owes its sundried application to the ease of preparation of extermely small particles with a microporous structure leading to a remarkably high surface area per unit weight of material. One gram will display up to 800 square meters of surface. The literature is riddled with attempts to understand the properties of silica surfaces; much of the experiment being redundant and some lesser amount of the analysis. Surprisingly little has been determined since Iler's book published in 1955. Commercial preparative methods have not changed since then. With the help of the electron micrograph the physical structure of the particles (down to 5 in diameter) and aggregates was known. The standard method of surface area determination (by N_2 adsorption) was then in use. Hydrocarbon 'esters' of silica surfaces had been produced and their oleophilic and hydrophobic properties studied.

Since then the major efforts have been toward the elucidation of the adsorptive mechanism. In particular much time has been spent on the nature of adsorbed waters and the arrangement of surface hydroxyl groups. The following is a sketchy survey of developements of the last five years.

It is certain that on exposure to air silica (the surfaces reviewed here are of the intermediate surface area type, known as

Cab-o-Sils) picks up several monolayers of water. By heating in vacuo this water and to a certain extent surface hydroxyls are lost. It was desired to determine the arrangement of the risidual -OH groups. It was known (DeBoer and Vleeskens[2]) that after repeated annealing and rehydroxylation a limiting surface density of 4.6 -OH/100 $Å^2$ was attained. It had also been found[3] that of these 3.2/100 $Å^2$ existed in hydrogen bonded pair and 1.4/100 $Å^2$ as free Si-OH, the free groups being stable to much higher temperatures. The most valuable analytical tool at this time was infrared spectroscopy. The band observed at 3750 cm^{-1} was assigned to the free hydroxyls and the 3550 cm^{-1} band to those paired. A third band at 3650 cm^{-1} was ascribed to non-hydrogen bonded or 'internal' -OH's and was lost on heating. These assignments are still generally accepted as correct. Peri and Hensley[4] modeled the silica surface by using a monte-carlo method to randomly dehydrate a β-cristobalite (100) face. This gave 4.56 -OH/100 $Å^2$ with 1.22 of these being geminal. Karger and Hartkopf[5] found that of the free hydroxyls 40% are isolated and 60% are geminal pair. Hertl and Hair[6], who have done much of the work on silica surfaces, found hydrocarbons to adsorb preferentially on the free lone -OH groups and non-hydrocarbon adsorbates to be accepted by both the free and geminal groups, the latter acting as one reactive site. The vicinal pair did not adsorb in the absence of water, this being explained by the following mechanism;

The paired -OH's are hydrogen bonded too strongly to interact with external molecules. The adsorbed water on the other hand can hydrogen bond as well as a water surface. Robert[7] et al felt that a water surface would be a useful model for silica gel (wet). This being based on a correlation between interfacial surface tention of various organic liquid- water systems and the adsorptive affinities of these organics for silica gel. Tyler[3] et al modeled silica gel as a mixture of crystalline silica surface planes.

In 1968 Hertl and Hair[8] studied the reaction of $MeSi(OMe)_3$ and Cab-oSil. At room temperature the silane was only physically bound and could be removed by pumping. At 100° chemically bonded siloxanes were formed. These produced a broad peak at 3350 cm^{-1}. The rates of reaction of a few siloxanes were given in a later paper.[9]

$$r = A \exp(-E/RT) [OH]^m [\theta]^n$$

	m	n	$E_{activation}$ (kcal/mole)
$MeOSi(Me)_3$	1.6	1.7	22 ± 3
$(MeO)_2Si(Me)_2$	2.2	2.2	32.0 ± 1.5
$(MeO)_3SiMe$	3.0	3.0	30.6

$[\theta]$ is the fraction of $[OH]$, the surface hydroxyl density, covered by physically adsorbed siloxane. They note the equvalence of m and n indicates the configuration of the chemically bonded molecule is like that of the adsorbed molecule. In no case were any changes observed in the intensity of the band at 3650 cm^{-1}, showing that the hydrogen bonded hydroxyl groups are non reactive toward methoxy silanes. The same authors later found the rate $r = k[OH]^2[HMDS]$ with E_a = 18.5 kcal/mole for reaction of

Cab-o-Sil with $[(Me)_3Si]_2NH$.

Low and Morterra[10] found that after the rather severe treatment of methoxylating with MeOH and demethoxylating at 600°C $\geqslant$Si-H and $\geqslant Si\langle_H^H$ groups (2300cm^{-1} and 2227cm^{-1}) appeared and the surface activity increased dramatically to the point of adsorbing H_2.

Hertl and Hair[11] discovered a layered structure of water adsorbed on silica by examination of adsorbtion isotherms. These showed knees at 1.3 and 6 H_2O's/ pair surface -OH. Bermudez[12] calculated 4.2 -OH/100 Å^2 from NMR data of Kamiyoshi.[13] Hertl and Hair[14] determined the silica pK_a to be 7.1 = 0.5 from solvent shifts of the OH vibration. Morrow and Devi[15] found the BF_3 surface product to be -Si-O-BF_2 utlizing IR and isotopic exchange (^{18}O). Kagiya[16] et al in a study of preferential adsorption from binary liquid systems, showed a correlation between the surface coverage and the Hammitt values of the adsorbate. By comparing coverages to the BET (N_2) values they predicted a flat orientation for benzene (parallel to the surface) and an end on packing for 1,4-dioxane. Liebich and Fink[17] found an increase in the adsorptive power of a silica surface for Hg on esterification to produce $\geqslant$Si-O-Si$(CH_3)_3$. Isotherms at 120°C gave 140 ng/m^2 at 4x10^{-2} torr for the esterified surface. This is equvalent to 4.2x10^{-4} Hg atoms/100 Å^2.

Bascom[18] showed the utility of CCl_4 as a media for IR studies. He found Cab-o-Sil with greater than .9 H_2O/100 Å^2 to promote the reaction: $(Me)_3SiOMe + H_2O_{surface} \xrightarrow{CCl_4} (Me)_3SiOH + MeOH$

$\not\rightarrow (Me)_3Si\text{-}O\text{-}Si(Me)_3$

Fripiat[19] et al found this region of water coverage to entertain changes in entropy losses indicating the onset of a transition

from an immobile to a mobile water layer. Surface conductivity also increased indicating more mobile charge carriers, possibly a $H_3O^+ + H_2O \longrightarrow H_2O + H_3O^+$ mechanism. Bascom suggested a four center mechanism for the hydroysis, consistant with solution chemistry of silyl ethers. M. Takeda[23] has already presented a brief review of the literature of ligands chemically supported on silica in his research report.

This work is concerned with the functionalization of a ligand esterified to a silica gel surface. The immediate purpose being to prepare a heterogeneous hydrogenation catalyst by coordination of a transition metal compound to this functional ligand and to investigate its properties. The work of M. Takeda[23] in this lab has resulted in the preparation of the ligand: $EtOSi(CH_3)_2CH_2CH_2P\emptyset_2Rh(COD)Cl$ COD ≡ 1,5 cyclooctadiene and its product with Cab-o-Sil, an active hydrogenation catalyst. This compound was chosen as a possible analogue of Wilkinson's catalyst.[20,21,22] In application Takeda's catalyst exhibits a number of interesting properties. There is an initiation period which increases as the catalyst is stored for longer times before the first use. The rate of the first run is invariably slower (by an order of magnitude) than subsequent runs. A two fold increase in Rh content (by elemental analysis) can effect a sixty fold increase in rate.

My interests were to study this type of catalyst utilizing electron microscopy and to duplicate some of the kinetic results mentioned above. The electron microscope lends itself nicely to this problem due to the relative ease of sample preparation. It is the state of the metal that is of primary importance; not only

in the catalysis problem but also in the interest this group has had in thin metal films and their potential electrical properties. Although a good amount of care is necessary to prevent foreign material from becoming a problem a minimal amount of sample manipulation is required. The silica gels are dusted onto a copper grid (400 mesh) supporting a thin carbon film. Since the object of interest is a heavy metal no shadowing is necessary. The density of the silica is also different enough from the carbon film to render it plainly visible. The silica particles are on the order of .01μ (100 Å) in diameter. Any metal particles to be visible would need to be 1 mμ (10 Å) or greater.

Results and Discussion

The electron microscope used was a Philips EM 200. All micrographs were taken on 35 mm film and printed on polycontrast paper without alteration. Absolute dimensions have uncertainties up to 10% due to sample position. This is evidenced in micrographs 1 and 2 taken of spheres in the same grid square. These spheres are a 10% polystyrene latex prepared by Dow and used in Pecora's group as standards for light scattering experiments. They measure 0.109μ in diameter with a standard deviation of .0027 on 318 measurements. All dimensions indicated are averages taken from the latex standard. The micrographs refered to in the text can be found in appendix 3 along with a discription of each.

Metal particles are plainly visible in a number of samples photographed. The dark spots in micrograph 16, measuring 10-50 A in diameter are metallic in nature. Similar centers are visible in 13 and 14. That they are crystallites of metal is suggested by their higher density and verified in micrograph 15 which is a dark field image of an area close to 14. This type of photograph is produced by tilting the incident electron beam off axis. By

this procedure the transmission image is no longer visualized but rather those electrons which are deflected by the sample. A crystalline sample will at certain angles Bragg reflect the beam and bright spots will be seen in the field of view.

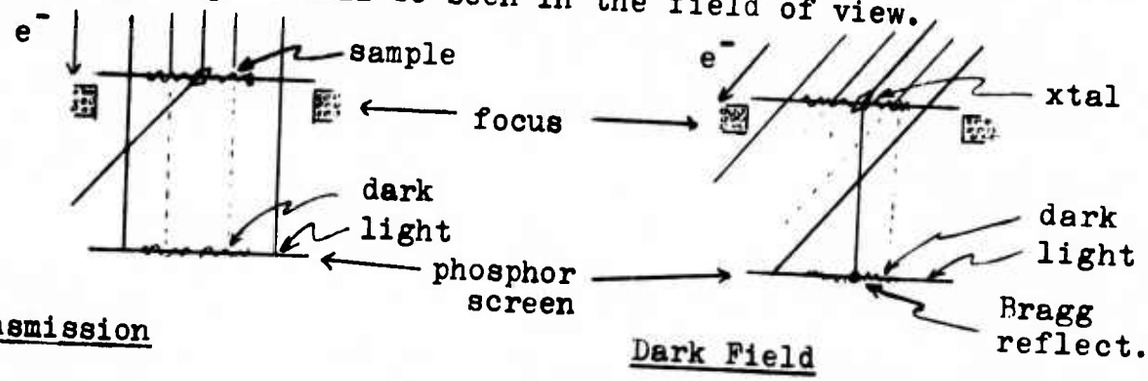

The sample now diffuses the beam which is refocused onto the screen. The crystals do not destroy the collimation of the beam and on focusing are essentially points. The presence of a bright spot in dark field coincident with a high density area in the normal micrograph demonstrates the metallic crystallite nature of these areas. If the particles are sufficiently large (ca 100 Å) a selected area diffraction pattern may be produced. This is shown for micrograph 13 in pattern A. This pattern shows the crystallite at an arbitrary angle as sample orientation was not possible on the instrument used. It shows sixfold symmetry which is consistant with the cubic structure of Rh metal. Samples of Rh on alumina give patterns which appear similar. Work is in progress to confirm this by taking patterns at known crystal orientation. Characteristic rings can be produced if the molecular density is high enough. This has not been the case for Rh compounds in our samples. Micrograph 17 shows three types of particles found in MT-28-4 prepared by M. Takeda. One mass of silica is free of crystallites, one seems to have several centers and the third object seems to contain a metal sphere 300 Å across.

A diffraction pattern of this object was unfortunately not obtained. Although not shown dark field confirmed its metallic nature.

Micrographs 20 and 21 are of a polystyrene Rh product produced by D. Marquardt. Preparation of these samples for microscopy necessitates embedding in epoxy resin and sectioning with an ultramicrotome to 1000 Å. Apparent are chatter marks produced in sectioning. These are quite difficult to avoid and the skilled microscopist, I understand, tries to make them large and photograph between them. Also obvious are the metallic centers. Why these prefer to lie on chatter edges I don't know. They seem to surround slightly denser regions, perhaps due to their formation on the surface of small globules of polystyrene.

Of paramount interest is the great dominance of metallic centers in Takeda's samples relative to those prepared by this author. This is ture both before and after their use in hydrogenation. For comparison see micrographs 4-12 prepared for this study and 13-17 by Takeda. My first attempts to produce the catalyst followed formulations which represented concentrations of Rh complex which were near the mean of those used by Takeda. M-10Y (9&10) however contained a 15 fold excess of Rh reactant to facilitate greater coverage. Micrographs show this sample appeared essentially the same before and after use and contained a few orders of magnitude less metal centers than Takeda's samples. An effect first noticed in micrograph 17 was again evident with M-10Y (9 & 10). A silica aggregate either contained no crystallites or at least a few. Only two aggregates out of 24 examined of M-10Y contained metal centers. Their Bragg reflections were also just noticeable suggesting they were smaller.

An attempt was made to image $Rh_6(CO)_{16}$ clusters by

solution in epoxy and sectioning. These attempts failed, in part due to the low solubility of these clusters in all solvents tried. A grainyness was noted; however this sort of artifact is easily produced by improper focus and must be discounted.

Experiments to determine catalytic rate were initially frustrated by lack of observable activity. All measurements were done at one atmosphere of H_2, using the apparatus described by Takeda. The catalysts were to be duplicates of those first prepared by Takeda with the exception that their preparation and use was to exclude entirely air and water. The possible effects of a surface layer of water were covered in the first section of this report. Hertl and Hair justify their study of surface water, " since small quantities of water are known to have a great effect in either accelerating or poisoning the rate of catalytic reaction on surfaces." The initiation period and its dependence on storage time noted by Takeda might have been due to oxide formation. The procedure first applied was to perform all transfers, filtering etc. in the dry box, which were otherwise done in air. See appendix 2 for preparatory methods.

Of five preparations rates were detected only for the last two, M-9 and M-10Y. A rate was also measured for a sample which had been heated to 250° in the absence of air. This sample, M-7, was grey in color and shows numerous metal particles in the micrographs (11& 12). The catalysts are normally tan in color before use and the active catalyst will become grey (grey-green in solution) during the hydrogenation. This was found to be true by Takeda as well as myself. These rates were all slower than those measured by Takeda; however M-9 showed the storage dependent initiation. The discrepancies are either due to a poisoning

effect or the different preparative method. The dry box atmosphere is free of water and O_2 but other experiments necessitate the presence of sundry volatiles. An inferior (or even sufficiently different, as catalysts have been known to be remarkably fickle) technique to that of Takeda might also have influenced the results. Experiments to show poisoning by Hg were frustrated by an undeliberate loss of activity before the Hg could be introduced.

These results contrast with those of Takeda in two respects. First catalytic activity was either not attained or was an order of magnitude slower in this study. Second, all samples prepared by this author showed no crystallites in the micrographs, while all of Takeda's samples examined showed numerous metal centers. Exceptions to this were M-10Y, which was prepared using a 15 fold excess of $Rh(COD)Cl/_2$, showing only a few crystallites; and M-7 which was heated to 250°, presumably destroying the surface ligand, showing a large number of metal particles. The fastest rate measured in this study was that sample showing the most crystallites. Faster rates were measured by Takeda whose samples contained a greater number of crystallites. Rh on alumina exhibiting somewhat more metal gave the fastest rate found by either of us. There would seem to be a definite correlation between the existence of these centers and catalytic rate. The problem now becomes to discover the mechanism of their formation. New techniques are being used to insure the integrity of the samples against air and water. Drying is done at diffusion pump pressure (with appropriate Hg traps) and reactions are carried out in modified Fischer-Porter bottles to avoid use of bench line N_2 not rigorously dry.

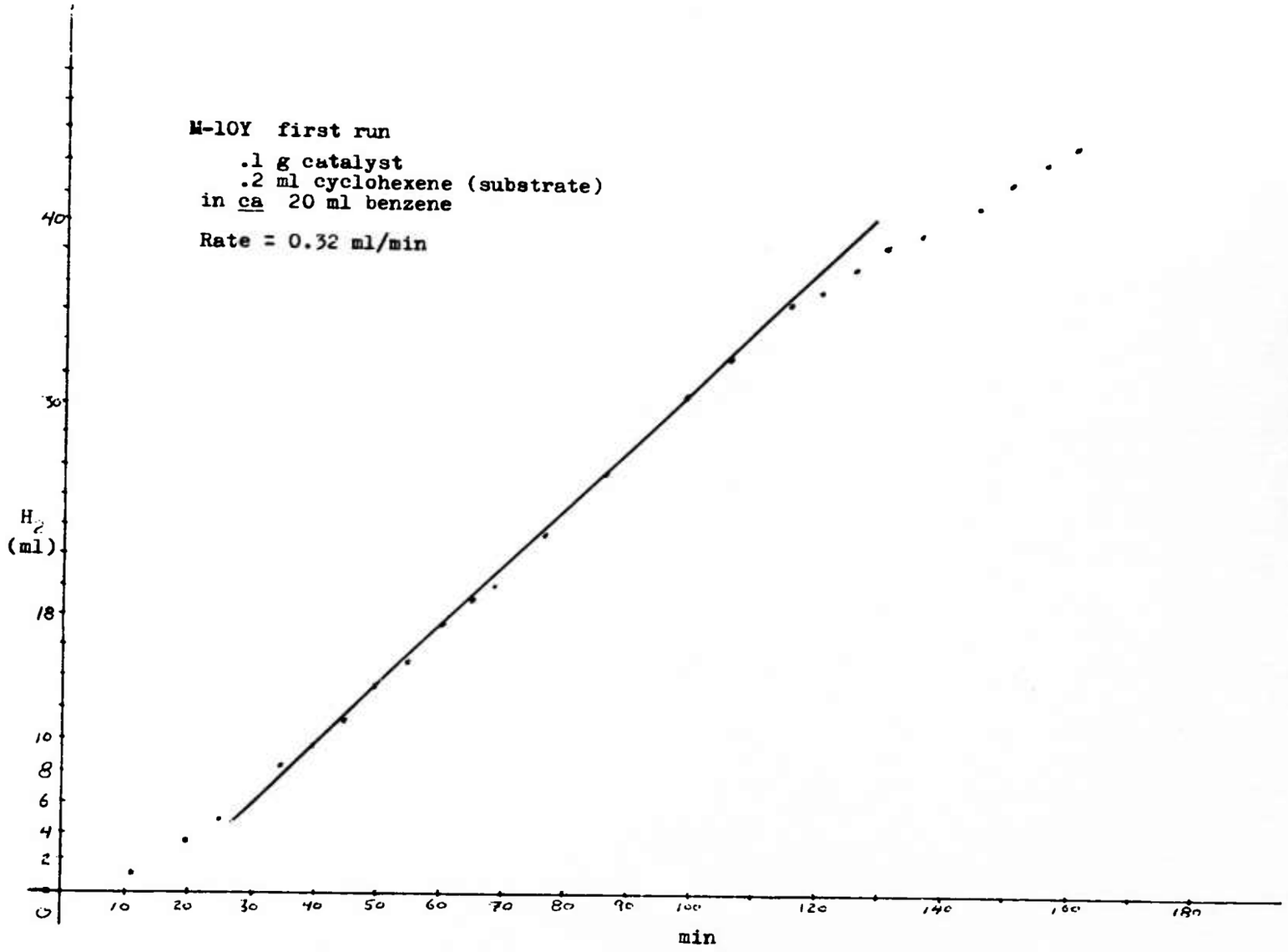
M-10Y first run
.1 g catalyst
.2 ml cyclohexene (substrate)
in ca 20 ml benzene
Rate = 0.32 ml/min
H2 (ml)
40
30
18
10
8
6
4
2
0
10
20
30
40
50
60
70
80
90
100
120
140
160
180
min

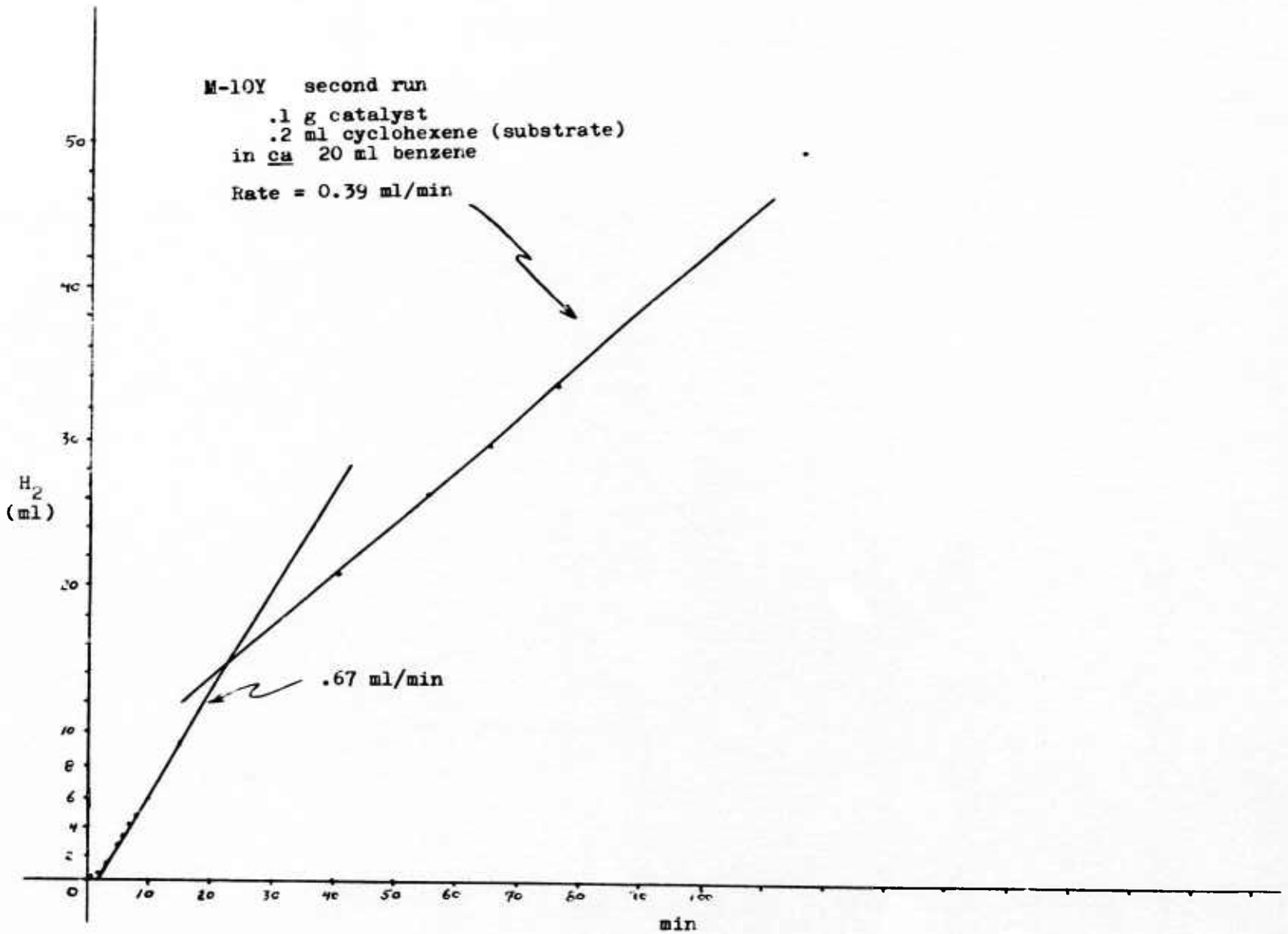
M-10Y second run
.1 g catalyst
.2 ml cyclohexene (substrate)
in ca 20 ml benzene
Rate = 0.39 ml/min
.67 ml/min
H2 (ml)
min
0
10
20
30
40
50
60
70
80
90
100

M-10Y third run

.1 g catalyst
.1 ml cyclohexene (substrate)
in ca 20 ml benzene

Rate = 0.71 ml/min

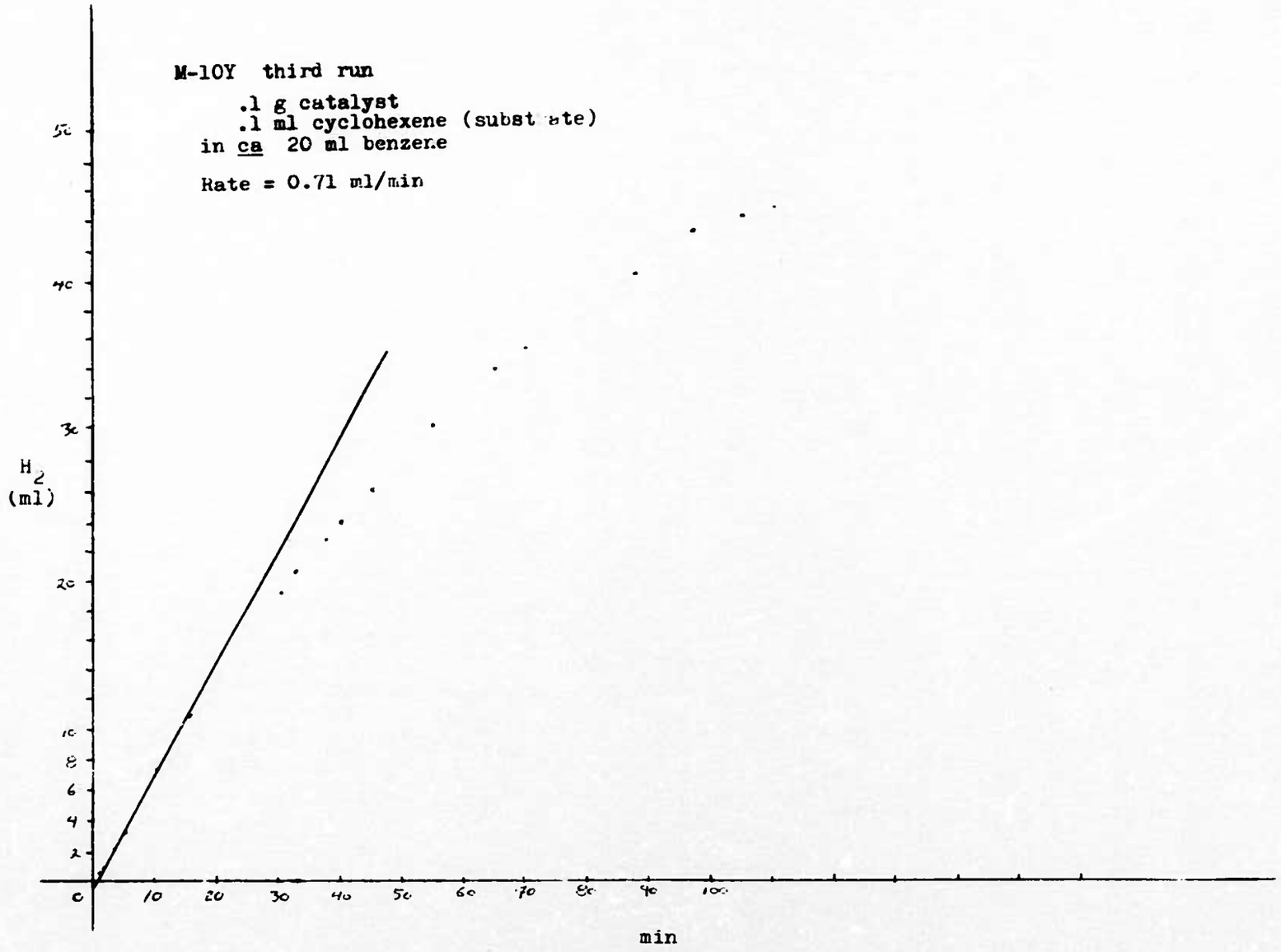

M-9 first run
(immediately after prepn)

.1 g catalyst
.2 ml cyclohexene (substrate)
in ca 20 ml benzene
Rate = 0.37 ml/min

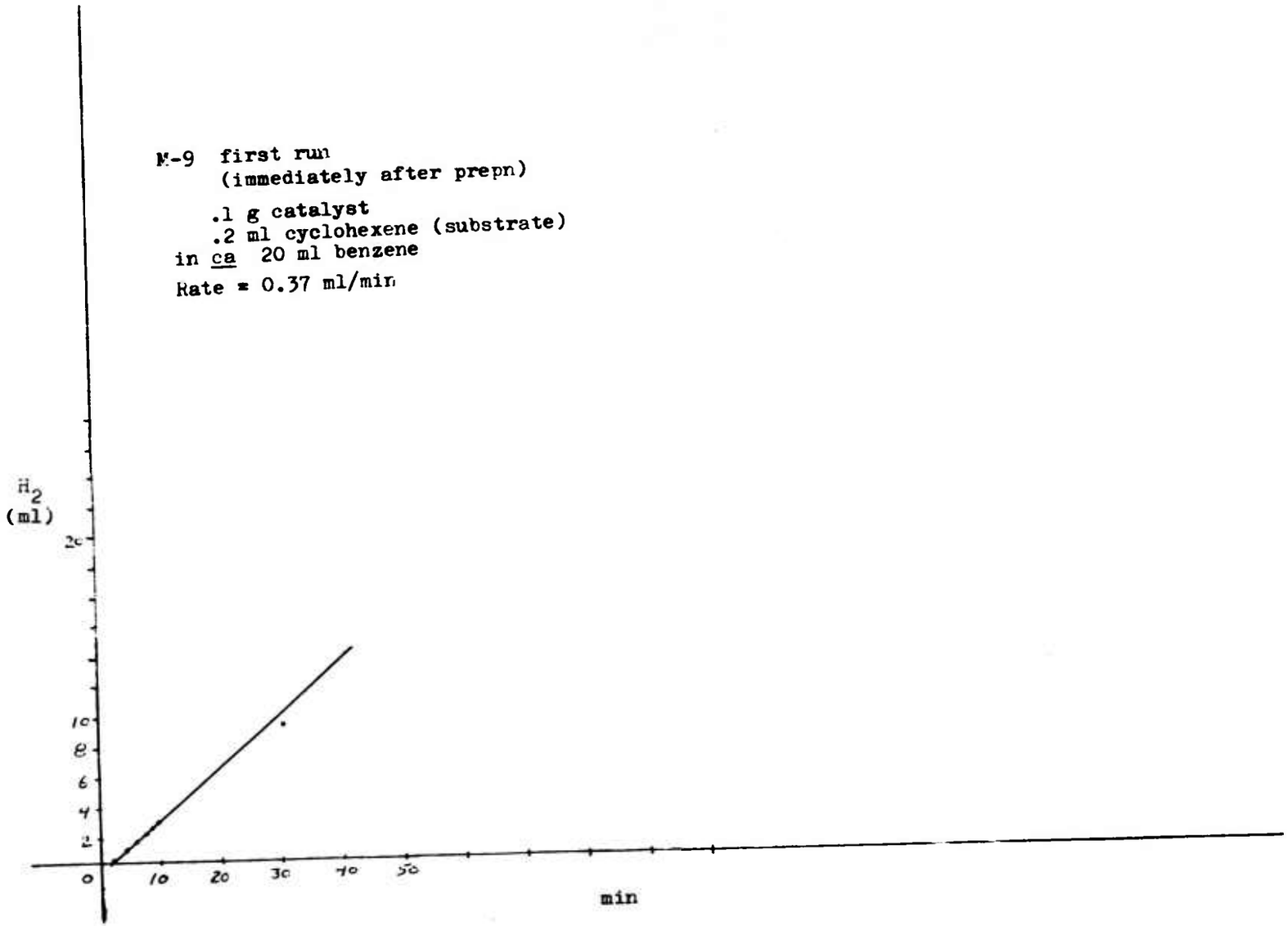

M-9 Catalyst had been stored 10 days before use. The first run showed no activity over 4 hrs. The catalyst was left in benzene under H_2 for 3 days. Additional substrate was added and the rate shown recorded.

second run
.1 g catalyst
.2 ml cyclohexene (substrate)
in ca 20 ml benzene

Rate = 1.2 ml/min

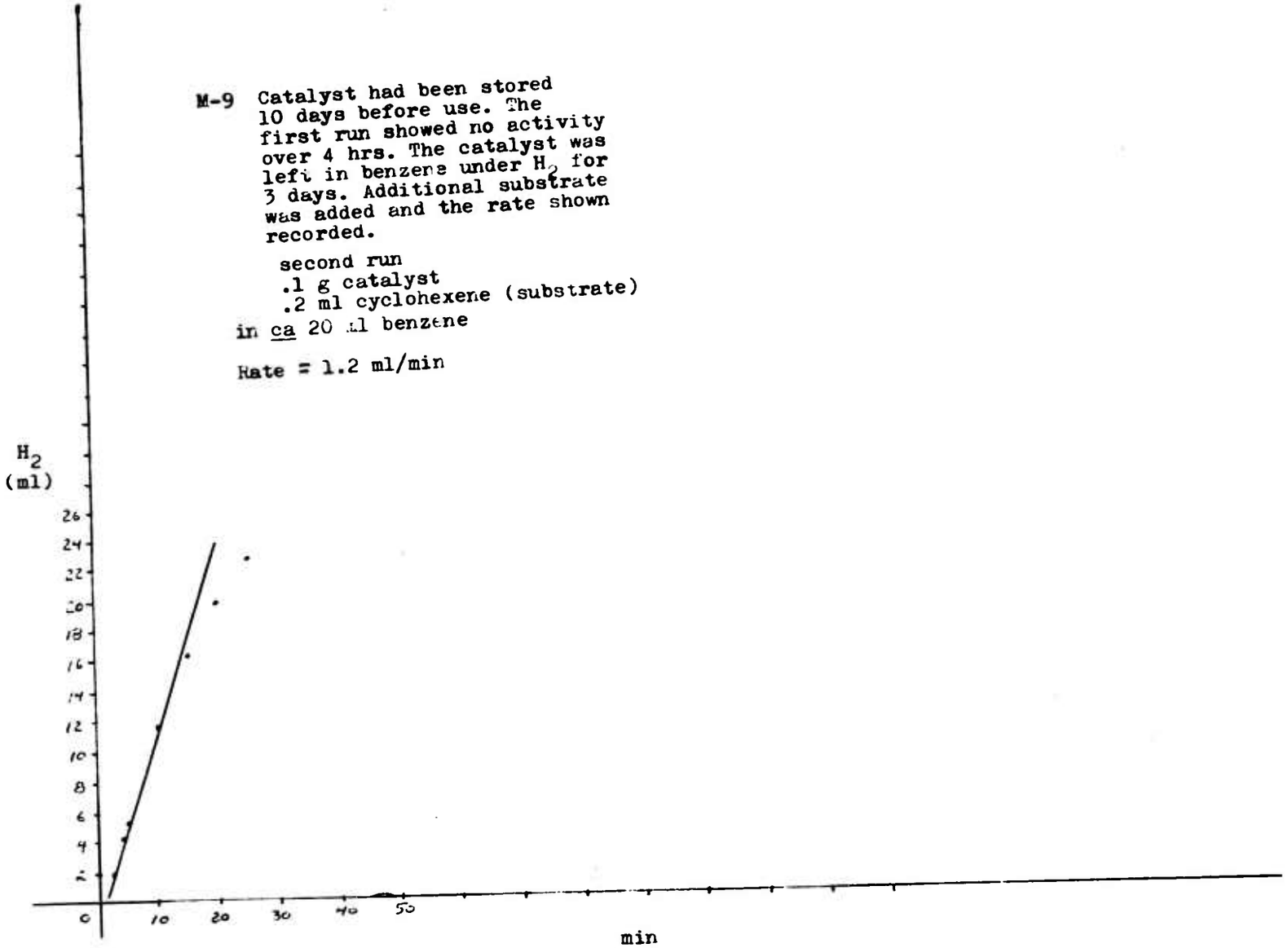

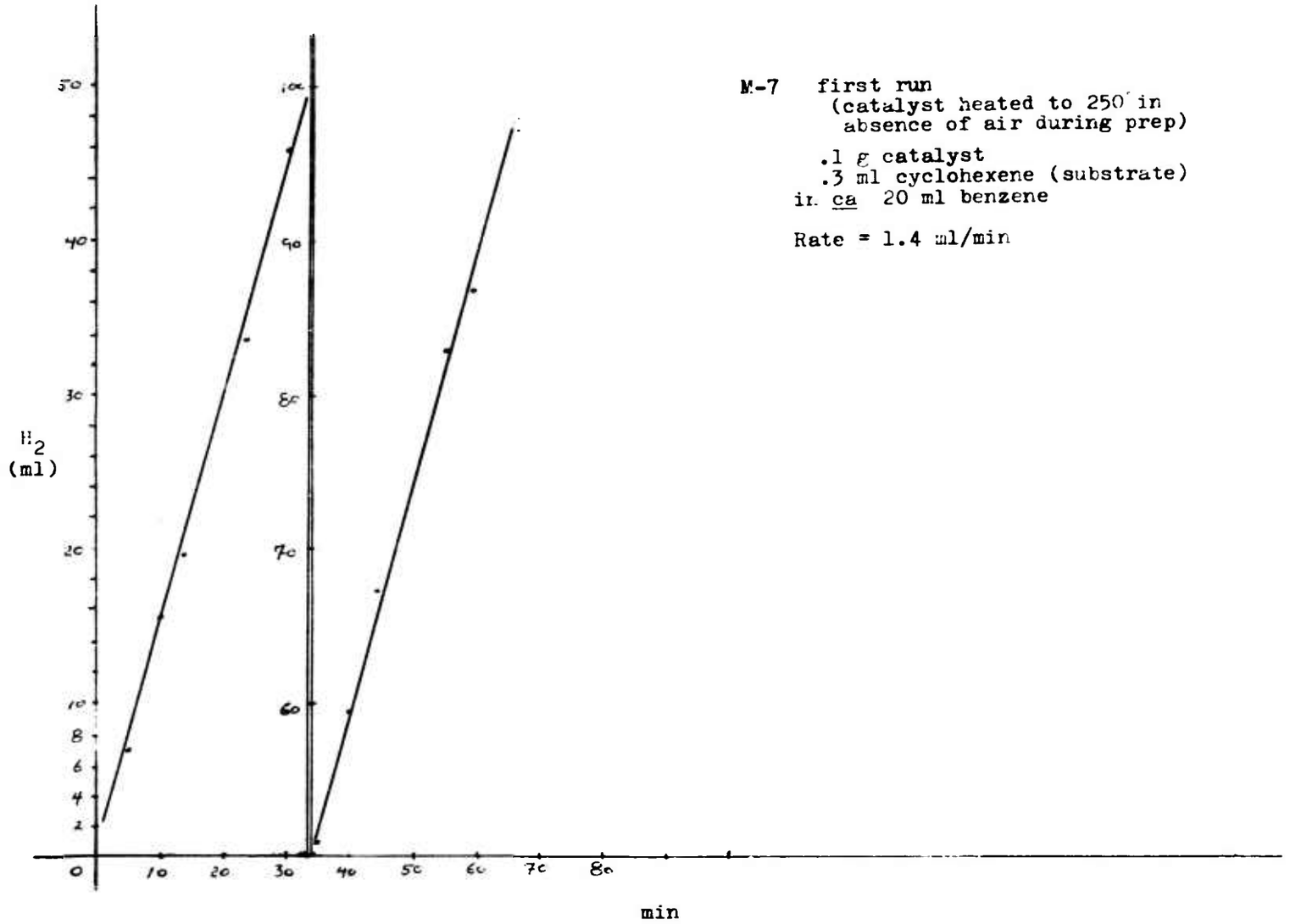

M-7 first run
(catalyst heated to 250° in absence of air during prep)

.1 g catalyst
.3 ml cyclohexene (substrate)
in ca 20 ml benzene

Rate = 1.4 ml/min

Appendix 2

Typical catalyst preparation:

Cab-o-Sil M-5 (200 m^2/g) Cabot Corp. was dried on a mechanical pump vacuum line in ca 20 gram quantities at 350 C for 24 hrs. .5 g (assuming 4.6 -OH/100 A^2 .5 g = 7.7×10^{-4} mol Si-OH) was transferred (in dry box) to a reflux apparatus with .25 g (7.9×10^{-4} mol) $EtOSi(CH_3)_2CH_2CH_2P\phi_2Rh(COD)Cl$ in ca 25 ml dry xylene. This system was closed, removed from the dry box and set up to reflux under a slight positive pressure of dry N_2 for 18-24 hrs. The system was then closed and reopened in the dry box where the product (tan-orange) was filtered and washed with 3x15 ml xylene (- 15 ml CH_2Cl_2 on some runs). The product was then left to dry, weighed and loaded into a sealable hydrogenation vessel. This was brought out, adjoined to the body of the hydrogenation apparatus and run immediately. M10-Y differed from this prep in that the Rh was introduced as $Rh(COD)Cl/_2$ after the silica surface was esterified with $EtOSi(CH_3)_2CH_2CH_2P\phi_2$. The silane and $Rh(COD)Cl/_2$ concentrations were also in 15 fold excess. The hydrogenation substrate in all cases was cyclohexene freshly passed through an activated alumina column (10 in.). In the latter runs (M-9 on) this step was carried out under N_2. The solvent in hydrogenation was always ca 25 ml dry-O_2 free benzene. Hydrogenation data is included in appendix 1.

Appendix 3

Micrograph	Description
1,2& 3	0.109 polystyrene spheres (Dow)
4 & 5	catalyst M-9 before use (see appendix 2 for prep)
6,7& 8	catalyst M-9 after use
9& 10	catalyst M-10Y after use (see appendix 2 for prep) samples appeared the same before use
11	catalyst M-7 (prepared as in appendix 2 but heated to 250 in absence of air)
12	catalyst M-7 dark field of #11
13	catalyst MT-28-4 (prepared by M. Takeda) Rh, 2.88% after use
14	catalyst MT-28 (prepared by M. Takeda) Rh, 2.88% before use
15	catalyst MT-28 dark field of # 14
16	catalyst MT-48 (prepared by M. Takeda) Rh, 8.22% after use
17	catalyst MT-28-4 (prepared by M. Takeda) Rh, 2.88% after use
18& 19	Rh (5%) on alumina
20& 21	catalyst prepared by D. Marquardt $RhCl(CO)(P\phi_3)_2$ + functionalized polystyrene: 
Pattern A	electron diffraction of a high density region of micrograph #13 crystallite orientation is unknown note sixfold symmetry

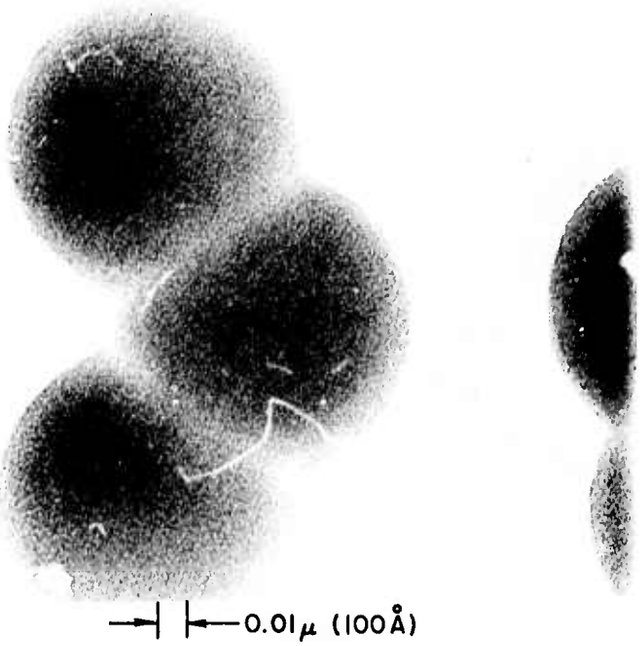

MICROGRAPH #1

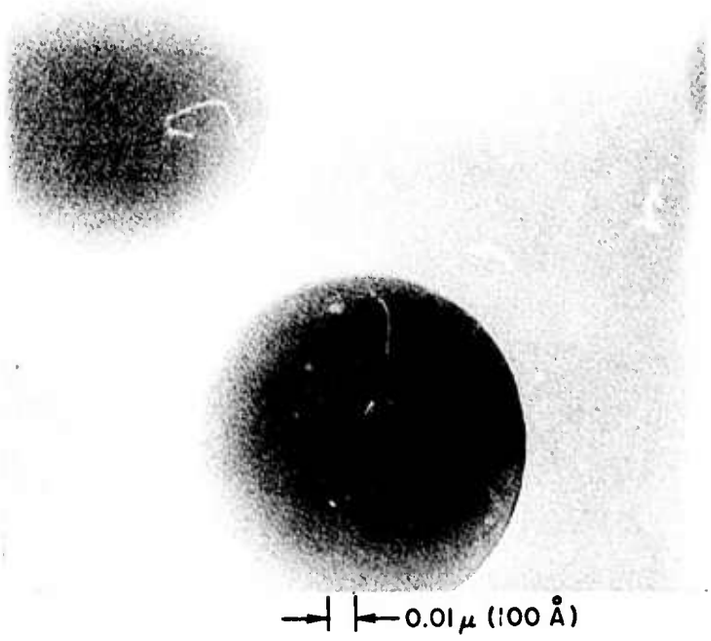

MICROGRAPH #2

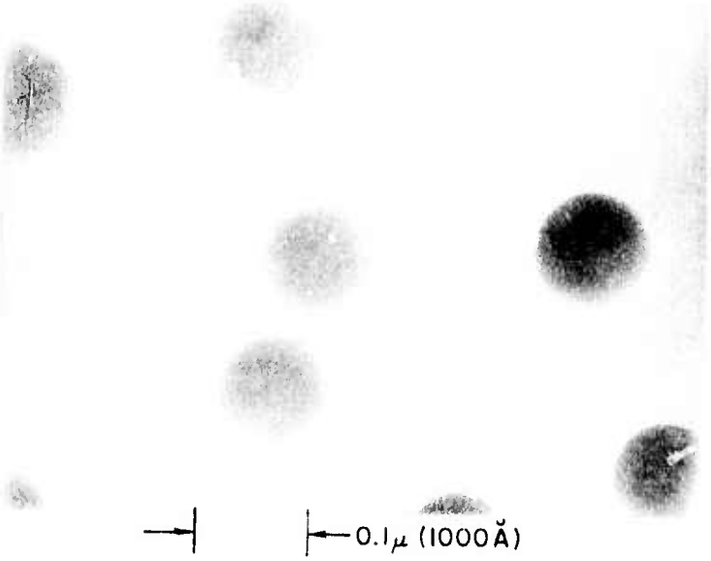

MICROGRAPH #3

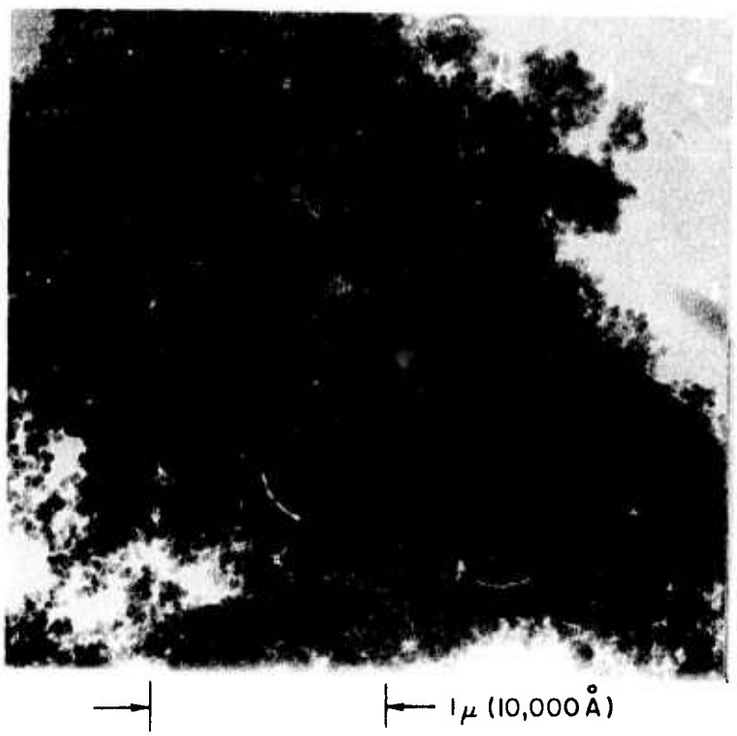

MICROGRAPH #4

0.01 μ (100 Å)

MICROGRAPH #5

0.01 μ (100 Å)

MICROGRAPH #6

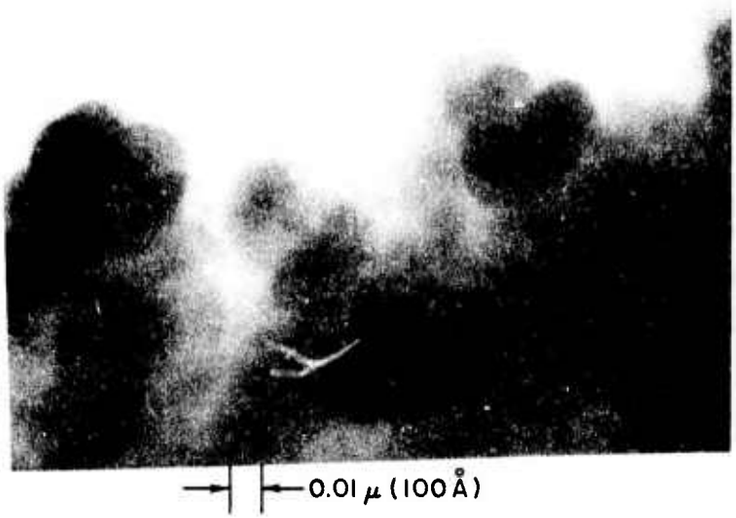

MICROGRAPH #7

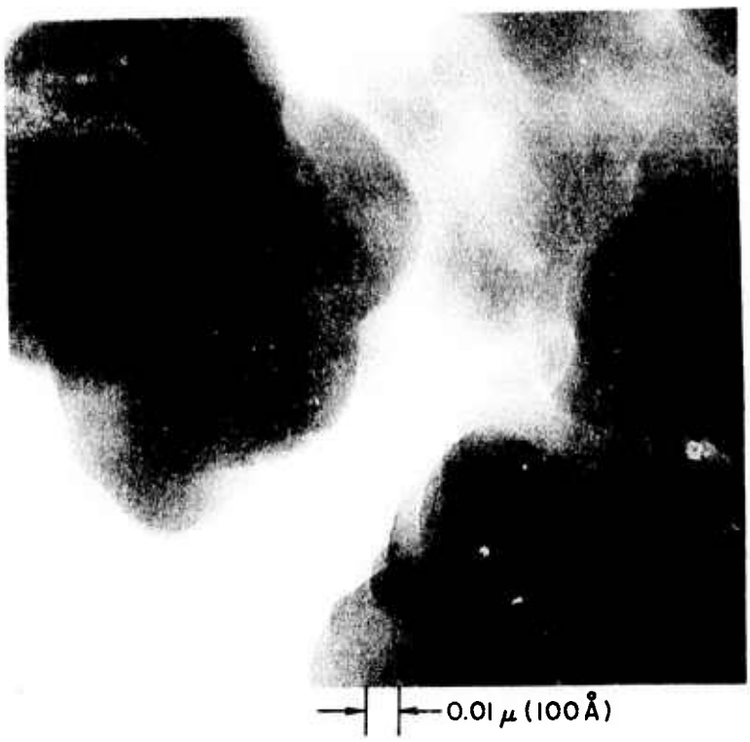

MICROGRAPH #8

MICROGRAPH #9

MICROGRAPH #10

0.01 μ (100 Å)

MICROGRAPH #11

0.01 μ (100 Å)

MICROGRAPH #12

DIFFRACTION PATTERN 'A'

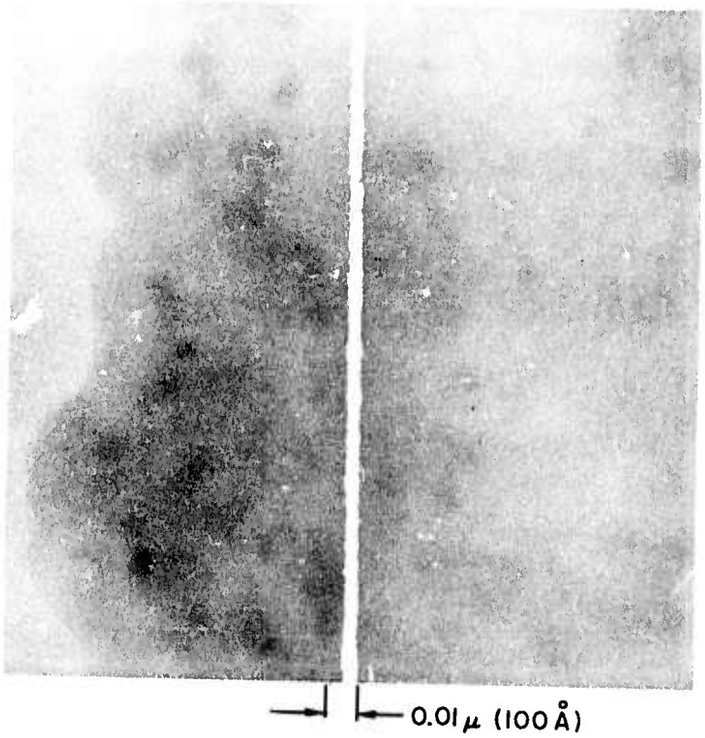

MICROGRAPH #13

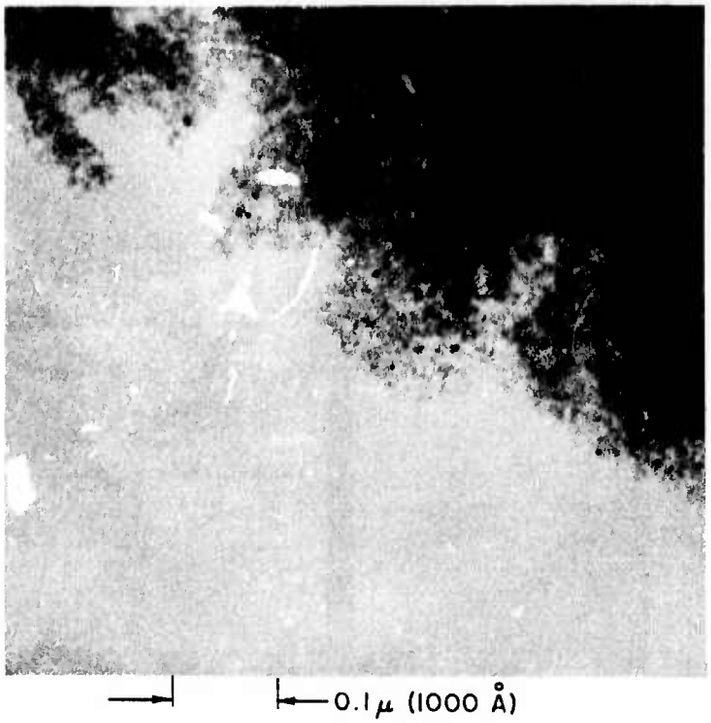

MICROGRAPH #14

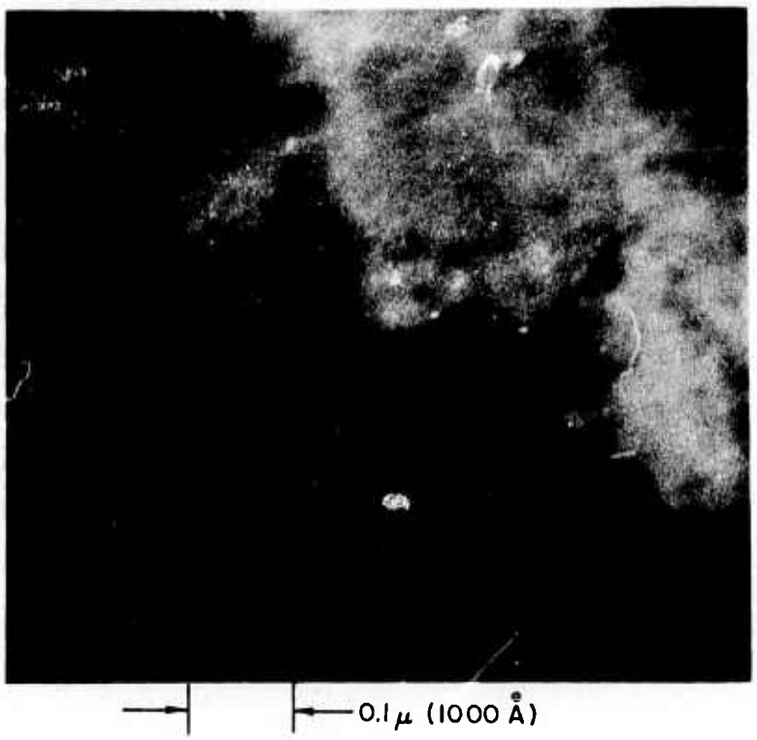

MICROGRAPH #15

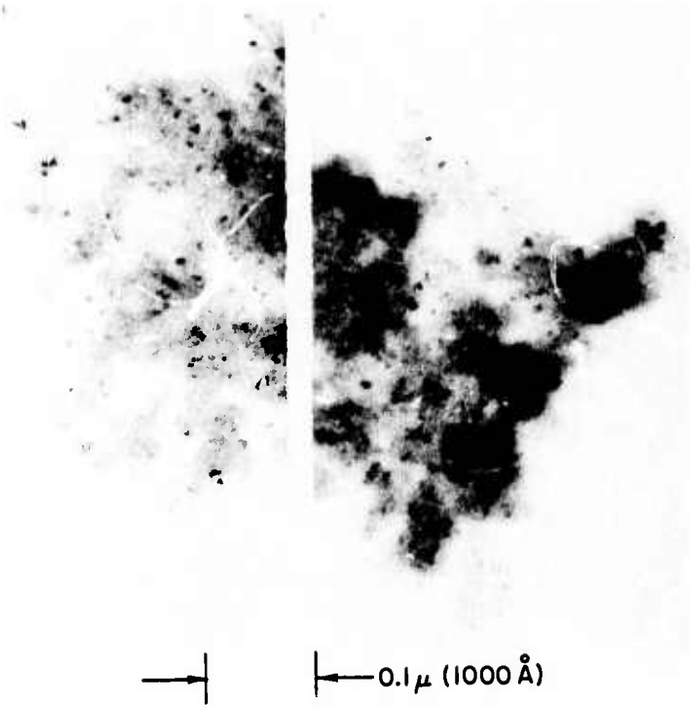

MICROGRAPH #16

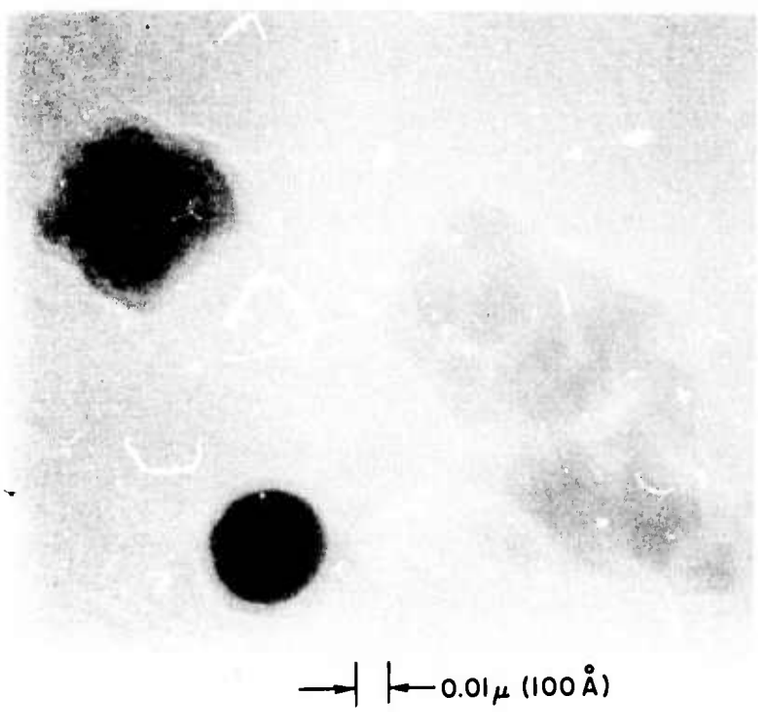

MICROGRAPH #17

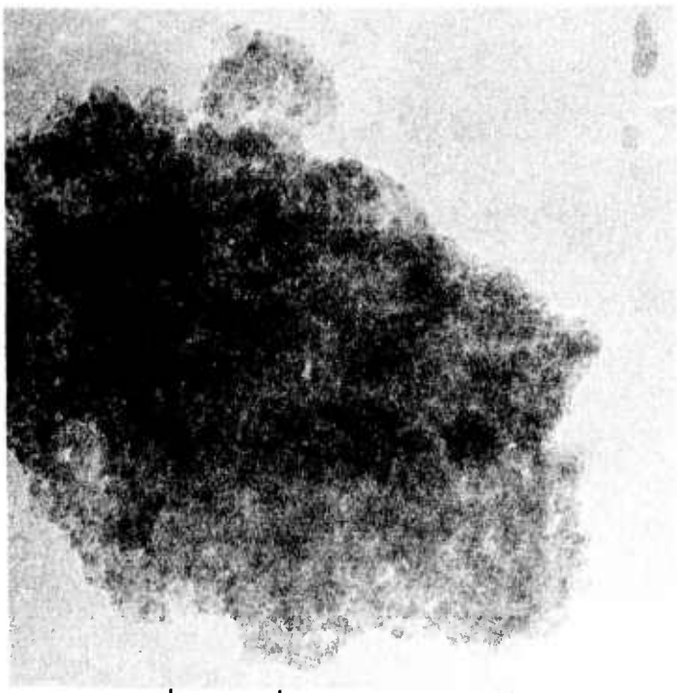

MICROGRAPH #18

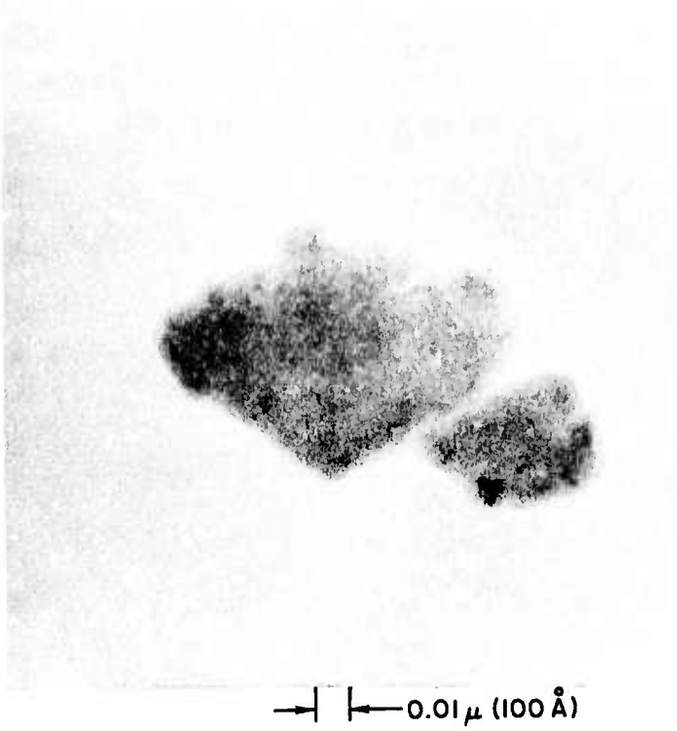

MICROGRAPH #19

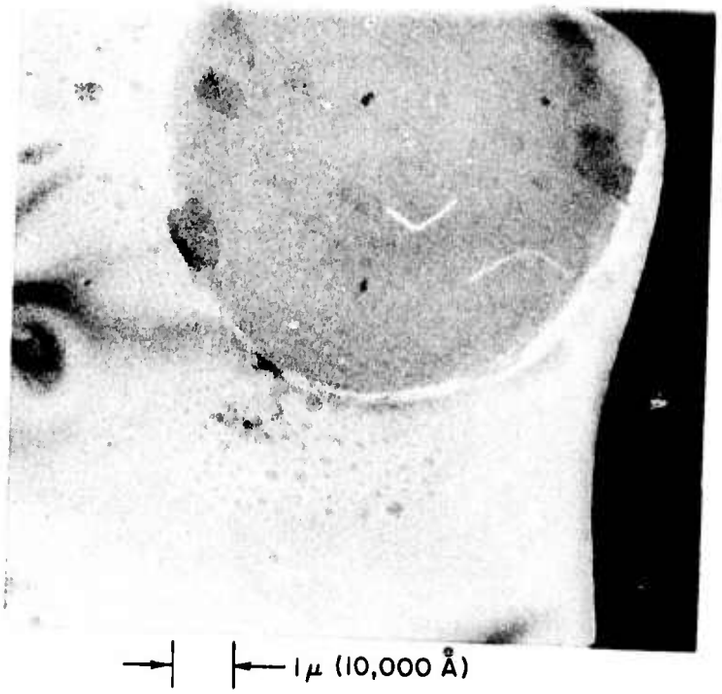

MICROGRAPH #20

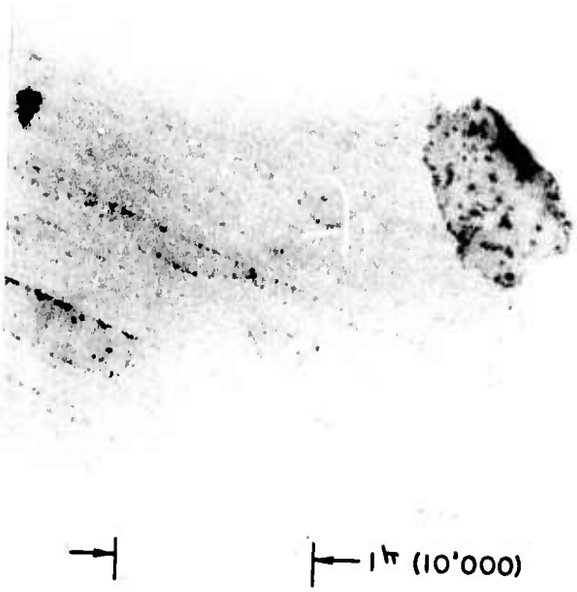

MICROGRAPH #21

References

(1) R. K. Iler, The Colloid Chemistry of Silica and Silicates, Cornell Univ. Press, 1955.

(2) DeBoer and Vleeskens, Proc. Kon. Inkl. Ned. Akad. Wetenshap., B, 60, 44, 1957.

(3) A. J. Tyler, C. G. Armistead, F. H. Hambleton, and J. A. Hockey, J. Phys. Chem., 73, 3947 (1969).

(4) J. B. Peri and A. L. Hensley, J. Phys. Chem., 72, 2926 (1968).

(5) R. L. Karger and A. Hartkopf, Anal. Chem., 40, 215 (1968).

(6) W. Hertl and M. L. Hair, J. Phys. Chem., 73, 4269 (1969).

(7) L. Robert, Z. Kessaissia, and G. Tabak, C. R. (C), 276, 451 (1973).

(8) W. Hertl and M. L. Hair, J. Phys. Chem., 72, 1242 (1968).

(9) W. Hertl and M. L. Hair, ibid., 75, 2181 (1971).

(10) M. Low and C. Morterra, ibid., 73, 321 (1969).

(11) W. Hertl and M. L. Hair, Nature, 223, 1150 (1970).

(12) V. M. Bermudez, J. Phys. Chem., 74, 4160 (1970).

(13) K. Kamiyoshi, J. Phys. Radium, 20, 60 (1959).

(14) W. Hertl and M. L. Hair, J. Phys. Chem., 74, 91 (1970).

(15) B. A. Morrow and A. Devi, Can. J. Chem., 48, 2454 (1970).

(16) T. Kagiya, Y. Sumida, and T. Tachi, Bull. Chem. Soc. Japan, 44, 1219 (1971).

(17) R. Liebich and P. Fink, Z. Chem., 11, 34 (1971).

(18) a. W. D. Bascom, J. Phys. Chem., 76, 3188 (1972).

b. W. D. Bascom and R. B. Timmons, ibid., 76, 3192 (1972).

(19) J. J. Fripiat, A. Jelli, C. Punclet, and J. Andre, Ibid., 69, 2185 (1965).

(20) C. A. Tolman and J. P. Jesson, Science, 181, 501 (1973).

(21) J. A. Osborn, F. H. Jardine, J. F. Young, and G. Wilkinson, J. Chem. Soc., A (1966), p. 1711.

(22) P. Meakin, J. P. Jesson, and C. A. Tolman, J. Amer. Chem. Soc., 94, 3240 (1972).

(23) M. Takeda, Research Report, 1973.

D. Studies on Sulfur Containing Rhodium and Platinum Catalysts

H. Heitner

Introduction. One of the chief problems of homogeneous catalysis is separation of the catalyst from the reaction products. This is of particular importance in high volume industrial applications where even slight losses of expensive metals would prove to be very costly. One approach to the recovery problem is to anchor the catalytic species to ligands which are chemically bonded to a polymeric support. This idea was first suggested by Manassen[1]. Since then a number of catalysts have been made based on phosphine containing organic polymers or silica gel[2]. The present work originated when it was observed that one of the materials prepared for reduction to form metal clusters was a hydrogenation catalyst. This material (27-1) was prepared by reacting ethanolic rhodium chloride with a silica gel coated with mercaptopropyl groups. (See report on surface bound clusters for discussion of ligands and silica gel). The object of this study was to elucidate the nature of the active species and to prove if possible that this material and related materials were truly supported homogeneous catalysts. It was decided to use chemical rather than physical experiments (ie. electron microscopy) to investigate these catalysts, principally

because there was some doubt as to the interpretation and reliability of results in the latter case.

Experimental Sequence

1. Steric Effects

Wilkinson's catalyst, $Rh(\emptyset_3P)_3Cl$, has been studied with a number of substrates. It shows a large amount of steric selectivity for olefins[3]. The relative difference in rate between cyclohexane and 1-methylcyclohexane is 50:1. In contrast a heterogeneous platinum catalyst showed a relative rate difference of 2:1[4] for this system. It was supposed that if Wilkinson's catalyst were taken as a model, a supported homogeneous catalyst should show a similar steric effect in the cyclohexene-1-methylcyclohexene system. A kinetic run at 1 atm showed a rate differential of 2:1. Some benzene was reduced with this catalyst (27-1) to cyclohexane indicating that perhaps some rhodium metal had been bound on the silica gel by reduction of $RhCl_3$ by ethanol. A blank made by refluxing ethanolic $RhCl_3$ with untreated silica gel gave an active hydrogenation catalyst. A blank made using aqueous $RhCl_3$ showed no catalytic activity. A new catalyst 68-1 was made by reacting aqueous rhodium chloride with mercaptopropyl silica. The rate of reduction with this new catalyst was smaller. It did not catalyze the reduction of benzene. Treating this catalyst with excess aqueous $SnCl_2$ gave a new catalyst 68-2 which showed enhanced reactivity (Table I). This catalyst showed a steric differential of nearly 10:1 for the cyclo-

hexene-1-methylcyclohexene system. The principal species in this material and most probably the active species is a Rh(I) complex containing $SnCl_3^-$ ligands. The reduction of Rh(III) to Rh(I) by Sn(II) has been reported by Wilkinson.[5]

Table I. Relative Hydrogenation Rates for Catalysts

Catalyst	1-methyl-cyclohexene	cyclohexene
63-2	0.55	1.18
68-2	0.47	3.98
68-1		0.40

2. Effect of HNO_3

Catalyst 68-2 which had been exposed to H_2 in a kinetic experiment was treated with concentrated HNO_3 and washed and the acid treatment and washing repeated. The dark catalyst was now pale yellow. In a Fisher-Porter bottle experiment it showed only a trace of catalytic activity. Acid treatment of Rh on Al_2O_3 did not noticeably lower its activity. A catalyst made using ethanolic $RhCl_3$ also losts its activity on acid treatment.

Conclusions. These two experiments indicate that the active catalyst of 68-2 does not contain any appreciable amount of rhodium metal since the kinetic behavior and chemical properties are completely different from metallic rhodium. (One is assuming that metallic rhodium is similar to platinum, this was not checked).

3. Effect of Chelating Ligands

68-1 didn't catalyze the reduction of 1, 5 cyclooctadiene (only traces of product). Rhodium on alumina catalyzed this reduction at a rapid rate. 1, 5 cyclooctadiene prevented the reduction of cyclohexene with 68-1. Treating 68-1 with ethanolic solutions of dimethylglyoxime or salen prior to hydrogenation also produced a strong inhibition of reduction. Addition of salen to 68-1 under hydrogen also inhibited reduction.

Conclusions. These experiments indicate that the active species of 68-1 is probably a monomeric rhodium complex since it is strongly inhibited by chelating ligands.

4. Reduced Species and Hydride Formation

68-1 could be reacted with aqueous $NaBH_4$ to give a dark substance 73-2. The reaction probably involves replacement of halide since prior treatment with ethanolic salen prevents this reaction. 73-2 does not catalyze the reduction of 1, 5 COD, but causes considerable isomerization even in the absence of H_2. The material lightened after a few days. It did catalyze the hydrogenation of benzene though not at a rapid rate. These properties indicate that this material probably contains a hydrido species and possibly a small rhodium cluster species. 68-2 also was capable of isomerizing 1, 5 COD in benzene in the absence of H_2 indicating that it too may contain a hydrido ligand. Another possibility is that 73-2 contains a metal boride species. Such compounds

have been reported as products in the reaction of BH_4^- with metal salts in solution[6].

Platinum Catalyst

Reaction of mercaptopropyl silica with aqueous K_2PtCl_4 gave a yellow material which was active for the hydrogenation of cyclohexene. No further experiments were done with this catalyst. An experimental sequence similar to that followed in the rhodium case would be useful in further characterizing this catalyst.

Other Reactions

$RhCl_3 \cdot 3H_2O$ catalyzes the dimerization of olefins in alcohol solution[7]. A test reaction was run at ~50°C to see whether 68-1 would catalyze the reaction of butadiene with ethylene to give hexadienes. After ≃ 20 hr at 80-110 psi of ethylene no hexadiene was observed by gc (considerable butadiene was observed). Hydrogenation of an aliquot of the reaction mixture using a rhodium catalyst gave no hexane.

A control reaction was run at 35°C using a homogeneous $RhCl_3$ catalyst. The result was apparently a mixture of hexadienes. Hydrogenation of this mixture gave several products, among them was hexane.

Homogeneous solutions containing various Rh species and iodine compounds catalyze the carbonylation of methanol to acetic acid[8]. A control reaction run in a Fisher-Porter bottle using a $RhCl_3$-CH_3I solution gave a considerable yield of methyl acetate at 120°C. Several supported catalyst systems were tested at ≃ 120°C under CO pressures of ≈80 psi. The catalyst preparation and results are summarized in the following table.

Table II. Carbonylation Catalysts

Catalyst	Results
8-2, catalyst 68-1 treated with aqueous KI, turned black	trace of methyl acetate slight leaching
9-II, catalyst 62-1 (same as 63-2) + CH_3I	high yield of methyl acetate, considerable leaching
8-III, catalyst 68-2 and CH_3I	same methyl acetate, some leaching
10-1, catalyst 68-1 and I_2	no activity

The two catalysts which showed activity comparable to the homogeneous system were extensively leached off the silica to give dark solutions. In the 9-II run the solid catalyst was filtered off and washed with methanol. It showed only slight catalytic activity. The filtrate was evaporated and the residue dissolved in fresh methanol. This solution also only showed slight catalytic activity. Evidently both components are necessary for catalysis. This system should be further investigated to determine whether or not it is a true supported homogeneous catalyst or a homogeneous catalyst of the usual type.

Experimental

Most test reactions were run in Fisher-Porter bottles under semi-quantitative conditions. Olefins were purified by passing them through activated alumina. 1,5 COD was distilled prior to passage through alumina. Products were identified by gas chromatography using a 10% carbowax column.

Catalyst Syntheses

Silica 26-2. Ten grams of Davison 62 silica was stirred for 2 days with 2 ml trimethoxymercaptopropylsilane and 1 ml di-i-propyl amine in 120 ml of dry benzene. A wrist action shaker was used in this step. The silica gel was filtered off and washed with benzene, acetone and ether.

Analysis: Sulfur, 2.24%.

Catalyst 62-1. Rhodium trichloride (0.2 gm) was dissolved in 100 ml of absolute ethanol, 1 gm of mercaptopropyl silica was added and the mixture was refluxed for 45 minutes. The dark red silica was filtered off and washed with ethanol and ether.

Analysis: Rhodium, 6.21%.

Other catalysts were synthesized by similar methods. Exact details can be obtained from the notebook references.

References

(1) J. Manassen, Chim. Ind. (Milan) 1969, 1058 (1969) and references contained therein.

(2) K. G. Allum, R. D. Hancock, S. McKenzie and R. C. Pitkethly, Proc. Fifth Int. Congress on Catalysis, Amsterdam, 1972.

(3) F. H. Jardine, J. A. Osborn and G. Wilkinson, J. Chem. Soc. A, 1967, 1574 (1967).

(4) A. S. Hussey, G. W. Keulks, G. P. Nowack, and R. H. Baker, J. Org. Chem., 33, 610 (1968).

(5) J. F. Young, R. D. Gillard and G. Wilkinson, J. Chem. Soc., 1964, (1964).

(6) H. C. Brown and C. A. Brown, J. Amer. Chem. Soc., 85, 1003 (1963).

(7) T. Alderson, E. L. Jenner and R. V. Lindsey, Jr., J. Amer. Chem. Soc., 87, 5638 (1965).

(8) J. F. Roth, J. H. Craddock, A. Hershman and F. E. Paulik, Chem. Tech., 1971, 600 (1971).

VII. DEVELOPMENT OF ELEVATED TEMPERATURES ELECTROCRYSTALLIZATION TECHNIQUES

R. C. DeMattei

Research Associate, Center
for Materials Research

I. V. Zubeck

Research Metallurgist, Center
for Materials Research

and

R. A. Huggins

Professor of Materials Science
and Engineering

A. Introduction

The electrochemical synthesis program was initiated to develop the facilities, techniques and understanding necessary for the preparation of a variety of materials by controlled electrolysis of molten salt systems at elevated temperatures. The potential advantages of the electrocrystallization technique are numerous. A broad range of unusual materials may be synthesized in this way. The relatively low temperature at which this type of synthesis can be accomplished (generally 500 - 1000°C) can also be advantageous, especially in the case of materials with very high melting points, materials which do not melt congruently, and those in which the vapor pressure of one of the components is high.

The technique can be operated isothermally with determination of the deposition parameters exercised electrically. This provides the opportunity for great precision and reproducibility in both measurements and the control of process parameters. This represents a substantial advantage over normal high temperature crystal growth, where thermal parameters are dominant. In addition, one has the possibility of producing both uniform and reproducible stoichiometry.

A very large fraction of the work done in this area to date has centered about the exploratory use of this method for the synthesis of various compounds, primarily of the transition elements. Essentially no previous effort has gone into the development of sufficiently sophisticated understanding and technology for the control of the growth morphology necessary for the production of useful bulk samples, including single crystals, of a wide range of materials. In order to do this, however, it is necessary to understand how to produce and maintain the pertinent thermodynamic and kinetic conditions at the growth interface during the electrocrystallization process. It is in this direction that the major emphasis of this program is oriented.

In addition, attention is being given to the development of the electrochemical conditions necessary for the production of a group of specific materials of special interest. These include intermetallic

niobium compounds with high superconductive transition temperatures, several high melting point boride compounds with either unusual hardness or good electron emissivities, and other materials of interest because of their potential technological use as optical materials or as mixed conductors in new types of battery systems.

The body of this report consists of the individual research reports of the investigators currently working in the areas of boride synthesis, niobium intermetallic synthesis, and continuous growth techniques.

B. Investigation of the LaB_6 System

I. V. Zubeck

Activities of the past six months have led to significant advances in the understanding of electrolytic crystal growth, and of the LaB_6 system in particular. The MB_6 system (where M is a lanthanide or an alkaline earth metal, and B=boron) was chosen as a pilot system for development of electrolytic crystal growth techniques. LaB_6 was chosen because of its many potential industrial applications. The hexaborides have a cubic tunnel structure (Fig. 1) in which the central ion is free to move and can be present over a stoichiometry range of $La_{.67}B_6$ to $La_{1.0}B_6$. This makes them of interest as potential electrode materials for solid electrolyte batteries.

The MB_6 can be a metal or a semiconductor, depending upon the valence of the central ion. The compounds possess a hardness approaching that of diamond and melting points in excess of 2000°C. LaB_6 has been used successfully as an electron emitter material in electron microscope filaments.

To the present, LaB_6 for industrial use has been obtainable only by high temperature synthesis methods which preclude any control of morphology or physical properties. In contrast, it can be grown electrolytically, in a manner similar to that of conventional electroplating, at 800°C. Powdery deposits were obtained electrolytically by Andrieux (1). Understanding of electrochemistry and of crystal growth techniques has advanced considerably during the forty years following Andrieux's publication. Polycrystalline deposits of LaB_6 can now be routinely grown electrolytically. We are confident that by control of appropriate kinetic and thermodynamic parameters, single crystalline material and polycrystalline deposits of good quality can be obtained from many useful materials.

EXPERIMENTS

Initial experiments, based on early work of Andrieux, sought to obtain LaB_6 deposits of a better quality and larger grain size

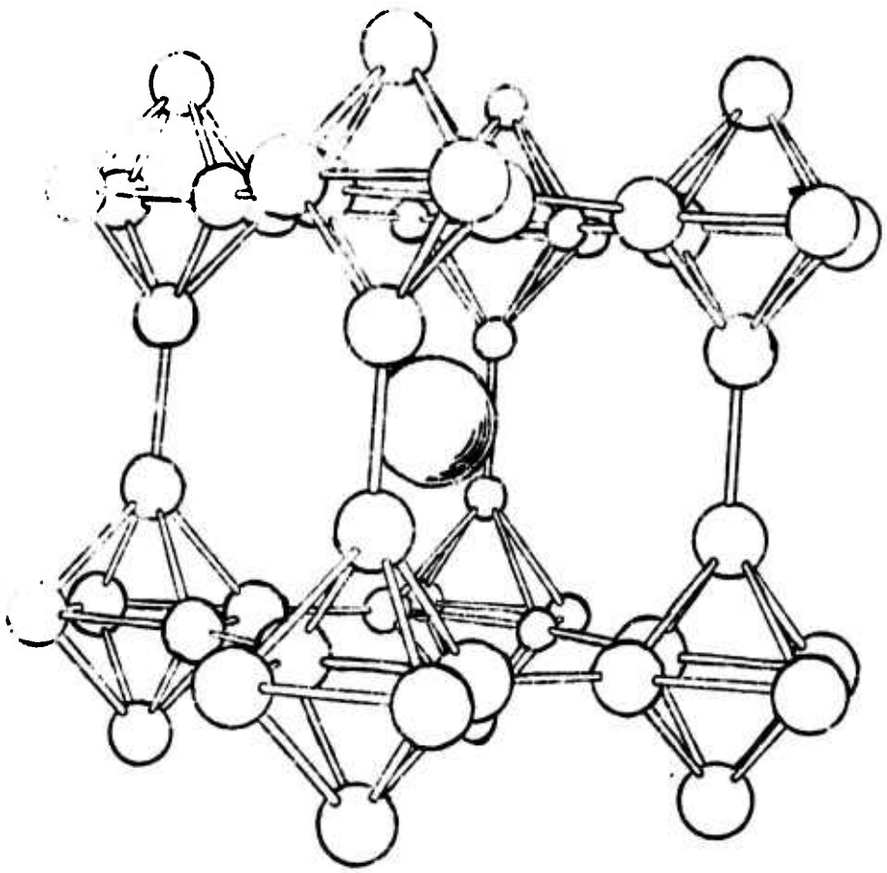

Fig. 1. The cubic metal hexaboride structure. The simple three-dimensional framework of interlocked B_6 octahedra is shown in perspective.

than those reported previously. Material was deposited on Au wire cathodes at 800°C from a molten salt mixture of La_2O_3, B_2O_3, Li_2O, and LiF. Electrolysis at low currents (~5mA) lasting several days produced clusters of magenta colored cubic crystals containing crystallites approximately 1 mm on a side. Efforts to accelerate material production by increasing the electrolysis current produced material of differing morphology, and, often bath failure, in which the molten salt bath would consistently give poor deposits or would cease to deposit material at all. Efforts were next directed toward documenting the types of crystal morphologies obtained under given growth conditions.

1. Morphology

A set of experiments was done in which samples were run at various initial current densities. An Au cathode was inserted into the bath, and the electrolysis voltage was set to a value corresponding to initial currents of 1.0, 2.0, 3.0, 4.0, 5.5, 7.0, 10.0, and 13.0 mA. Cathode area was maintained the same so that these samples could be compared in terms of current density. Electrolysis was allowed to proceed as the voltage and current were continuously monitored, until the current and voltage vs time reached stable values (almost immediately for the low current samples, 20-30 min. for the 7.0 and 10.0 mA samples). Evaluation of the samples grown and of their current-voltage vs time characteristics showed the necessity of using constant voltage power supplies if reproducible results were ever to be obtained.

Using constant voltage power supplies, the set of experiments was repeated. The resulting samples showed that cubic material was obtained at and below initial currents of 4.0 mA and that the current during the runs stayed essentially constant. The material obtained at 4.0 mA showed distorted cubes in which one corner was more acute than cubic (tending toward dendritic behavior). At initial currents of 5.5 mA and greater, the current increased during the run, the amount of the increase being greater, the greater the initial current.

Samples showing this behavior were V-shaped dendrites, whose length to width ratio increased with starting current. At an initial current of 13 mA, the deposits were powdery, finger-like dendrites, indicating that the useful range of operation had been exceeded.

2. Stoichiometry

The available literature on LaB_6 indicated that the compound could exist over a range of stoichiometry, $La_{.67}B_6$ to $La_{1.0}B_6$. A set of experiments was run to investigate whether LaB_6 covering this stoichiometry range could be obtained electrolytically.

A set of molten salt baths was prepared in which the mole-percent of La_2O_3 was varied. Samples were grown from melts containing 0.1, 0.5, 1.0, 2.2, and 4.0 mole-percent La_2O_3. Due to the excessively high melting points, baths containing more than 4.0 mole-percent La_2O_3 were not investigated. The melting point, decomposition potential, and a current-voltage plot were recorded for each bath. Quantitative analysis was performed on the samples using an electron microprobe, and x-ray techniques were used to check for changes in lattice parameter with composition.

Analysis showed the samples to vary from $La_{.672}B_6$ to $La_{.87}B_6$. The stoichiometry of the compound vs the La_2O_3 content of the electrolysis bath is shown in Table I. (Due to the low atomic number of boron, the accuracy of the determinations is highly dependent upon the type of standard used, the orientation of the sample with respect to the detector, etc.) The 1.0-4.0 mole-percent samples yielded the familiar magneta colored metallic cubes. The sample grown at 0.5% was still cubic, though of a deeper blue metallic luster. The sample grown from the 0.1% La_2O_3 bath yielded a mixture of rectangular and cubic crystals of a deep purple color. Voltage vs current data showed that the effects of La_2O_3 content and temperature on the decomposition potential of the electrolysis bath were negligible. Analysis of x-ray data showed no changes in lattice parameter with composition.

TABLE I

Mole % in La_2O_3 in bath	Microprobe Analyses	
	#1	#2
0.1%	-	$La_{.672}B_6$
0.5	$La_{.858}B_6$	-
1.0	$La_{.864}B_6$	$La_{.822}B_6$
2.2	$La_{.867}B_6$	$La_{.834}B_6$
4.0	$La_{.867}B_6$	$La_{.834}B_6$

3. The Electrolysis Bath

During the course of experimentation, it became obvious that a bath could never be electrolyzed long enough to use up more than a small portion of the La_2O_3 and B_2O_3 it contained. Baths consistently failed when less than 10% of the total La_2O_3 present had been consumed by electrolysis. Although the decomposition potential of the bath appeared to remain the same and current flowed through the cell, no cathode product was deposited. The condition could not be reversed.

Senderoff and Mellors (2), in electrodepositing ZrB_2 from a bath composed of LiF, NaF, KF, and ZrF_2+B_2O_3, also reported bath failure, which they correlated with the O/B ratio of their melts. Their analyses showed that when the O/B ratio of the bath exceeded 1.75, the bath failed, depositing only powder of ZrB_2 and ZrO_2. In selected cases, when enough B_2O_3 was added to an electrolysis bath to reduce the O/B ratio to 1.5, the cathode product would again be coherent ZrB_2. They believed the mechanism to be as follows: as the system is electrolyzed and boron is removed from the melt, the O/B ratio increases above 1.5 (that of B_2O_3) and the reaction occurs

$$2B_2O_3 + O^{-2} \rightarrow B_4O_7^{-2}.$$

What is certain is that B_2O_3 acts as a getter for O^{-2} ions and that there are several complex ions containing boron and oxygen. K. E. Johnson (3) prepared a series of electrode potentials (vs Cl_2 and F_2 reference electrodes) which contain entries for the reduction of B_2O_3, $B_2O_4^{-2}$, $B_4O_7^{-2}$, and $B_2O_5^{-4}$ (TableII). B_2O_3, in the presence of O_2, is easily reduced to one of the above complex oxyanions at a cathode.

In our experimental system, an Au anode of small surface area encouraged the dissolution of the anode product (O_2) in the bath. The excess O_2 would have combined with B_2O_3, forming one of the complex ions. The passage of current without deposition of a cathode

TABLE II

Electrode Potentials for Systems Containing Oxyanions

Electrode Reaction	E° v. Cl_2 at 1200°K	E° v. F_2 at 1800°k
$Ca^{2+} + 2e = Ca$	-3.25	-4.77
$SiO_4^{4-} + 4e = Si + 4O^{2-}$	-2.76	-4.34
$SiO_5^{6-} + 4e = Si + 5O^{2-}$	-2.73	-4.36
$SiO_3^{2-} + 4e = Si + 3O^{2-}$	-2.63	-4.22
$B_2O_5^{4-} + 6e = 2B + 5O^{2-}$	-2.62	-4.28
$B_4O_7^{2-} + 12e = 4B + 7O^{2-}$	-2.62	-4.06
$B_2O_4^{2-} + 6e = 2B + 4O^{2-}$	-2.50	-4.15
$SiO_2 + 4e = Si + 2O^{2-}$	-2.40	-3.29
$B_2O_3 + 6e = 2B + 3O^{2-}$	-2.29	-3.94
$P_2O_9^{8-} + 10e = P_2 + 9O^{2-}$	-2.27	-3.80
$P_2O_8^{6-} + 10e = P_2 + 8O^{2-}$	-2.26	-3.79
$P_2O_5 + 10e = P_2 + 5O^{2-}$	-1.63	-3.21
$CO_2 + 2e = CO + O^2$	-1.53	-3.13
$CO_3^{2-} + 2e = CO + 2O^{2-}$	-1.49	
$2CO_2 + O_2 + 4e = 2CO_3^2$	-0.64	
$O_2 + 4e = 2O^{2-}$	-0.61	-2.48
$2SiO_2 + 3O_2 + 12e = 2SiO_5^{6-}$	-0.39	-2.24
$SiO_2 + O_2 + 4e = SiO_4^{4-}$	-0.26	-2.08
$2SiO_2 + O_2 + 4e = 2SiO_3^{2-}$	-0.16	-2.05
$4B_2O_3 + O_2 + 4e = 2B_4O_7^{2-}$	-0.15	-1.78
$B_2O_3 + O_2 + 4e = B_2O_5^{4-}$	-0.10	-1.97
$Cl_2 + 2e = 2Cl-$	0	-1.86
$2B_2O_3 + O_2 + 4e = 2B_2O_4^{2-}$	+0.01	-1.84
$P_2O_5 + 2O_2 + Se = P_2O_9^{8-}$	+0.19	-1.73
$2P_2O_3 + 3O_2 + 12e = 2P_2O_8^{6-}$	+0.44	-1.49
$F_2 + 2e = 2F^-$	+2.00	0

product indicates the operation of a cyclic oxidation-reduction process involving B_2O_3 and its complex oxyanions. The presence of oxide compounds, La_2O_3 and Li_2O, in the bath compounded the problem.

Work is presently underway on the deposition of LaB_6 from a bath containing only fluorides and/or chlorides plus B_2O_3. Metal-boron compounds are commonly deposited from such melts. It is hoped that excluding oxides from the electrolysis bath will avoid the formation of O-B complexes, and will enable consistent results to be obtained.

RESULTS AND CONCLUSIONS

While becoming familiar with a variety of techniques pertinent to the electrolytic method of crystal growth, we have obtained cubic crystallites of LaB_6 approximately 1 mm on a side. These have been grown having a stoichiometry range of $La_{.67}B_6$ to $La_{.87}B_6$. The crystal morphologies obtainable under various growth conditions have been documented. In addition, knowledge of the characteristics of fluoride and oxide melts, and of the crucible, anode, and cathode materials appropriate to various conditions has been acquired.

In the coming months, we intend, first, to design an electrolysis bath for LaB_6 which will deposit the material reproducibly. That being accomplished, the understanding and control of crystal growth parameters will be pursued in order to obtain larger single crystals of LaB_6. In addition, it is planned to start work on the electro-deposition of sulfides and/or phosphides.

References

(1) L. Andrieux, Ann. de Chim., 12 424, (1929).

(2) G. W. Mellors, S. Senderoff, J. Electrochem Soc., 118, 220 (1971).

(3) K. E. Johnson, Proceedings of the Third International Symposium on High Temperature Technology, Pacific Grove, California, Sept. 1971. Butterworths, London.

C. Nb_3X Systems

U. Cohen

The conventional preparation of bulk superconductors of the type A-15 (β-tungsten) suffers from too many disadvantages. Arc melting, powder compacting, and sintering all result in non-homogeneous, highly brittle materials which cannot be machined, and are, therefore, very difficult to handle from the commercial viewpoint.

Vapor deposition techniques to prepare these materials are known, and it is possible to make thin coatings of these materials on ready-formed articles thereby avoiding the necessity for machining. The disadvantage of the vapor deposition technique is that it is difficult to deposit complex shapes uniformly. Also, the rate of deposition is very slow, and such deposits are limited to thin films. This imposes a severe restriction on the values of critical current that can be attained. One of the most important uses of these hard superconductors is for high magnetic field coils. However, these require heavy currents, and therefore relatively thick superconductor layers. For such purposes, vapor deposition techniques are not sufficiently satisfactory. Also, accurate control of stoichiometry is a critical problem in both bulk preparation and vapor deposition techniques.

It is believed that if a successful electrodeposition of uniform and well-bonded deposits of such superconductors can be achieved, this technique will find a wide and diverse application. It is hoped that easy control of thickness, composition, mechanical properties and reproducibility will be characteristic of such a technique.

Because of the recognition of the great advantage of fluoride systems in producing high purity, dense and coherent deposits, particularly of highly reactive metals such as niobium, a good fraction of the effort to date has been aimed toward the development

of molten fluoride salt technology. Three growth systems have been designed and put into operation that permit batch-type electrocrystallization in fluoride salts under controlled atmosphere up to 1000°C. In addition, a fourth unit, incorporating Czochralski-type rotation and pulling features is nearing completion. Support facilities include vacuum drying and electrolyte purification and pretreatment systems.

The elimination of water and oxygen from molten fluorides is a general problem encountered by those working with such materials. However, this difficulty has been overcome by pretreatment of the fluoride baths and the incorporation of decomposable constituents to provide flushing action.

By use of quasi-steady state current-voltage measurements of appropriate salt compositions, previously unknown values of the electrode potential in fluoride melts for both niobium (2.8 volts) and germanium (2.7 volts) have been evaluated using a gold anode. Similar work is presently being undertaken for tin.

High quality deposits of elemental niobium have been produced, using alkali metal fluoride electrolytes. Initial experiments aimed at producing niobium-germanium and niobium-tin compounds are underway, but have not yet been completed. The latter system presents complications due to the multiple valency of tin. Earlier work on the niobium-aluminum system has been discontinued because of difficulties inherent in the wide disparity between the decomposition potentials of the reducible species.

Decomposition potentials of NbF_5 were taken at different temperatures and solution concentrations in a solvent of KF-LiF eutectic at 490°C. A gold wire served as a reference anode electrode. It was found that gold dissolution corresponds to less than 1% of the current, the rest of the current resulting in the formation of fluorine gas. Molar concentrations of K_2NbF_7 investigated were 0.02%, 0.2%, 2% and

80%. The decomposition potential was determined by automatic I-V plots, with extrapolation to the I = 0 point, giving a precision and reproducibility of the order of 20-40 mV.

It was found that the decomposition potential varied with the temperature as expected, the effect of concentration being much less important than that of temperature. A concentration change by a factor of 10, resulted in a shift of the decomposition potential shift of about 20 mV. Representative values of the decomposition potential at 800°C were 1.82 Volts for 2% and 1.75 Volts for 80% K_2NbF_7.

In order to separately evaluate the fluoride solvents, decomposition potentials were measured in pure KF, as well as for the eutectic of LiF-KF. Values of 3.47 V were found for KF and 3.49 V for the KF-LiF eutectic at 800°C. Measurements of the decomposition potential of a 1.5% solution of AlF_3 in the fluoride eutectic gave values of about 3.27 V at 565°C. This large value explains the exclusive Nb deposition from all mixtures of Nb and Al fluoride solutions.

Decomposition potentials of Sn-fluoride solutions have also been measured. A value of 1.71 V was found for a 0.1% solution of SnF_2 at 600°C. Another wave is always formed at a higher potential, although its location is ill-defined. It is believed that one wave is due to the decomposition SnF_2, and that the other is due to the reduction of Sn^{+4} to Sn. The electrode reactions are thus: at the cathode; $Sn^{+2} + 2e^- \rightarrow Sn$, and at the anode; $Sn^{+2} \rightarrow Sn^{+4} + 2e^-$.

Studies of the electrolytic decomposition of solutions containing both Sn and Nb fluorides, as well as Ge and Nb combinations have also been undertaken. However, these experiments have not yet progressed to the point that definitive results can be reported.

D. Continuous Growth

R. De Mattei

INTRODUCTION

In order to move toward the development of continuous growth methods, work has been undertaken upon growth in low temperature molten salt systems with the deposition of copper from chloride electrolytes as the model system. This allows the study of continuous growth and morphological effects under relatively simple experimental conditions. Transfer of the acquired know-how to the more demanding high temperature atmosphere-controlled systems will be made later.

An important constituent of this problem is the understanding and control of the interface morphology during growth and the development of appropriate steady state conditions. Of primary importance in this regard is an understanding of the conditions leading to and the means of avoiding dendrite formation. The mechanism of formation and propagation of a dendrite is represented schematically in Figure 1. Interface instability starts as a microscopic protrusion whose growth rate accelerates under the influence of the concentration gradient of the diffusion layer near the cathode surface, until the protrusion tip extends far enough from the electrode surface to form its own independent diffusion layer. At this point, dendritic growth takes over and the dendrite grows at a constant rate.[1]

The mechanistic steps of the deposition process are represented in Figure 2.[2] As in many kinetic processes, the rate of the total event, in this case deposition, depends primarily on the slowest step in the kinetic chain. In the case of electrochemical synthesis, this leads to two distinct growth regimes: one in which the diffusion step is the slowest mechanism, and another in which one of the surface steps dominates the rate. This second condition is most desirable, since the diffusion limited mechanism favors dendritic growth consistent with the mechanism previously outlined. The problem thus reduces to finding a set of conditions that will insure rapid transport of material

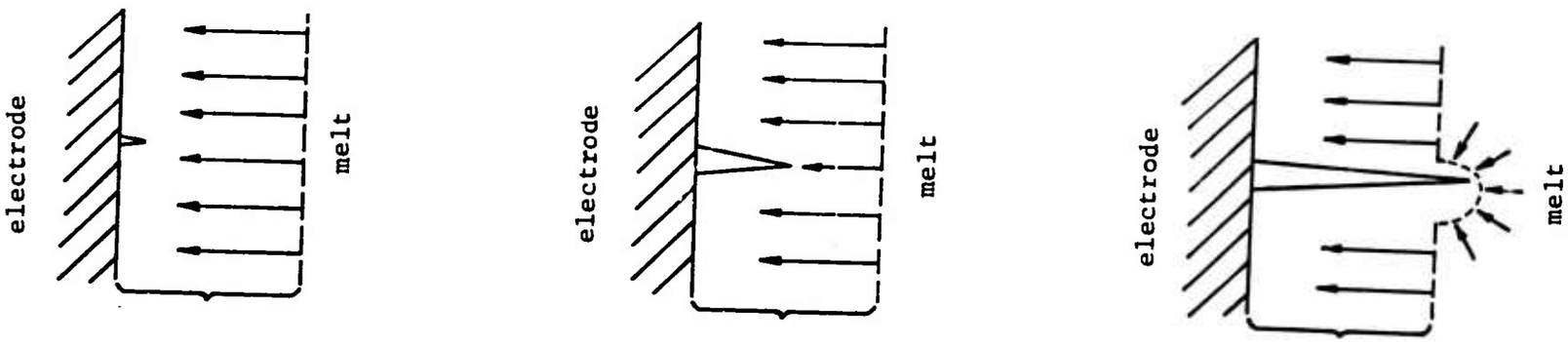

Figure 1. Schematic representation of initiation and growth processes leading to dendrite formation.

Figure 1a. Initiation of surface instability. Small protrusion forms on electrode surface. Protrusion is fed by linear diffusion (arrows) through diffusion layer (S). Shape and thickness of S is governed by electrode shape, electrochemical and hydrodynamic conditions.

Figure 1b. Protrusion grows at increasing rate due to increased concentration gradient as it moves through diffusion layer.

Figure 1c. True dendritic growth. Protrusion has grown long enough to extend beyond general boundary layer and forms its own diffusion-controlled layer. Growth now proceeds at a linear rate, independent of rate of progress of the overall electrode-melt interface.

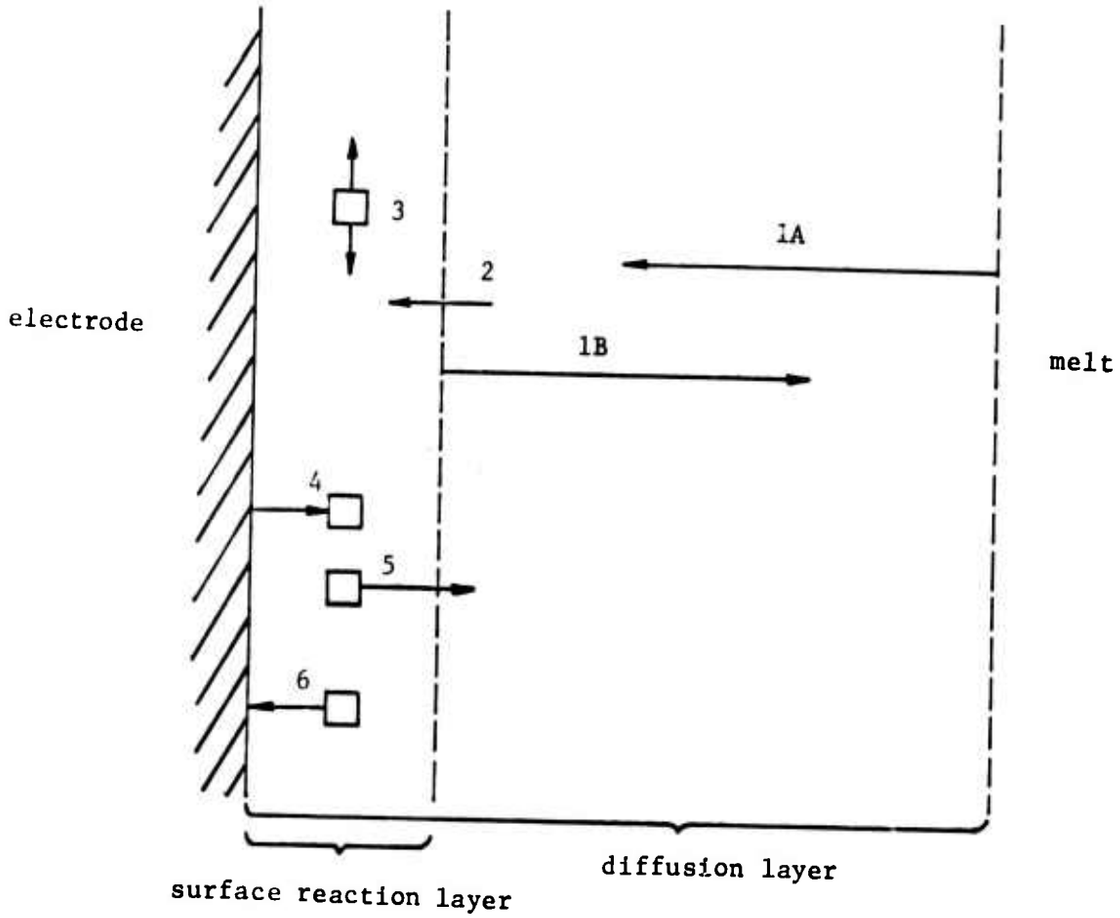

Figure 2. Schematic representation of kinetic processes involved in electrolytic growth.

1A Diffusion of solute to electrode interface
1B Diffusion of excess solvent, impurities, and electrolysis products away from interface
2 Partial desolvation
3 Surface diffusion to reaction site
4 Electron transfer (single or multistep)
5 Diffusion of solvent and electrolysis product away from interface
6 Attachment of electrolysis product to interface

across the diffusion layer, so that interfacial processes dominate the growth process.

The work of previous investigators[2,3,4,5] has indicated several approaches that separately or in conjunction with one another may prove fruitful. These include studies involving bulk melt concentration, stirred melts and/or rotating electrodes to reduce the boundary layer thickness, alternating deposition potential or superimposed alternating potential on steady dc, and ultrasonic energy input to growth interface. A series of experiments to evaluate these techniques alone and in combination is underway.

EXPERIMENTS AND RESULTS

The system chosen for the continuous growth investigation was the KCl (46 mole %) - $ZnCl_2$ eutectic with 5 mole % $CuCl_2 \cdot 2H_2O$ added initially. This system was chosen for its relatively low melting point (228°C) and the fact that it could be handled in air.

The first series of experiments run with this system were designed to investigate the effect of alternating potentials on the growth morphology. In the course of these experiments another problem presented itself. Under virtually all combinations of growth conditions, the cathode showed what has come to be called an "umbrella" - the rate of dendritic growth was greater near the surface of the melt. Various hypotheses concerning temperature gradients, chemical changes due to dissolved oxygen at the molten salt surface, uneven potential distribution along electrodes, and convective effects were put forward as possible causes of this phenomenon. A series of experiments testing these hypotheses was run, with the conclusion that the umbrella-type of growth morphology is caused by the convective movement of depleted solvent. This is schematically shown in Figure 3. A volume of solvent is partially depleted of its solute. Being somewhat less dense than the surrounding solvent it rises along the electrode face, continuously losing more solute. Eventually the solute concentration becomes low enough that

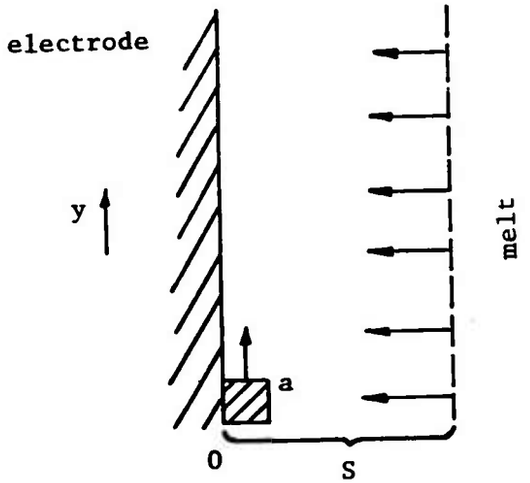

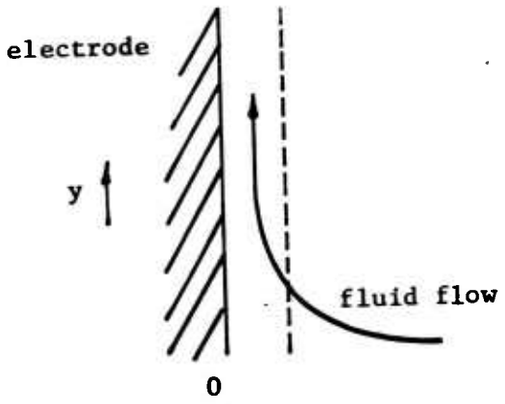

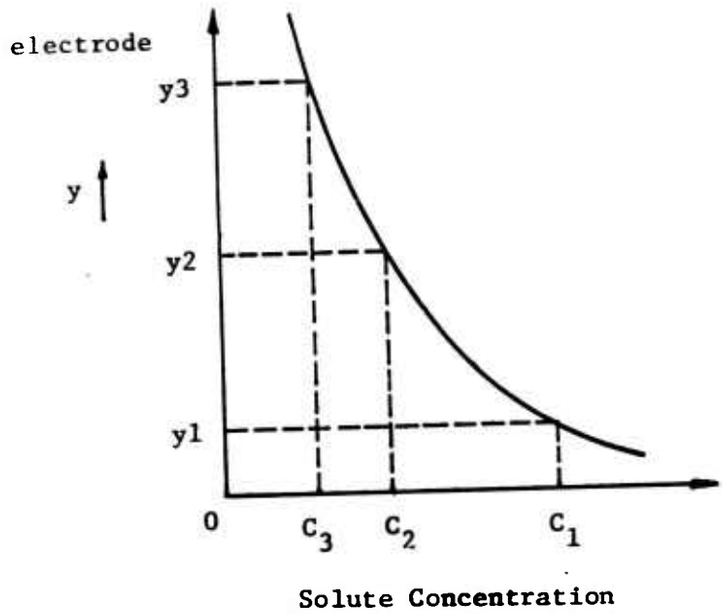

Figure 3. Schematic representation of process leading to umbrella formation.

Figure 3a. Small volume of melt (a) slightly depleted of solute moves in y-direction due to decreased density. (a) is further depleted as it moves along electrode.

Figure 3b. Process described in Figure 3a leads to a fluid flow pattern as shown (if there is no stirring) and leads to a region which is depleted of solute.

Figure 3c. Schematic plot of solute concentration in depleted region versus vertical position y.

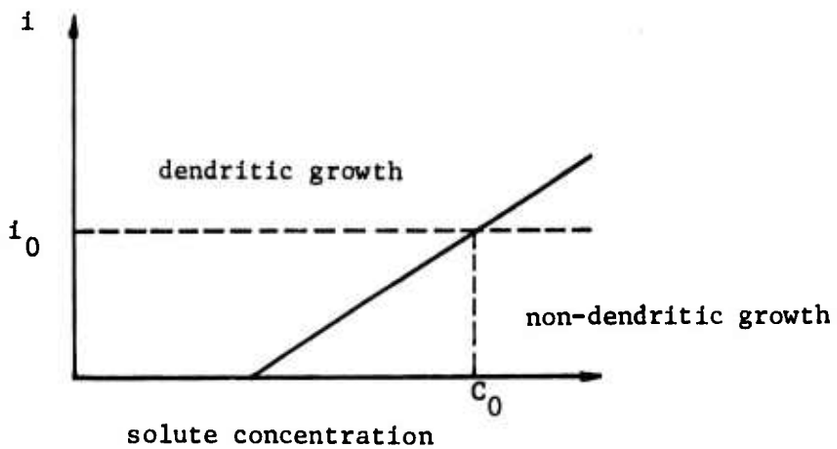

Figure 3d. Schematic plot of current density (i) versus concentration showing region in which dendrites can occur. At an operating current density (i_0), with changing solute concentration, a range of morphologies will be obtained on the same electrode. At local concentrations lower than C_0, dendrite growth will occur.

growth becomes diffusion-limited and dendrites form, the formation becoming more extreme as solute concentration diminishes. This hypothesis was tested using various electrode geometries and flow conditions. It was found that any area which was allowed to stagnate showed increased dendrite growth. Experiments concerning the effects of alternating potentials were postponed until some means of assuring a non-convective interface could be found.

A series of experiments was initiated utilizing a rotating electrode. The thickness of a boundary layer is dependent on the relative velocity of the melt past the interface,

$$\delta = KU^{\frac{1}{2}}$$

where δ is the boundary layer thickness, K is a constant incorporating solution viscosity and density, diffusion constant, interface length and a constant related to solute concentration along the interface, and U is the relative velocity.[2] If the boundary layer is made thinner, solute transport across it should be increased, leading to a smoother deposit morphology.

An apparatus for spinning the cathode at speeds of 94, 176, 351, 468, 936, and 1872 rpm was constructed, and a series of experiments at different ranges of current density and rotational speeds conducted. The distribution of the deposit was more uniform from top to bottom, with the improvement increasing with rotational speed (see Figure 4.).

Concurrent with these experiments, another series of experiments was run aimed at deliberately growing dendrites of copper, so as to attack the problem at the other extreme. This also allowed the introduction of the technique of continuous pulling of the deposited product from the melt during growth. Under properly adjusted conditions, dendrites several centimeters long and with variations in morphology were obtained from a melt containing 2.5 mole % $CuCl_2 \cdot 2H_2O$ (Figure 5).

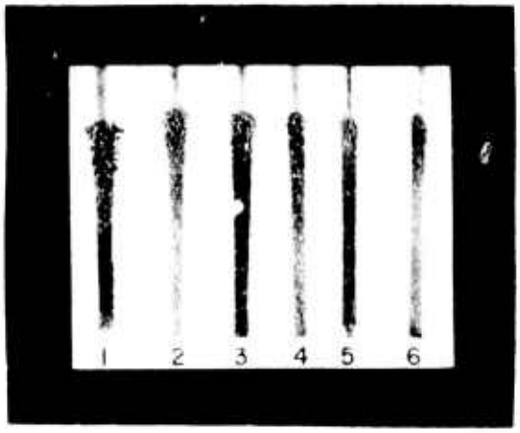

Figure 4. Effect of electrode rotation on deposit morphology.

From left to right:
(1) $i = 3.6\ ma/cm^2$, rpm = 0, time = 23 hrs.
(2) $i = 3.4\ ma/cm^2$, rpm = 94, time = 15 hrs.
(3) $i = 4.1\ ma/cm^2$, rpm = 176, time = 15 hrs.
(4) $i = 3.5\ ma/cm^2$, rpm = 468, time = 7 hrs.
(5) $i = 3.9\ ma/cm^2$, rpm = 936, time = 7 hrs.
(6) $i = 4.4\ ma/cm^2$, rpm = 1872, time = 6 hrs.

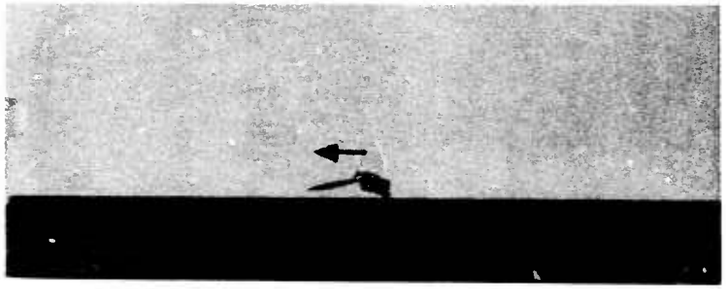

(a) Total current (I) = 20 ma
Pull Rate (P) = .01 cm/min.
Rotation (R) = 5 rpm

(b) I = 30 ma
P = .015 cm/min.
R = 5 rpm

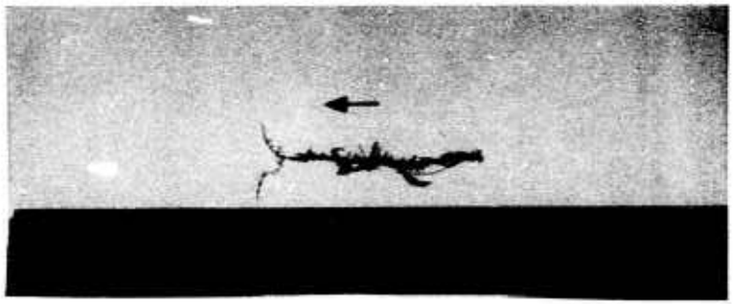

(c) I = 30 ma
P = .025 cm/min.
R = 5 rpm

(d) I = 30 ma
P = .035 cm/min.
R = 0 rpm

Figure 5. Examples of copper dendrites produced under various conditions. Melt composition was KCl (46 mole %) - $ZnCl_2$ with 2.5 mole % $CuCl_2.2H_2O$.
Arrows indicate growth direction.

References

(1) Despic', A. R. and K. I. Popov, "Transport-Controlled Deposition and Dissolution of Metals," Modern Aspects of Electrochemistry, edited by B. F. Conway and J. O'M Bockris, Plenum Press, New York, 1972, p.199.

(2) Scheel Hans J. and D. Elwell, "Stability and Stirring in Crystal Growth from High-Temperature Solutions," J. Electrochem. Soc. Vol. 120, No. 6.

(3) Despic', A. R. and K. I. Popov, "The Effect of Pulsating Potential on the Morphology of Metal Deposits Obtained by Mass-transport controlled Electro-deposition." J. Appl. Electrochem. Vol. 1 (1971), p. 275.

(4) Hinzner, F. W., "Solution Kinetics in Solid-Liquid Metal Systems." Thesis. Department of Materials Science, Stanford University, January 1962.

(5) Barton, S. L. and J. O'M. Bockris, "The Electrolytic Growth of Dendrites from Ionic Solutions". Proc. Roy. Soc. Vol. 268A p. 485.